Winter 12-15-2014

Study of II-VI Colloidal Semiconductor Magic-size Nanoclusters and Crystalline Quantum Platelets

Yuanyuan Wang
Washington University in St. Louis

WASHINGTON UNIVERSITY IN ST. LOUIS

Department of Chemistry

Dissertation Examination Committee:

William E. Buhro, Chair
Richard A. Loomis
Liviu Mirica
Bryce Sadtler
Li Yang

Study of II-VI Colloidal Semiconductor Magic-size Nanoclusters and Crystalline Quantum Platelets

by

Yuanyuan Wang

A dissertation presented to the
Graduate school of Arts and Sciences
of Washington University in
partial fulfillment of the
requirements for the degree
of Doctor of Philosophy

December 2014

Saint Louis, Missouri

TABLE OF CONTENTS

LIST OF FIGURES

Introduction:

Chapter 1:

Chapter 2:

LIST OF SCHEMES

LIST OF TABLES

ACKNOWLEDGEMENTS

I would like to express my great appreciation and deep regard to my advisor, Professor William E. Buhro, for his patient guidance, enthusiastic encouragement, and invaluable and constructive suggestions throughout my research work. Professor Buhro also provides much-needed assistance in preparing me to search for and find a postdoctoral position. It is my honor to work with him.

I also thank my dissertation committee members Professor Richard A. Loomis, Professor Liviu Mirica, Professor Bryce Sadtler, and Professor Li Yang for taking time from their busy schedules to accommodate me.

I would also like to thank Professor Richard A. Loomis, and Professor Vladimir Birman for interviewing me and bringing me to Saint Louis in 2009, in which I had the chance to study at Washington University in St. Louis.

Professor Loomis contributed in many helpful discussions of photoluminescence and kinetic studies. The photoluminescence spectra of CdSe quantum platelets were collected by Dr. Jessica Hoy. Professor Patrick C. Gibbons provided training in low-resolution TEM analyses. And Dr. Tyrone Daulton provided traning in high-resolution TEM analyses.

Laser-desorption-ionization (LDI) mass spectrometry experiments were conducted by Ying Zhang, Dr. Henry W. Rohrs, and Dr. Paul J. Kowalski (Bruker Daltonics, Inc). Mass spectra for the ligand-ratio studies were collected by Ying Zhang and Dr. Daryl E. Giblin. Special thanks go to Ying Zhang for teaching and guiding me about sample preparation and data analysis.

Elemental analysis was performed by Christy Love in Galbraith Laboratories, Inc.

Rutherford backscattering spectrometry data was collected by Greg Haugstad from the Characterization Facility, College of Science and Engineering, University of Minnesota.

I am particularly grateful for the assistance given by Karen Klein, Dr. Rachel Dunn, Phyllis Noelken and other department staff members. I also thank my friends, the current and past members in Buhro group and Loomis group, for help. Special thanks go to Dr. Fudong Wang and Dr. Yi-hsin Liu for their generous help and valuable suggestions in the beginning of my research. I would also like to extend my appreciation to Dr. Vernal Richards, PJ Morrison, Waynie Schuette, Linjia Mu, and Yang Zhou for their helpful scientific discussions.

Finally, my very special thanks go to my parents for their unconditional support and encouragement throughout my life. I also thank my girlfriend Xi Deng who supported me whenever I needed it during these years.

ABSTRACT OF THE DISSERTATION

Study of II-VI Colloidal Semiconductor Magic-size Nanoclusters
and Crystalline Quantum Platelets

by
Yuanyuan Wang

Doctor of Philosophy in Chemistry

Washington University in St. Louis, 2014

Professor William E. Buhro, Chairperson

The main objective of this project is to prepare and isolate the smallest, discrete, magic-size nanoclusters of cadmium selenide (CdSe) and to grow crystalline, wurtzite CdSe quantum platelets (QPs) at room temperature. The achievement of these goals enables us to provide a general synthesis of II-VI semiconductor magic-size nanoclusters and low-temperature routes to well-passivated nanocrystals having a range of compositions and morphologies.

The magic-size nanocluster $(CdSe)_{13}$ is grown in a lamellar-bilayer soft template at room temperature. The results described in this thesis strongly suggest that $[(CdSe)_{13}(n\text{-octylamine})_{13}]$ is the most thermodynamically stable nanocluster and serves as a key intermediate in the formation of CdSe quantum belts. Upon ligand exchange, sheet-like structures of $[(CdSe)_{13}(n\text{-octylamine})_x(oleylamine)_{13-x}]$ and free clusters of $[(CdSe)_{13}(oleylamine)_{13}]$ are released from the template. The kinetically stabilized magic-size nanolcusters prefer to grow to larger sizes once the steric protection of the primary-amine ligation is compromised by small-ligand substitution.

Several discrete $[(CdSe)_{13}(RNH_2)_{13}]$ derivatives (R = *n*-propyl, *n*-pentyl, *n*-octyl, and oleyl) are prepared in the corresponding primary amine solvent. For the first time, the soft-template method has been employed on the gram scale to prepare pure $(CdSe)_{13}$ as a solid, isolable derivative. This achievement enables us to study the intrinsic physical properties of $(CdSe)_{13}$, like size and melting points. The access to preparative quantities of $(CdSe)_{13}$ will promote further experimental studies of its structure, reactivity, and use as a nanocrystal precursor.

A novel method is introduced to synthesize crystalline wurtzite, two-dimensional CdSe quantum platelets (QPs) by employing primary amine and secondary amine cosolvent mixtures. This is the first preparation of thickness-controlled CdSe nanocrystals under mild conditions. The thickness of the QPs is dependent on temperature, and the length is affected by the nature of secondary amine. Reaction monitoring establishes that the magic-size nanocluster $(CdSe)_{34}$ is a key intermediate in the formation of the QPs. $[(CdSe)_{34}(n\text{-octylamine})_{16}(\text{di-}n\text{-pentylamine})_2]$ is isolated, which functions as critical size crystal nuclei that may be stored in a bottle.

Introduction

This dissertation first reports the low temperature growth of colloidal, semiconductor single-size $(CdSe)_{13}$ nanoclusters (Chapter 1), as various primary-amine derivatives (Chapter 2). Bundled $(CdSe)_{13}$ nanoclusters were initially generated in an *n*-octylamine-based lamellar-bilayer-template structure. Colloidal $(CdSe)_{13}$ sheets were exfoliated from bundled $(CdSe)_{13}$ upon partial ligand exchange. Full ligand exchange released free, soluble $(CdSe)_{13}$ as $(CdSe)_{13}(oleylamine)_{13}$. Kinetic data showed that small alcoholic ligands broke the steric protection of free, soluble $(CdSe)_{13}(oleylamine)_{13}$ nanoclusters, and caused cluster growth by a first-order kinetics (Chapter 1). Further studies showed that even shorter-chain primary amines formed amine-bilayer templates, in which $(CdSe)_{13}(RHN_2)_{13}$ derivatives were generated. Among all the $(CdSe)_{13}$ derivatives, $(CdSe)_{13}$(*n*-propylamine)$_{13}$, which was prepared as a solid on the gram scale will promote further experimental studies and use as a nanocrystal precursor. Low-angle diffraction data experimentally estimated the diameter of the bare $(CdSe)_{13}$ cluster at 0.8 nm, in agreement with molecular modeling (Chapter 2).

Furthermore, this dissertation also describes a room temperature growth of crystalline two-dimensional CdSe quantum platelets (QPs) (Chapter 3). Reaction monitoring established $(CdSe)_{34}$ as a key intermediate isolated in the formation of QPs with an empirical formula [$(CdSe)_{34}$(*n*-octylamine)$_{16}$(di-*n*-pentylamine)$_2$], which functioned as critical-size crystal nuclei and could be store in a bottle (Chapter 3).

II-VI semiconductor nanocrystals (NCs) (II = Cd, Zn; VI = S, Se, Te) have attracted tremendous attention due to their special size- and shape-dependent electrical and optical properties.[1] Investigation of these materials reveal several original characteristics, , such as a large band gap range, bright photoluminescence, large extinction coefficients, tunable

emission features, specific effects with magnetic ions in the crystal lattice, etc.[2] According to these properties, II-VI semiconductor NCs are recognized as important potential materials in optoelectronic,[3] lasing devices,[4] and as building blocks for new electronic and optical nanodevices.[5] Recent studies also indicate II-VI semiconductor NCs have great potential in biological labels,[6] and solar cells.[7]

Recently, significant interest has arisen in molecular-like intermediates or precursors to NCs, called magic-size nanoclusters (MSNCs) partly because of the ability to design the size and shape of the NCs with atomic precision.[8] MSNCs are ultra-small clusters containing a well-defined number of atoms with closed shells, and only stable in certain sizes.[9] Since such materials are metastable and may merge with neighboring clusters to destroy their discrete nature, only a few nanocluster materials exist in purity and stability at present.[10] Among them, the most famous ones are C_{60} and C_{70}.[11] After the initial report of CdSe clusters in 2004,[12] intense interest in II-VI semiconductor MSNCs is arising.[13] CdSe MSNCs as a model system have been investigated most for studying size-dependent properties in a strong confinement regime.[14] These magic-size nanoclusters with dimensions in the range of 1-2 nm can act as the smallest building blocks of cluster-assembled materials,[9a, 15] including quantum dots,[16] rods,[17] wire,[14] and belts.[18]

Among various nanostructures currently available that are assembled from MSNCs, semiconductor quantum platelets (QPs) (nanobelts, or quantum belts) have been recognized as a novel class of two-dimensional (2D) nanostructures, not only because of their relatively convenient synthesis pathway, but also because their special size and shape-dependent electrical[19], optical[20] and mechanical[21] properties. Since these flat

materials have thicknesses much smaller than their lateral dimensions and their Bohr radii, the electron-hole pairs are strongly confined in one dimension.[22] Thus the properties they exhibit are close to those of quantum wells, which is a thin layer confining electrons and holes in the dimension perpendicular to the layer surface, and the movement of electrons and holes in the other dimensions is not restricted. Besides, thanks to their intrinsic crystalstructure, zinc-blende (cubic) or wurtzite (hexagonal), and mild solution syntheses, 2D nanocrystals have better passivation on their large surface areas, which gives them remarkable optical properties, for example astonishingly high photoluminescence efficiencies compared with other anisotropic semiconductor nanocrystals like rods and wires. Due to these unique chemical and physical characteristics, we believe 2D semiconductor nanocrystals will have a great potential in solar-energy conversion and other emerging technologies.

Several methods have been applied to synthesize 2D-structured materials, including molecular beam epitaxy (MBE),[23] the solvothermal method[24] and solution-based synthesis.[25] In addition to these bottom-up synthetic methods, the top-down physical methods have also been used to make high-quality 2D-structured materials.[26] However, all methods mentioned above require high reaction temperatures. In some cases, phosphines, such as trioctylphosphine (TOP)[27] and trioctylphospine oxide (TOPO),[28] are also required as key coordinating solvents. These toxic and expensive starting materials are not environmentally friendly, and also limit the semiconductor-nanocrystal products to milligram quantities. Due to the limitation of lithographic resolution, top-down techniques cannot produce 2D structures with thickness under the nanoscale, or control

their thicknesses with atomic precision.[26]

In order to obtain a large quantity of 2D-structured materials with a precise controllable thickness via a green chemistry pathway, a novel technique is required. This goal can be achieved by double-lamellar-soft-template method. (Chapter 3)

Synthesis and isolation of cadmium selenide magic-size nanoclusters. Colloidal semiconductor nanocrystals, in particular, cadmium and zinc chalcogenide nanocrystals, represent the most popular research models in this field because of the ease of synthesis, and their size tunable absorption and emission properties in a strong-confinement regime. Due to the importance of strong quantum confinement effects in both fundamental research and technical applications, precisely controlling the size of nanocrystals is necessary. Compared with large-size nanocrystals, this goal seems to be easily achieved with nanoclusters consisting with less than hundreds atoms. Furthermore, MSNCs show sharper absorption and PL spectra and larger Stoke shifts than that of large size nanocrystals, like quantum dots, rods and wires, which make them potential materials for future devices and also an ideal platform for investigation of the molecular-to-nanocrystal transition.[29] Furthermore, recent experiments indicate MSNCs can serve as versatile building blocks for functional materials in nanoscience and nanotechnology.[18, 25]

Among all II-VI semiconductor MSNCs, cadmium chalcogenide MSNCs are the most studied, but only a few papers have been published concerning zinc chalcogenide clusters. Cadmium chalcogenide MSNCs especially $(CdSe)_{13}$ had been prepared only in mixtures of various sizes, and no single, discrete-size nanoclusters had been isolated in purity prior to our work.[9b, 13c, 30]

In chapter 1, a novel method is introduced to synthesize and isolate discrete, magic-size $(CdSe)_{13}$(*n*-octylamine)$_{13}$ nanoclusters. The smallest-known magic-size CdSe nanocluster generated in an *n*-octylamine-based lamellar-template structure by reaction of cadmium acetate dihydrate [$Cd(OAc)_2 \cdot 2H_2O$] and selenourea [$H_2NC(Se)NH_2$] at room temperature is the most thermodynamically stable. The stoichiometry of the nanoclusters is established by UV-visible spectroscopy and matrix-assisted laser-desorption ionization (MALDI) mass spectrometry. Elemental analysis further confirms the composition of the isolated material to be [$(CdSe)_{13}$(*n*-octylamine)$_{13}$]. Study shows that free $(CdSe)_{13}$ nanoclusters are liberated from the synthetic templates by sonication of [$(CdSe)_{13}$(*n*-octylamine)$_{13}$] in the presence of oleylamine. The growth behavior of free and templated nanoclusters in the presence of polar solvents is also discussed in this chapter.

To function as building blocks, a large amount of MSNCs is required in solution and also in the solid phase. However, no data have been reported on either preparing quantities of pure MSNCs, or isolating and storing them as solids. Chapter 2 describes several [$(CdSe)_{13}(RNH_2)_{13}$] derivatives (R = *n*-propyl, *n*-pentyl, *n*-octyl, and oleyl) obtained in the corresponding primary-amine solvents. The nanoclusters grew in spontaneously formed amine-bilayer templates, and were characterized by elemental analysis, IR spectroscopy, UV-visible spectroscopy, TEM, and low angle XRD. The derivative [$(CdSe)_{13}$(*n*-propylamine)$_{13}$] was isolated as a yellowish-white solid (MP 98 ℃) on the gram scale. These compounds were the first derivatives of magic-size CdSe nanoclusters to be isolated in purity. Chapter 2 also describes a novel $(CdSe)_{13}$ derivative synthesized in ethylenediamine (en). TEM images showed $(CdSe)_{13}$ assembled in sheet-like structures.

UV-visible spectroscopy indicated that nanoclusters passivated by en were more thermally stable. They were more stable at high temperature (70-80 ℃), and in polar solvents, and had better solubility in solution compared with those passivated by primary amine. These features give $(CdSe)_{13}$ prepared in en potential advantages for a crystal-structure study in the future.

Room temperature nucleation. Nucleation is an initiating, irreversible process of a first-order phase transition where a new, low-energy phase is generated from a mother phase with a higher energy. This transformation requires passage over a free-energy barrier.[31] The higher the barrier, the more activation energy is required, and thus more severe conditions are necessary to initiate the transformation. Normally, nucleation happens in phase boundaries (Fig I-1) because of the prerequisite of nucleation which requires the system to be in a thermodynamically metastable state.[32]

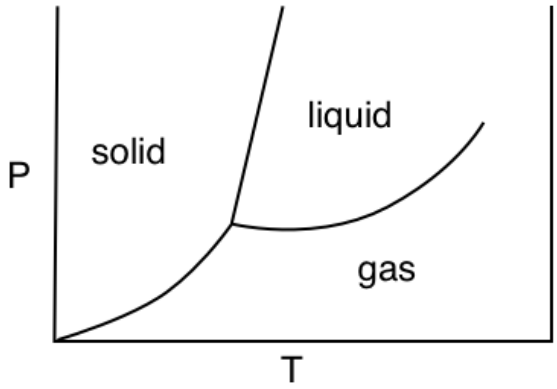

Figure I-1. Phase diagram of solid, liquid and gas.

For a chemical reaction, a crystal nucleation and growth process requires a proper ordering of reaction, nucleation, and growth barriers. Figure I-2 illustrates a typical process for the formation of nanocrystals. According to the classic crystal-growth model, in order to make nanocrystals grow, the chemical reaction barrier must be higher than that of the

nucleation (black solid line). However, if the reaction barrier is lower than that of nucleation, no nucleation stage exists in the reaction, thus only amorphous or non-crystalline materials are generated (red dashed line). Since the process of forming semiconductor nuclei often has a high nucleation barrier, a high reaction temperature then is necessary in the formation of nanocrystals. We suspect that high synthesis temperatures may reflect high nucleation barriers for assembling the critical-size nuclei, such that high-barrier chemical reaction is also required. That's the reason why crystalline semiconductor nanoparticles can only be prepared at high temperatures under traditional synthetic pathways. However, if a critical-size nucleus can be assembled under milder conditions, then in principle, nucleation and growth processes can be achieved at lower temperature.

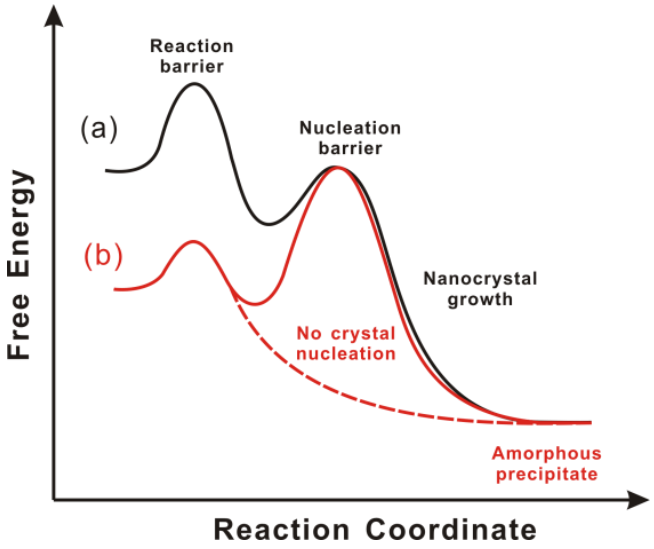

Figure I-2. Reaction-coordinate diagrams for alternate ordering of the monomer-generating-reaction and crystal-nucleation barriers.

In Chapter 3, a new species, magic-size nanoclusters were introduced as a potential, room temperature precursor for crystalline CdSe nanomaterials. The stoichiometry of the discrete nanoclusters was established by UV-visible spectroscopy and matrix-assisted laser-desorption ionization (MALDI) mass spectrometry. Elemental analysis further

confirms that the composition was [$(CdSe)_{34}$(*n*-octylamine)$_{16}$(di-*n*-pentylamine)$_2$]. Since this magic-size nanocluster assembled at room temperature, and its size was close to the critical crystal nucleus size, $(CdSe)_{34}$ nanoclusters under such reaction system later acted as a nucleant in the subsequent crystallization where the high nucleation barrier was largely surmounted. Consequently, low temperature nanocrystal synthesis was achieved. Then the magic-size nanocluster was obtained in an isolated form that can could be stored in a bottle. Using semiconductor magic-size nanoclusters as potent nucleating agents in different mesophase-templates may provide low-temperature routes to well-passivated nanocrystals having controllable compositions and morphologies.

Low temperature synthesis of crystalline quantum platelets. Two dimensional (2D) nanomaterials beyond graphene have received significant attention due to their special size-dependant chemical and physical properties. Among those materials, II-VI colloidal binary 2D nanocrystals are of the greatest interest for both fundamental research and technical applications. By using 1-octadecene (ODE) as non-coordinate solvent, the Dubertret group[20] obtained zinc-blend CdSe, CdTe and CdS atomically flat quasi-two-dimensional colloidal nanoplatelets with well-defined thickness at high temperature. These nanoplatelets have a narrow emission spectrum with less than 40 meV full-width at half-maximum (FWHM). Further study demonstrated that CdSe nanoplatelets can function as the fastest colloidal fluorescent emitters, and have a giant-oscillator-strength transition. However, their method requires extremely high reaction temperatures (>200 ℃). Besides, this system works only in synthesis of cadmium chalcogenide (CdE, E= S, Se, Te) nanocrystals. In the meantime, the Hyeon group[25] and our group[18] used a soft-template

method to obtain nanosheets or quantum belts under milder conditions (T = 70- 120 ℃). The nanocrysals prepared under such conditions have a wurtzite structure, and the thickness can be controlled by varying reaction temperature, while the lengths and widths are determined by the intrinsic properties of the spontaneously formed, double-lamellar templates. Then we sought to purposefully vary these dimensions by varying the nature of solvent, and these efforts led to experiments using cosolvent systems.

Chapter 3 reports a novel method to obtain crystalline wurtzite CdSe quantum platelets (QPs) at room temperature. $Cd(OAc)_2 \cdot 2H_2O$ and selenourea were used as cadmium and selenium precursors, respectively. $Cd(OAc)_2$ and a primary-amine solvent formed a lamellar, amine-bilayer mesophase, and then $(CdSe)_{34}$ clusters were formed within the template when primary-amine/secondary-amine cosolvents were employed. Then $(CdSe)_{34}$ clusters were converted to bundled QPs at room temperature, in which a long-chain primary amine resulted in the spontaneous exfoliation. The crystallinity of QPs was established by XRD, high-resolution TEM, and their sharp extinction and photoluminescence spectra. Reaction monitoring established the magic-size nanocluster $(CdSe)_{34}$ to be a key intermediate in the growth process, which converted to CdSe quantum platelets by first-order kinetics with no induction period. The results were interpreted to indicate that the critical crystal-nucleus size for CdSe under these conditions was in the range of $(CdSe)_{34}$ to $(CdSe)_{68}$. The nanocluster was obtained in isolated form as $[(CdSe)_{34}(\text{n-octylamine})_{16}(\text{di-n-pentylamine})_2]$, which was proposed to function as crystal nuclei that may be stored in a bottle.

Reference

1. (a) Peng, X., Manna, L., Yang, W., Wickham, J., Scher, E., Kadavanich, A., Alivisatos, A.P., *Nature* **2000,** *404*, 59-61; (b) Peng, Z. A., Peng, X.G, *J. Am. Chem. Soc.* **2001,** *124*, 3343-3353; (c) Son, J. S., Park, K., Kwon, S.G., Yang, J., Choi, M.K., Kim, J., Yu, J.H., Hyeon, T., *Small* **2012,** *8* (15), 2394-2402; (d) Zhuang, Z., Lu, X., Peng, Q., Li, Y, *Chem. Eur. J.* **2011,** *17*, 10445-10452.

2. (a) Azpiroz, J. M., Matxain, J.M., Infante, I., Lopez, X., Ugalde, J., *Phys. Chem. Chem. Phys* **2013,** *15*, 10996-11005; (b) Kukreja, L. M., Rohlfing, A., Misra, P., Hillenkamp, F., Dreisewerd, K., *Appl. Phys. A* **2004,** *78*, 641-644.

3. (a) Kim, S. K., Song, K.D., Kempa, T.J., Day, R.W., Lieber, C.M., Park, H.G., *ACS Nano* **2014,** *7*, 3707-3714; (b) Kim, J. Y., Voznyy, O., Zhitomirsky, D., Sargent, E.H., *Adv. Mater.* **2013,** *25*, 4986-5010.

4. (a) Duan, X., Huang, Y., Agarwal, R., Lieber, C.M., *Nature* **2003,** *421*, 241-245; (b) Klembt, S., Seyfried, M., Aschenbrenner, T., Sebald, K., Gutowski, J., Hommel, D., Kruse, C., *Appl. Phys. Lett.* **2012,** *100*, 121102/1-121102/4.

5. (a) Wang, M., Fei, G., *Nanoscale Res. Lett.* **2009,** *4*, 1166-1170; (b) Vanmaekelbergh, D., Liljeroth, P., *Chem. Soc. Rev.* **2005,** *34*, 299-312; (c) Mohanan, J. L., Arachchige, I.U., Brock, S.L., *Science* **2005,** *307*, 397-400; (d) Luo, J., Ma, L., He, T., Ng, C.F., Wang, S., Shun, H., Fan, H.J., *J.Phys. Chem. C* **2012,** *116*, 11956-11963; (e) Cao, L., White, J.S., Park, J.S., Schuller, J.A., Clemens, B.M., Brongersma, M.I., *Nat. Mater.* **2009,** *8*, 643-647.

6. (a) Choi, H., Radich, J.G., Kamat, P.V., *J.Phys. Chem. C* **2013,** *118*, 206-213; (b) Choi, H., Kuno, M., Hartland, G.V., Kamat, P.V., *J. Mater. Chem. A* **2013,** *1*, 5487-5491.

7. Fan, Z., Razavi, H., Do, J., Moriwaki, A., Ergen, O., Chueh, Y.L., Leu, P.W., Ho, J.C., Takahashi, T., Reichertz, L.A., *Nat. Mater.* **2009,** *8*, 648-653.

8. Evans, C. M., Guo, L., Peterson, J.J., Maccagnano-Zacher, S., Krauss, T.D., *Nano Lett.* **2008,** *8*, 2898-2899.

9. (a) Kudera, S., Zanella, M., Giannini, C., Rizzo, A., Li, Y., Gigli, G., Cingolani, R., Ciccarella, G., Spahl, W., Parak, W.J., Manna, L., *Adv. Mater.* **2007,** *19*, 548-552; (b) Dukes III, A. D., McBride, J.R., Rosenthal, J.R., *Chem. Mater.* **2010,** *22*, 6402-6408.

10. Seifert, G., *Nat. Mater.* **2004,** *3*, 77-78.

11. Kratschmer, W., Lamb, L.D., Fostiropoulos, F., Huffman, D., *Nature* **1990,** *347*, 354-358.

12. Kasuya, A., Sivamohan, R., Barnakov, Y. A., Dmitruk, I. M., Nirasawa, T., Romanyuk, V. R., Kumar, V., Mamykin, S. V., Tohji, K., Jeyadevan, B., Shinoda, K., Kudo, T., Terasaki, O., Liu, Z., Belosludov, R. V., Sundararajan, V., Kawazoe, Y., *Nat. Mater.* **2004,** *3* (2), 99-102.

13. (a) Bowers, M. J., II McBride, J. R., Rosenthal, S. J., *J. Am. Chem. Soc.* **2005,** *127* (44), 15378-15379; (b) Riehle, F. S., Bienert, R., Thomann, R., Urban, G. A., Kruger, M., *Nano Lett.* **2009,** *9* (2), 514-518; (c) Cossairt, B. M., Owen, J. S., *Chem. Mater.* **2011,** *23* (12), 3114-3119; (d) Scholes, G. D., *Nat. Mater.* **2011,** *10* (12), 906-907.

14. Sengupta, S., Sarma, D.D., Acharya, S., *J. Mater. Chem.* **2011,** *21*, 11585-11591.

15. Cossairt, B. M., Owen, J.S., *Chem. Mater.* **2011,** *23*, 3114-3119.

16. Evans, C. M., Love, A.M., Weiss, E.A., *J. Am. Chem. Soc.* **2012,** *134*, 17298-17305.

17. Jiang, Z. J., Kelley, D.F., *ACS Nano* **2010,** *4*, 1561-1572.

18. Liu, Y. H., Wang, F. D., Wang, Y. Y., Gibbons, P. C., & Buhro, W. E., *J. Am. Chem. Soc.* **2011,** *133*, 17005-17013.

19. Liu, Y. H., Wayman, V.L., Gibbons, P.C., Loomis, R.A., Buhro, W. E., *Nano Lett.* **2010,** *10*, 352-357.

20. Ithurria, S., Tessier, M.D., Mahler, B., Lobo, R.P., Dubertret, B., Efros, A.L., *Nat. Mater.* **2011,** *10*, 936-941.

21. Huang, M. H., Cavallo, F., Liu, F., Lagally, M.G., *Nanoscale* **2011,** *3*, 96-120.

22. Ithurria, S., Dubertret, B., *J. Am. Chem. Soc.* **2008,** *130*, 16504-16505.

23. Chu, C. P., Arafin,S., Huang, G., Nie, T., Wang, K.L., Wang, Y., Zou, J., Qasim, S.M., BenSaleh, M.S., *J. Vac. Sci. Technol. B* **2014,** *32*, 02C111-1-02C111-7.

24. Roushan, M., Zhang, X., Li, J., *Angew. Chem., Int. Ed.* **2012,** *51*, 436-439.

25. Yu, J. H., Liu, X. Y., Kewon, K. E., Joo, J., Park, J., Ko, K. T., Lee, D. W., Shen, S. P., Tivakornsasithorn, K., Son, J. S., Park, J. H., Kim, Y. W., Hwang, G. S., Dobrowolska, M., Furdynal, J. K. & Hyeon, T., *Nat. Mater.* **2010,** *9*, 47-53.

26. Baca, A. J., Meitl, M.A., Ko, H.C., Mack, S., Kim. H.S., Dong, J., Ferreira, P.M., Rogers, J.A., *Adv. Mater.* **2007,** *17*, 3051-3062.

27. Pedetti, S., Nadal, B., Lhuillier, E., Mahler, B., Bouet, C., Abecassis, B., Xu, X., Dubertret, B., *Chem. Mater.* **2013,** *25*, 2455-2462.

28. Garnweitner, G., Niederberger, M., *J. Mater. Chem.* **2009,** *18*, 1171-1182.

29. Achermann, M., Petruska, M.A., Kos, S., Smith, D.L., Koleske, D.D., Klimov, V.I., *Nature* **2004,** *429*, 642-646.

30. Noda, Y., Maekawa, H., Kasuya, A., *Eur. Phys. J. D* **2010,** *57*, 43-47.

31. De Yoreo, J. J., Vekilov, P.G., *Rev. Mineral. Geochem.* **2003,** *54*, 57-93.

32. Schmelzer, J. W. P., *Nucleation Theory and Applications*. John Wiley & Sons: New York,

2006.

Chapter 1
Isolation of the magic-size CdSe nanoclusters [$(CdSe)_{13}$(*n*-octylamine)$_{13}$] and [$(CdSe)_{13}$(*n*-oleylamine)$_{13}$]

Introduction

The preparation, isolation, stoichiometric characterization, and dissolution of purified $(CdSe)_{13}$ nanoclusters are described in this chapter. In previous studies, we[18] and others[33] reported that $(CdSe)_{13}$ nanoclusters were intermediates in the synthesis of CdSe quantum-belts (nanoribbons). Now we demonstrate that a lamellar intermediate phase[18] collected from the quantum-belt synthesis is $[(CdSe)_{13}(n\text{-octylamine})_{13}]$, the smallest, discrete, magic-size nanocluster of CdSe that has been isolated.[34] Kinetic data show that free, soluble $[(CdSe)_{13}(\text{oleylamine})_{13}]$ nanoclusters are released from the insoluble $[(CdSe)_{13}(n\text{-octylamine})_{13}]$ upon ligand exchange.

Intense research activity has focused on the study of so-called "magic-size" nanoclusters (MSNCs) of the II-VI (12-16) semiconductors[13a, b, 13d, 35] since the initial report of $(CdSe)_{33}$ and $(CdSe)_{34}$ formation in 2004.[36] MSNCs are those clusters with ultra-small size, well-defined number of atoms and only stable in discrete-size. The synthetic efforts to date have generated only mixtures of magic-size CdSe nanoclusters,[37] and the isolation of a discrete, magic-size nanocluster has not been achieved prior to this report. We note that the carbon fullerene field expanded dramatically following the isolation of C_{60},[38] and propose that related advances for II-VI nanoclusters may now be possible. Access to purified $(CdSe)_{13}$ nanoclusters should enable experimental structure solution, chemical-reactivity studies, and detailed investigations of physical and spectroscopic properties.

Nanoclusters of $(CdSe)_{13}$ are generated by reaction of cadmium acetate dihydrate, $[Cd(OAc)_2(H_2O)_2]$, with selenourea $[H_2NC(Se)NH_2]$ in *n*-octylamine solvent at room temperature. We and others have recently shown that combination of CdX_2 compounds (X

= halide,[18, 39] OAc[18]) with *n*-octylamine results in the spontaneous formation of lamellar mesophases consisting of CdX_2 layers separated by *n*-octylamine bilayers. Addition of selenourea generates a mixture of CdSe nanoclusters that converts completely to $(CdSe)_{13}$ within 2-5 h, as indicated by spectroscopic monitoring.[18] On the same time scale, a white precipitate is deposited, which we now show to be [$(CdSe)_{13}$(*n*-octylamine)$_{13}$].

Results and Discussion

CdSe nanoclusters were synthesized in *n*-octylamine solution. The cadmium precursor $Cd(OAc)_2(H_2O)_2$ was dissolved in *n*-octylamine at 70 ℃, and the then solution cooled to room temperature. Selenourea was dissolved in an appropriate amount of *n*-octylamine at room temperature. After mixing the cadmium precursor with the selenium precursor at room temperature with stirring, a greenish-yellow mixture of different size nanoclusters were generated in 5 min, in which $(CdSe)_{13}$, $(CdSe)_{19}$, $(CdSe)_{33}$, $(CdSe)_{34}$ were included. (Figure 1-1) The CdSe nanocluster mixture gradually converted to $(CdSe)_{13}$ in 20 h with the color changing from greenish-yellow to white, and with the relative absorption intensity of $(CdSe)_{13}$ to other nanoclusters increasing. Our interpretation of this result was that larger size nanoclusters under these conditions eventually converted to $(CdSe)_{13}$ (Figure 1-1, red curve). A white precipitate was deposited from the reaction mixture.

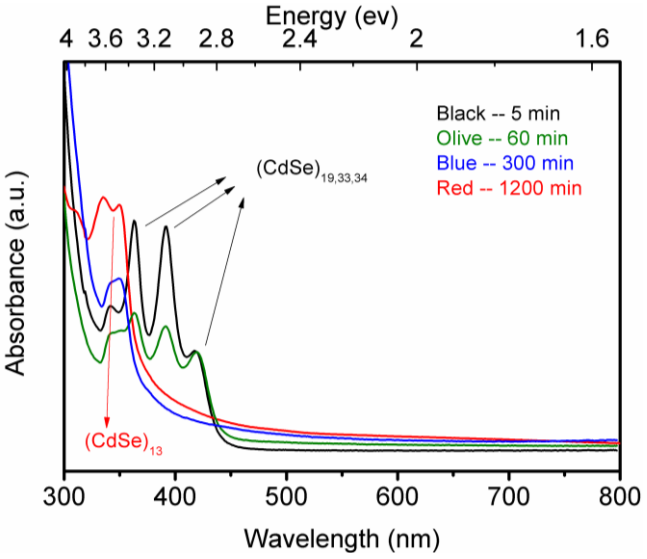

Figure 1-1 UV-visible spectral evolution upon transformation from mixture to $(CdSe)_{13}$. UV-visible extinction of CdSe nanoclusters after Se precursor injection 5 min (Black curve), 60 min (green curve), 300 min (blue curve) and 1200 min (red curve).

We previously demonstrated that the white precipitate contained bundles of lamellae (or layers) in which the $(CdSe)_{13}$ nanoclusters were entrained (Figure 1-2a).[18] The UV-visible spectrum of the material suspended in toluene (Figure 1-3a) exhibited the three expected absorbances at 312, 335, and 350 nm, closely matching the spectrum calculated theoretically for $(CdSe)_{13}$.[40] Note the significant scattering tail to longer wavelengths due to the large size of the $(CdSe)_{13}$ bundles. We also previously showed that individual layers or sheets could be exfoliated from the bundles by sonication in the presence of oleylamine (Figure 1-2b).[18] Figure 1-3a includes the UV-visible spectrum of the exfoliated sheets dispersed in toluene. The scattering tail was absent, indicating a reduction in the dimensions of the suspended particles. Significantly, absorptions at 363, 389 nm, and 413 nm, assigned to $(CdSe)_{19}$, $(CdSe)_{33}$, and $(CdSe)_{34}$, respectively,[18, 40] were also absent, establishing the spectroscopic purity of the $(CdSe)_{13}$ obtained by the synthetic procedure.

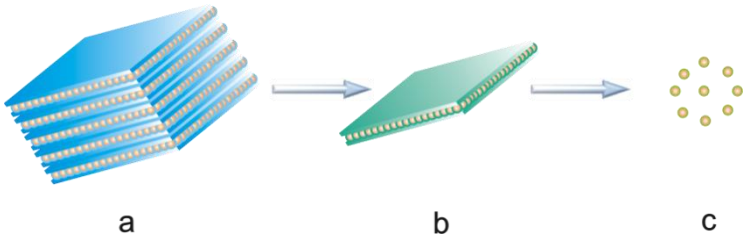

Figure 1-2 Disassembly of nanocluster-amine-bilayer aggregates. a, Bundled nanocluster-amine-bilayer aggregates from the templated synthesis of bundled [$(CdSe)_{13}$(*n*-octylamine)$_{13}$].[1] b, Exfoliation of colloidal sheets of aggregated nanoclusters. c, Release of freely soluble [$(CdSe)_{13}$(oleylamine)$_{13}$] nanoclusters by ligand exchange. The blue features represent *n*-octylamine self-assembled monolayers (a), the blue-green features the mixed-ligand *n*-octylamine-oleylamine monolayers (b), the green features theoleylamine ligand shells (c), and the orange features the $(CdSe)_{13}$ nanoclusters.

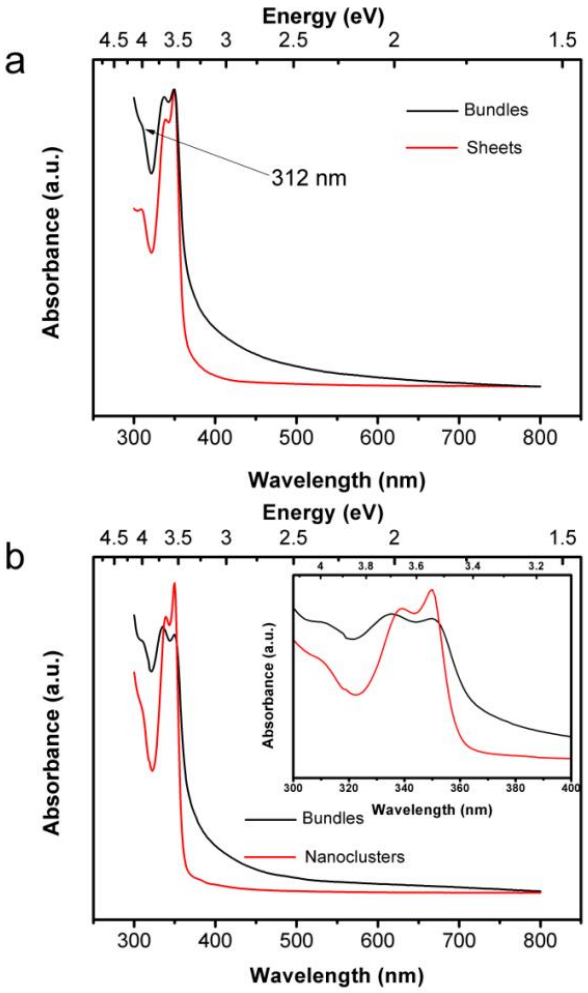

Figure 1-3 UV-visible spectra of $(CdSe)_{13}$. a, Spectra from bundles (black) and exfoliated sheets (red). b, Spectra from bundles and free nanoclusters. Inset: spectral expansion to show the small spectral shift between [$(CdSe)_{13}$(*n*-octylamine)$_{13}$] bundles (black) and free [$(CdSe)_{13}$(oleylamine)$_{13}$] nanoclusters (red).

Elemental analyses and the IR spectrum of the isolated bundles (white precipitate) established the empirical formula to be [(CdSe)(*n*-octylamine)]. Rutherford backscattering spectrometry found a Cd:Se ratio of 1.05:0.95. The C, H, N analyses were consistent with a CdSe:*n*-octylamine ratio of 1:1. The IR spectrum of the white precipitate showed no residual acetate or water absorptions (Figure 1-4). The results were consistent with a theoretical model that shows amine binding to each Cd atom in the nanocluster.[41]

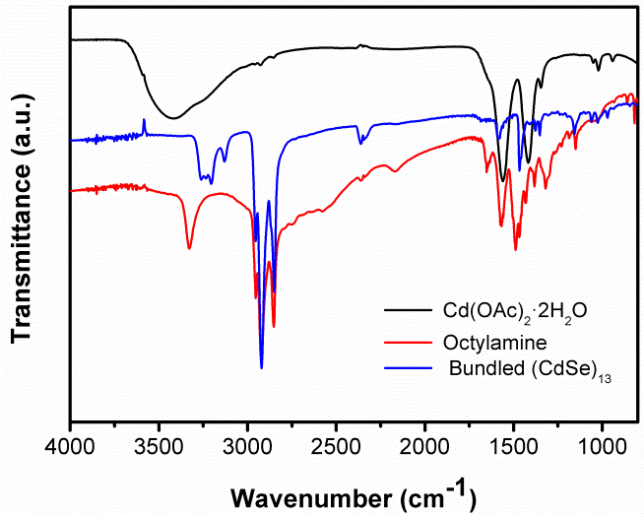

Figure 1-4. IR spectra from KBr pellets of the starting material $Cd(OAc)_2{\cdot}2H_2O$ (black curve), the solvent *n*-octylamine (red curve), and the bundled $[(CdSe)_{13}(n\text{-octylamine})_{13}]$ (blue curve).

The $(CdSe)_{13}$ stoichiometry of the nanoclusters was determined by laser-desorption-ionization (LDI) mass spectrometry (Figure 1-5). Detailed parameters are listed in Table 1-1. The base peak in the spectrum appeared at *m*/*z* 2488.57, matching the theoretical mass of $(CdSe)_{13}$. The results indicated that the *n*-octylamine ligands were detached by the LDI excitation. Small, higher-mass peaks also appeared at 3638.12, 6318.03, and 6507.51 corresponding to $(CdSe)_{19}$, $(CdSe)_{33}$, and $(CdSe)_{34}$, respectively. However, LDI delivers significant energy to a sample, and we assert that the small quantities of $(CdSe)_{19}$, $(CdSe)_{33}$, and $(CdSe)_{34}$ observed in the mass spectrum resulted from thermal

heating and subsequent growth of $(CdSe)_{13}$. As noted above and shown in Figure 1-3a, the absorption features of these larger nanoclusters were not detected in the UV-visible spectra of the bundled or exfoliated $(CdSe)_{13}$-containing material. We note that the spectrum in Figure 1-4 contrasts markedly from those published previously for mixtures of magic-sized CdSe nanoclusters[8] in that the peak for $(CdSe)_{13}$ is by far the predominant one; those for $(CdSe)_{19}$, $(CdSe)_{33}$, and $(CdSe)_{34}$ are very weak by comparison.

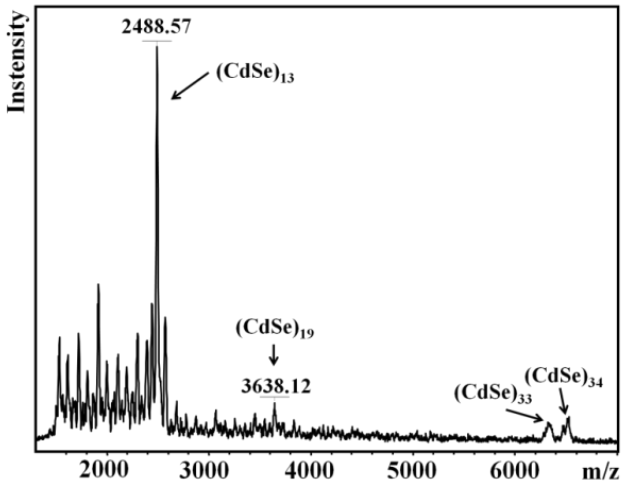

Figure 1-5 LDI mass spectrum of [$(CdSe)_{13}$(*n*-octylamine)$_{13}$] bundles. Various $(CdSe)_n$ nanocluster features are labeled.

Table 1-1. Parameters used in the LDI MS experiments.

Delay	57312 ns	Laser Attenuation	55
PIE delay	120 ns	Laser RepRate	1000 Hz
Electronic Gain	100 mV/fullscale	IS voltage 1	25 kV
SampleRate	0.25ns (4 GHz)	IS voltage 2	22.5 kV
Polarity	Positive	Lens voltage	7.75 kV
URefDet	2.367 kV	Reflector voltage 1	26.45 kV
# Shots	20000	Reflector voltage 2	13.4 kV

An expansion around the base peak at *m/z* 2488.57 (Figure 1-6a) revealed the isotopic distribution in the $(CdSe)_{13}$ nanoclusters, which was compared to the simulated isotopic distribution for $(CdSe)_{13}$ (Figure 1-6b). The two patterns match closely, further confirming the $(CdSe)_{13}$ stoichiometry of the nanoclusters. The combination of the UV-visible spectrum matching the theoretical prediction for $(CdSe)_{13}$,[40] the elemental analyses confirming the empirical formula [(CdSe)(*n*-octylamine)], and the LDI mass spectrum dominated by $(CdSe)_{13}$ establishes the white precipitate obtained from the synthesis to have the molecular formula $[(CdSe)_{13}(n\text{-octylamine})_{13}]$. The structures of $(CdSe)_{13}$ or $[(CdSe)_{13}(n\text{-alkylamine})_{13}]$ have not been experimentally determined. However, theoretical studies have found that $[(CdSe)_x(NH_3)_x]$ nanoclusters exhibit cage-like structures with one NH_3 ligand bound to each Cd atom.[41]

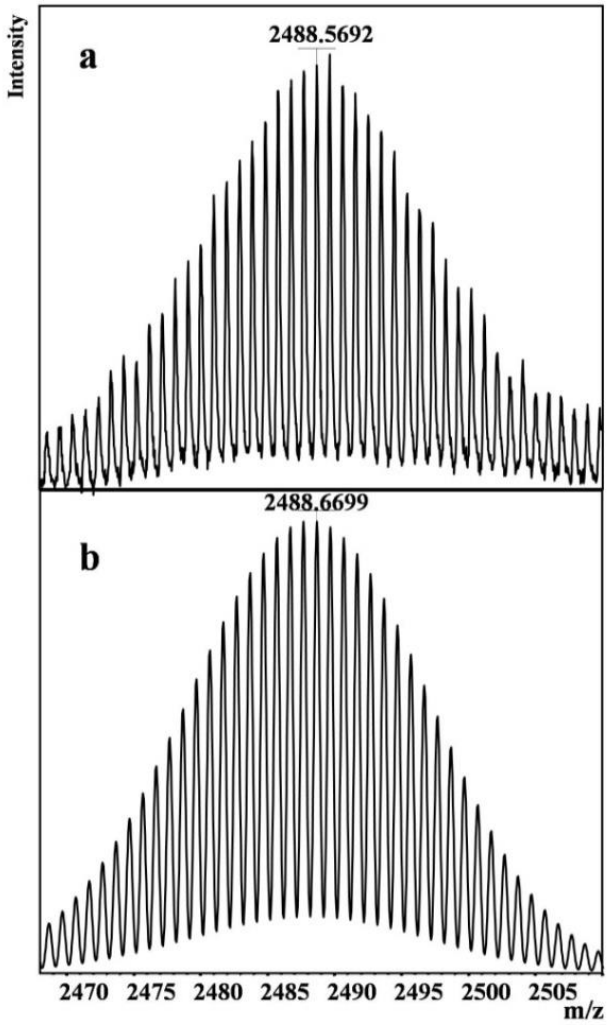

Figure 1-6 Isotope-distribution pattern from the mass spectrum of $(CdSe)_{13}$. a, Experimental data obtained by expansion of the spectrum in Figure 1-4. b, pattern simulated using natural isotopic abundances.

The sonication of mixtures of [$(CdSe)_{13}$(*n*-octylamine)$_{13}$] in toluene with an excess of oleylamine (oleylamine:$(CdSe)_{13}$ ≅ 20:1) resulted in the dissolution of [$(CdSe)_{13}$(*n*-octylamine)$_{13}$] and the release of free [$(CdSe)_{13}$(oleylamine)$_{13}$] nanoclusters into solution (Figure 1-2c and Scheme 1-1). As described above, sonication of [$(CdSe)_{13}$(*n*-octylamine)$_{13}$] bundles (Figure 1-7a, b) in oleylamine-toluene mixtures initially exfoliated nanosheets of [$(CdSe)_{13}$(*n*-octylamine)$_x$(oleylamine)$_{13-x}$] (Figure 1-7c, d), in which some ligand exchange was presumed to have occurred (Figure 1-2b).[13] Extended sonication

resulted in the destruction of the sheet structures (Figure 1-7e, f), whereas the $(CdSe)_{13}$ nanoclusters remained intact, as evidenced by the retention of their characteristic absorption features (Figure 1-3b). Free nanoclusters which were characterized as $[(CdSe)_{13}(oleylamine)_{13}]$ were released from the template gradually. The increasing intensity of the $(CdSe)_{13}$ absorption at 335, and 350 nm indicated that more and more free nanoclusters were dissolved in solution upon sonication. (Figure 1-8) During this procedure, the initially cloudy suspension was converted into a clear solution (Figure 1-9). The free $[(CdSe)_{13}(oleylamine)_{13}]$ nanoclusters could be remained dissolved and stable in toluene/oleylamine solution for at least overnight. Figure 1-10 indicated that $(CdSe)_{13}$ nanoclusters remained intact and no self-assembling occurred since no new peaks or scattering tail emerged.

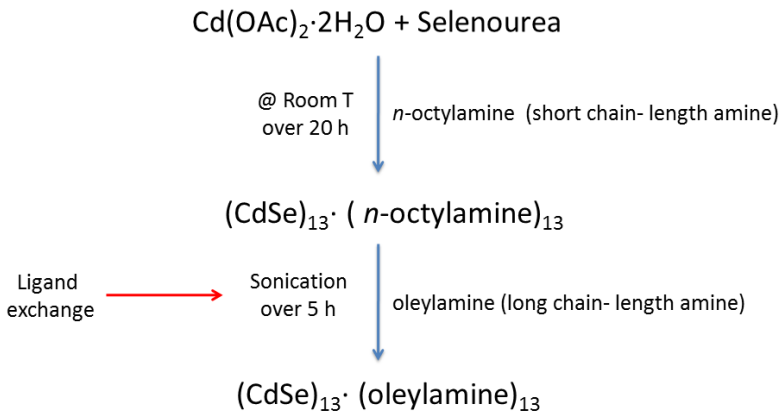

Scheme 1-1. Indirect pathway of forming $[(CdSe)_{13}(oleylamine)_{13}]$ nanoclusters.

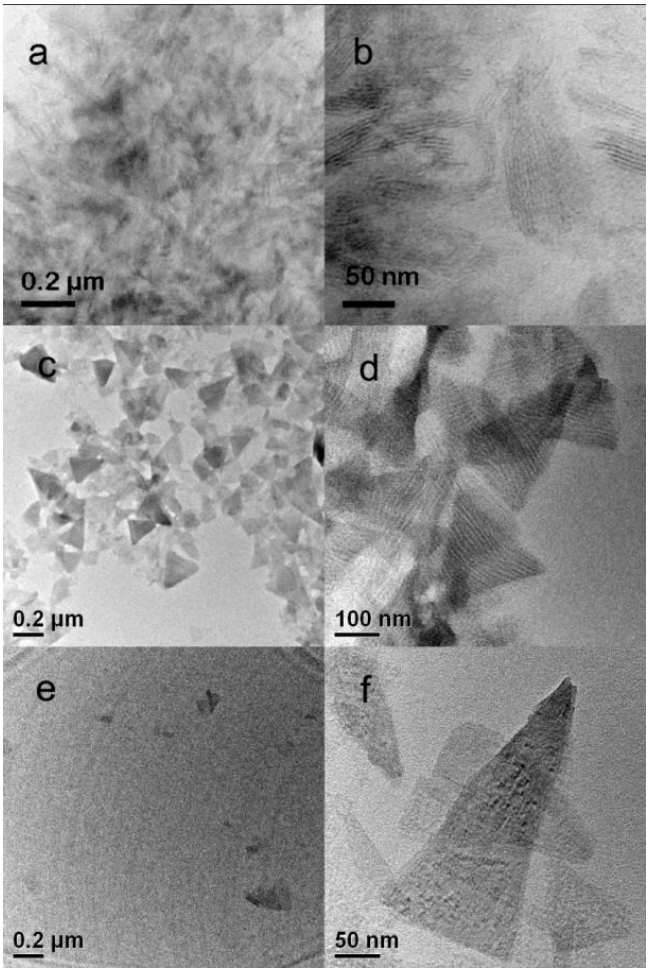

Figure 1-7 TEM images of $(CdSe)_{13}$ in its various forms. a, b, Bundled $[(CdSe)_{13}(n\text{-octylamine})_{13}]$; note the lamellar features evident in b. c, d, Exfoliated $[(CdSe)_{13}(n\text{-octylamine})_x(\text{oleylamine})_{13-x}]$ sheets; note the striped domain pattern in d.[1] e, f, Residual sheets after ligand exchange and release of freely soluble $[(CdSe)_{13}(\text{oleylamine})_{13}]$; note the lack of striped domains in f.

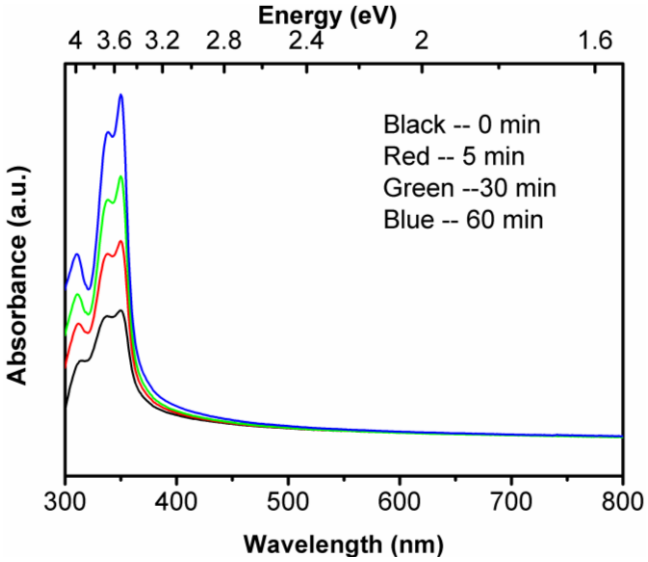

Figure 1-8 UV-visible spectra of $(CdSe)_{13}$ nanoclusters released from template. As-made bundled $(CdSe)_{13}$ nanoclusters (black curve), $(CdSe)_{13}$ nanoclusters after sonicaiotn in oleylamine-toluene solution for 5 min (red curve), 30 min (green curve) and 60 min (blue curve).

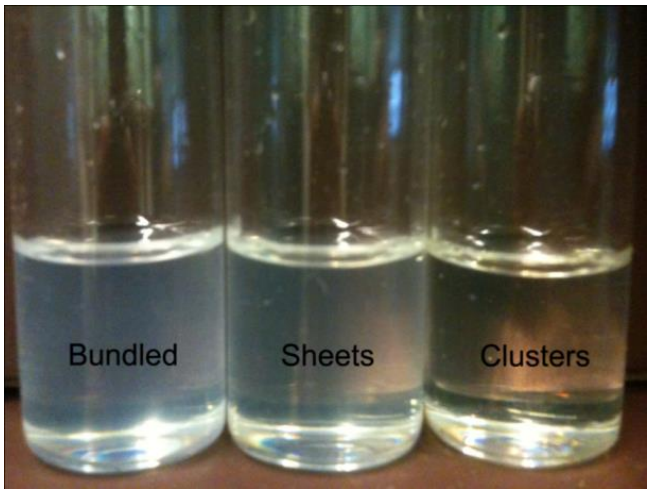

Figure 1-9 A photograph of a dispersion of bundled $[(CdSe)_{13}(n\text{-octylamine})_{13}]$ (left), a dispersion of $[(CdSe)_{13}(n\text{-octylamine})_x(oleylamine)_{13-x}]$ sheets (center), and a solution of $[(CdSe)_{13}(oleylamine)_{13}]$ nanoclusters.

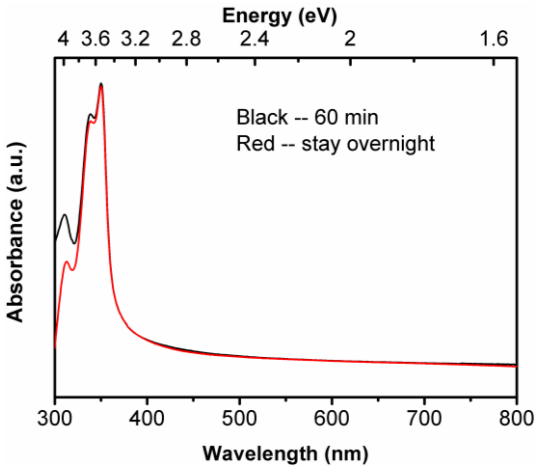

Figure 1-10 UV-visible spectra of $(CdSe)_{13}$ nanoclusters after sonication in oleylamine-toluene solution for 60 min (black curve) and after standing overnight after sonication (red curve).

The inset in Figure 1-3b is a spectral expansion in the region of the $(CdSe)_{13}$ absorbances, showing a slight shift of the 335-nm feature to 339 nm as a result of the ligand exchange. The $[(CdSe)_{13}(oleylamine)_{13}]$ stoichiometry was confirmed by elemental analysis. $[(CdSe)_{13}(oleylamine)_{13}]$ was also prepared directly from cadmium acetate dihydrate and selenourea in oleylamine (Scheme 1-2, Figure 1-11 and see the Experimental section). Consequently, sonication and ligand exchange afforded a means of solubilizing the $(CdSe)_{13}$ nanoclusters.

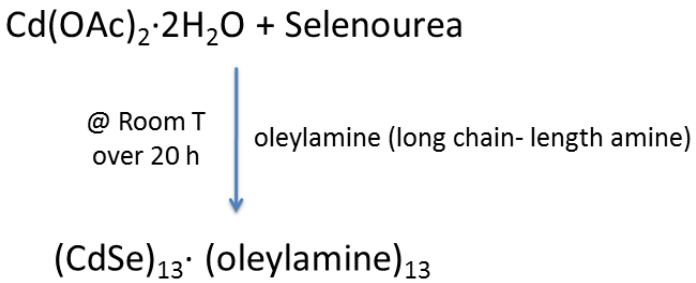

Scheme 1-2. Direct pathway of forming $[(CdSe)_{13}(oleylamine)_{13}]$ nanoclusters.

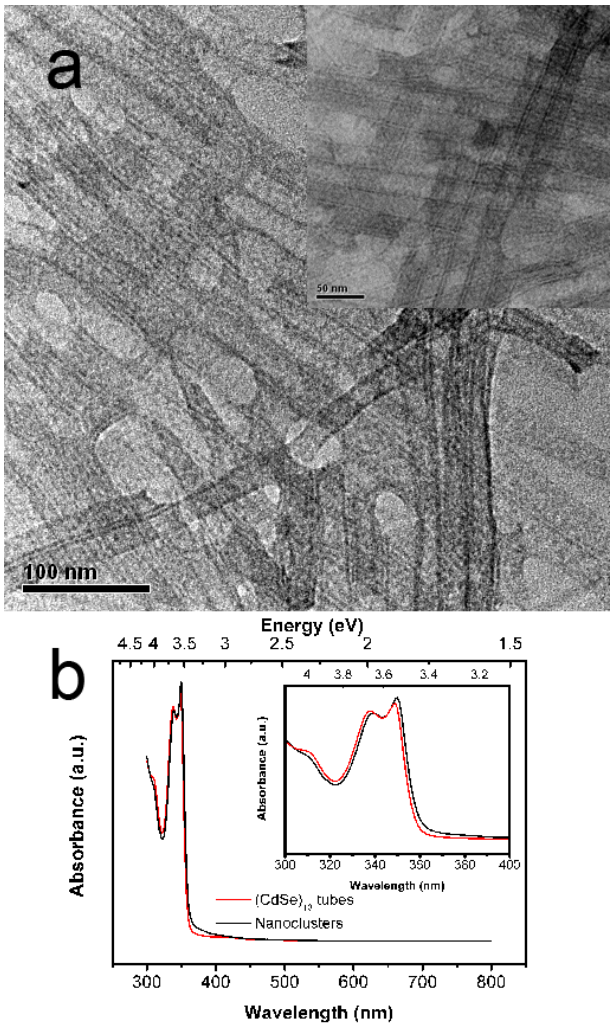

Figure 1-11. TEM images and UV-visible spectra of [$(CdSe)_{13}$(oleylamine)$_{13}$] nanoclusters. (a) TEM images at two magnifications of [$(CdSe)_{13}$(oleylamine)$_{13}$] obtained from the direct synthesis in oleylamine solvent. (b) Spectral comparison of [$(CdSe)_{13}$(oleylamine)$_{13}$] obtained from the direct synthesis (red curves) and by ligand exchange from [$(CdSe)_{13}$(*n*-octylamine)$_{13}$] (black curves).

We sought further confirmation of the formation of free, soluble [$(CdSe)_{13}$(oleylamine)$_{13}$] nanoclusters from nanocluster-growth kinetics. The [$(CdSe)_{13}$] bundles, sheets, and free nanoclusters were stable at room temperature in the solid state, in dispersion, or in solution for at least 6 months. However, addition of MeOH to dispersions of bundled [$(CdSe)_{13}$(*n*-octylamine)$_{13}$] (Figure 1-2a and Figure 1-12a), partially ligand-exchanged [$(CdSe)_{13}$(*n*-octylamine)$_x$(oleylamine)$_{13-x}$] nanosheets (Figure 1-2b and Figure 1-12b), and free [$(CdSe)_{13}$(oleylamine)$_{13}$] nanoclusters (Figure 1-2c) resulted in destroying the

lamellar-bilayer-template structures (Figure 1-12c, d) and the loss of the characteristic UV-visible absorptions at 335 and 350 nm with the appearance of a broad envelope of features to longer wavelength (Figure 1-13 and Figure 1-14), consistent with indiscriminate growth of the $(CdSe)_{13}$ nanoclusters. Presumably, substitution of the small ligand MeOH for *n*-octylamine reduced the steric protection of the nanoclusters, allowing their coalescence and growth.

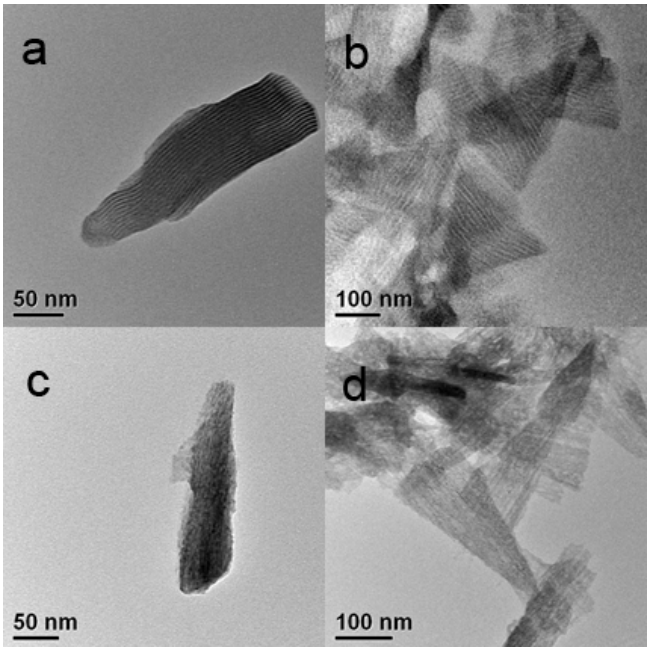

Figure 1-12. TEM images of bundled and sheet-like $(CdSe)_{13}$ before (a,b) and after (c,d) adding MeOH additive.

The growth process was monitored by UV-visible spectrometry (Figure 1-13). After addition of an appropriate amount of MeOH, the intensity of $(CdSe)_{13}$ characteristic peaks at 335 and 350 nm decreased in all cases (Figure 1-13a, b, c) along with the increased of new broad peaks at longer wavelength. This result indicated that $(CdSe)_{13}$ nanoclusters, inside or outside the template, were vulnerable to the polar solvent, and began to form larger size clusters in the presence of MeOH. However, the growth rates were different in each case. In figure 1-13a, the relative intensity of $(CdSe)_{13}$ to larger size clusters decreased slowest,

even after 390 min, only a very small amount of large-size nanoclusters could be observed in the spectrum. For free nanoclusters, the concentration of $(CdSe)_{13}$ decreased dramatically right after adding MeOH, and the growth rate was fastest. (Figure 1-13c) The growth rate of those nanoclusters entrained in sheets structure was in between. These results indicated that $(CdSe)_{13}$ nanoclusters were most stable in the bundled template and became vulnerable once template was destroyed.

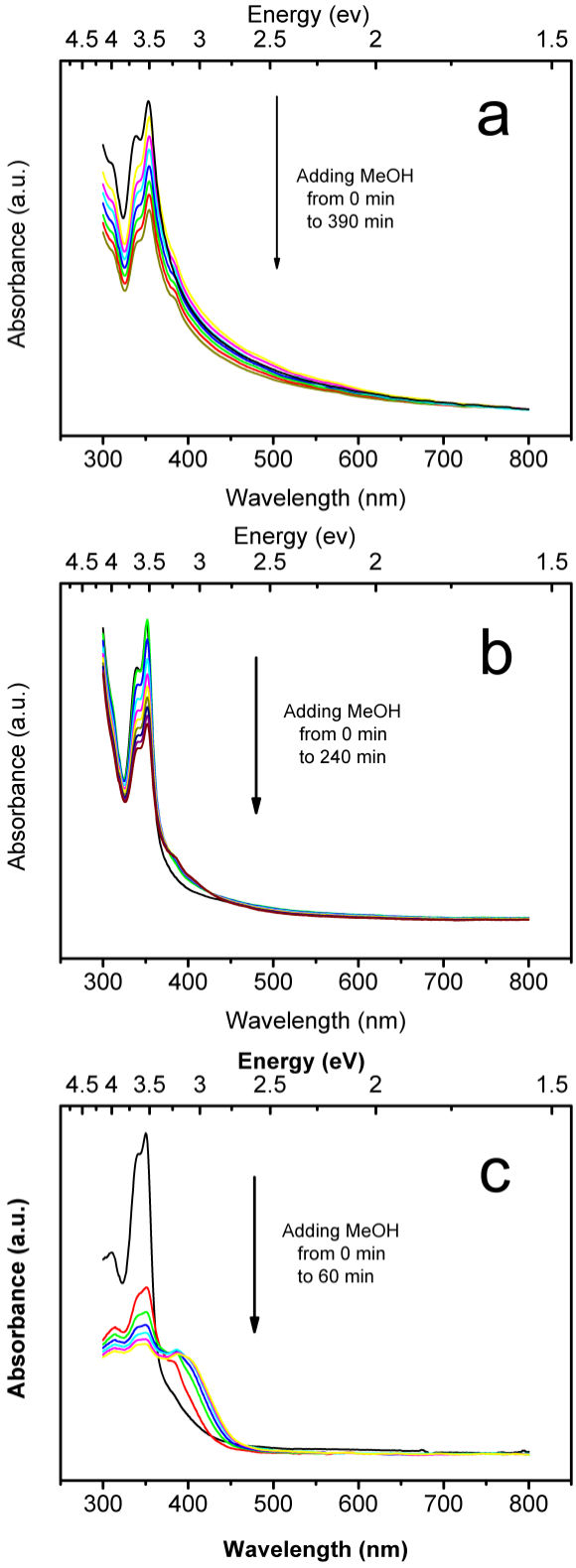

Figure 1-13 UV-visible spectral changes occurring during nanoclusters growth after adding MeOH in (a) bundled clusters, (b) sheets-like clusters, and (c) free clusters.

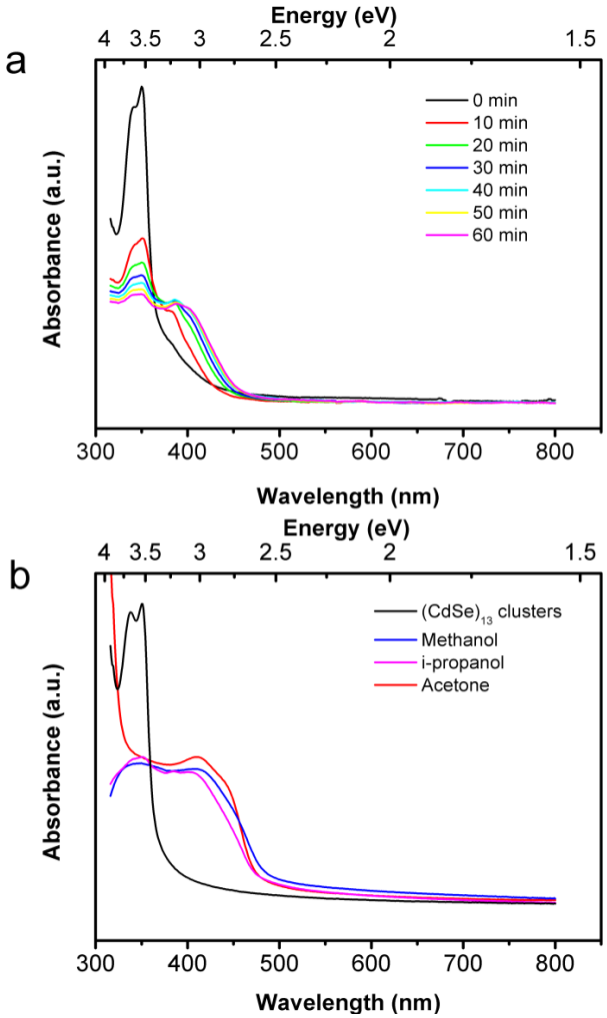

Figure 1-14 UV-visible spectral changes occurring during nanocluster growth. (a) Spectra as a function of time after addition of MeOH. (b) A spectrum of the starting $[(CdSe)_{13}(oleylamine)_{13}]$ nanoclusters (black) and those at the conclusion of nanocluster growth induced by MeOH (blue), *i*-propanol (magenta), and acetone (red).

We reasoned that the steric protection of the $(CdSe)_{13}$ nanoclusters should be greatest in the $(CdSe)_{13}$ bundles and sheets (Figure 1-2a, b), and least in the free nanoclusters (Figure 1-2c). Consequently, the MeOH-induced growth kinetics should distinguish aggregated and free nanoclusters. The growth rate was expected to be significantly faster for the free nanoclusters, and thus a faster experimentally determined growth rate would provide strong secondary verification for the release of free, soluble nanoclusters from the bundled and sheet materials.

The MeOH-induced growth of $(CdSe)_{13}$ was monitored by the decreasing absorbance of the UV-visible feature at 350 nm in the presence of a large excess of MeOH (Figure 1-14a). The disappearance of bundled [$(CdSe)_{13}$(*n*-octylamine)$_{13}$] followed pseudo-first-order kinetics over four half-lives (k_{obs} = 1.64 $\times 10^{-3} \pm 0.12 \times 10^{-3}$ s^{-1}, $t_{1/2}$ = 423 $\pm$ 31 s, Figure 1-15. Similarly, the disappearance of [$(CdSe)_{13}$(*n*-octylamine)$_{13}$] in the sheet structures followed pseudo-first-order kinetics with an identical rate constant within error (k_{obs} = 1.61 $\times 10^{-3} \pm 0.02 \times 10^{-3}$ s^{-1}, $t_{1/2}$ = 430 $\pm$ 5 s, Figure 1-15). In contrast, the kinetic data for the disappearance of free [$(CdSe)_{13}$(oleylamine)$_{13}$] contained two pseudo-first-order regimes. The initial, fast regime corresponded to k_{obs} = 8.35 $\times 10^{-3} \pm 0.20 \times 10^{-3}$ s^{-1} ($t_{1/2}$ = 83.0 $\pm$ 2 s, Figure 1-15), which is 5$\times$ faster than the growth rates of $(CdSe)_{13}$ in the bundles and sheets. The second, slow regime corresponded to k_{obs} = 1.68 $\times 10^{-3} \pm 0.03 \times 10^{-3}$ s^{-1} ($t_{1/2}$ = 413 $\pm$ 7 s, Figure 1-15), indicative of the residual sheet-like structures in the specimen (Figure 1-7e). Because the initial, fast regime persisted over 3 decades in concentration, we estimate the quantity of residual, aggregated $(CdSe)_{13}$ to be $\leq$ 0.1%. Thus, the kinetic results strongly supported the liberation of free, soluble [$(CdSe)_{13}$(oleylamine)$_{13}$] nanoclusters from the aggregated bundles and sheets.

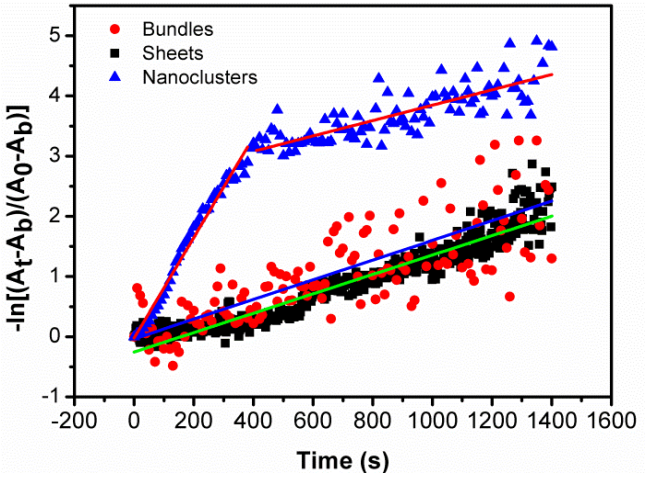

Figure 1-15 Kinetic data from the MeOH-induced growth of $(CdSe)_{13}$. The pseudo-first-order plots were constructed by monitoring the $(CdSe)_{13}$ absorbance at 350 nm, where A_t is the absorbance at time t, A_0 is the absorbance at t = 0 s, and A_b is the background absorbance measured at t = 1800 s. The slopes were extracted by linear least-squares fitting. The red circles and blue line correspond to bundled $[(CdSe)_{13}(n\text{-octylamine})_{13}]$; the black squares and green line to exfoliated $[(CdSe)_{13}(n\text{-octylamine})_x(oleylamine)_{13-x}]$ sheets; and the blue triangles and red lines to free $[(CdSe)_{13}(oleylamine)_{13}]$ nanoclusters.

Addition of *i*-propanol or acetone also induced the growth of $[(CdSe)_{13}(oleylamine)_{13}]$. Kinetic data collected under pseudo-first-order conditions as a function of additive concentration established that the growth processes were first-order in additive, for MeOH (Figure 1-16), *i*-propanol (Figure 1-17), and acetone (Figure 1-18). Assuming that growth is triggered by the substitution of the smaller additive ligands for oleylamine ligands, the first-order nature of the kinetics in additive suggests that the first ligand substitution is rate determining. Apparently, loss of the first oleylamine ligand compromises the steric protection of the nanocluster ligand shell, promoting rapid substitution of the remaining oleylamine ligands, and subsequently allowing coalescence and growth of the $(CdSe)_{13}$ nanoclusters.

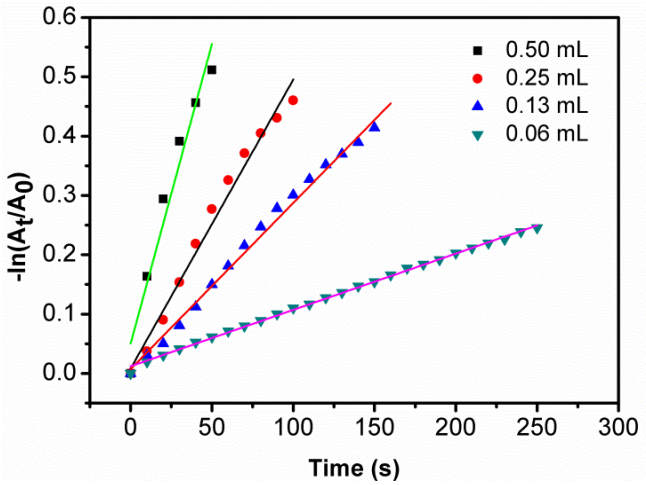

Figure 1-16 Initial $[(CdSe)_{13}(oleylamine)_{13}]$ nanocluster growth rates as a function of the amount of added MeOH. The slopes are 1.01×10^{-2} s^{-1} (green line, black points), 4.87×10^{-3} s^{-1} (black line, red points), 2.80×10^{-3} s^{-1} (red line, blue points), and 9.50×10^{-4} s^{-1} (magenta line, cyan points).

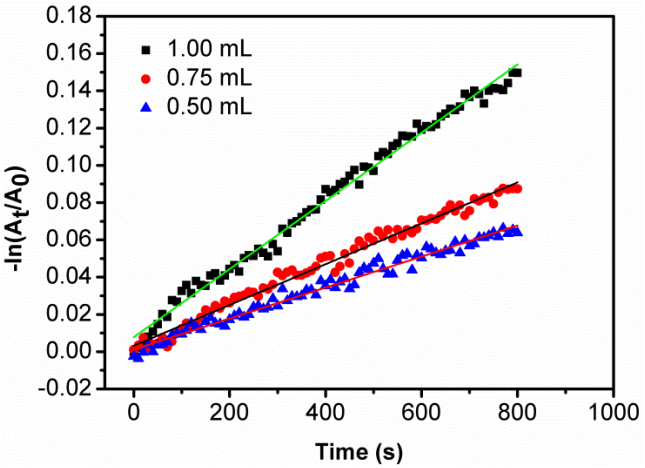

Figure 1-17 Initial $[(CdSe)_{13}(oleylamine)_{13}]$ nanocluster growth rates as a function of the amount of added *i*-propanol. The slopes are 1.83×10^{-4} s^{-1} (green line, black points), 1.09×10^{-4} s^{-1} (black line, red points), and 8.32×10^{-5} s^{-1} (red line, blue points).

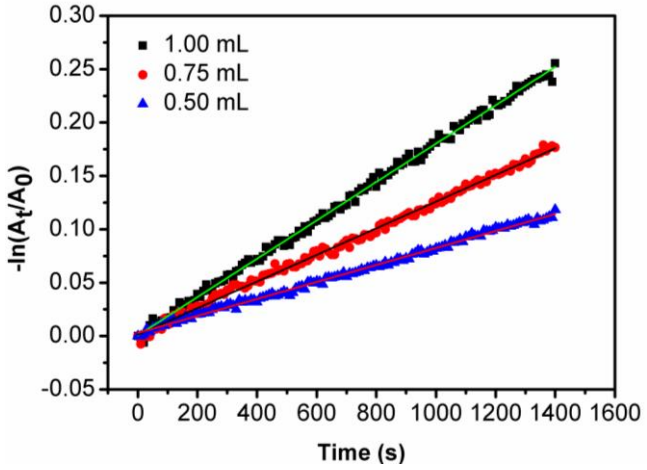

Figure 1-18 Initial [$(CdSe)_{13}$(oleylamine)$_{13}$] nanocluster growth rates as a function of the amount of added acetone. The slopes are 1.80×10^{-4} s^{-1} (green line, black points), 1.25×10^{-4} s^{-1} (black line, red points), and 7.96×10^{-5} s^{-1} (red line, blue points).

Conclusions

That the syntheses reported here provide $(CdSe)_{13}$, exclusive of nanoclusters of other sizes, is surprising. However, spectroscopic monitoring established the initial formation of mixtures of $(CdSe)_{13}$, $(CdSe)_{19}$, $(CdSe)_{33}$, and $(CdSe)_{34}$, which ultimately equilibrate to $(CdSe)_{13}$.[1] The results strongly suggest that $(CdSe)_{13}$ is the most thermodynamically stable nanocluster within the amine-bilayer template (Figure 1-1a)[1] in which it forms. The results further suggest that subsequent liberation by oleylamine-ligand exchange produces sterically protected, free $(CdSe)_{13}$ nanoclusters that are kinetically stabilized. After the steric protection is compromised by small-ligand substitution with MeOH, *i*-propanol, or acetone, the nanoclusters prefer to grow to larger sizes, which are more stable outside of the synthetic template. In summary, discrete, magic-size $(CdSe)_{13}$ nanoclusters have been prepared and isolated, and are thus now available for further studies.

Experimental Section

Materials. *n*-Octylamine (*n*-OA) was obtained from Aldrich (+99%) and Alfa Aesar (99%), selenourea (99.9%, metal basis) from Alpha Aesar, $Cd(OAc)_2 \cdot 2H_2O$ from Aldrich, trioctylphosphine (TOP) from Sigma-Aldrich (97%), and oleylamine (or cis-9-octadecenylamine) from TCI (> 40.0% by GC) and Sigma-Aldrich (technical grade, 70%). All were used as received, and stored under N_2. Toluene from Sigma-Aldrich (CHROMASOLV®, for HPLC, ≥ 99.9%) was purged with dry N_2 for at least 1 h and stored under N_2 prior to use.

Analyses. Elemental analyses (C, H, N) were obtained from Galbraith Laboratories, Inc. (Knoxville, TN). The analysis by Rutherford backscattering spectrometry was provided by the Characterization Facility at the University of Minnesota (Minneapolis, MN). UV-visible spectra were obtained from a Perkin Elmer Lambda 950 UV/Vis spectrometer. IR spectra were obtained from a Perkin Elmer Spectrum BX FT-IR System. The LDI mass spectra were recorded on a BrukerultrafleXtreme MALDI-TOF/TOF mass spectrometer. No matrix was employed in these mass-spectral analyses.

Synthesis of $[(CdSe)_{13}(n\text{-octylamine})_{13}]$.[1] All synthetic procedures were conducted under dry N_2. Cadmium acetate dihydrate [$Cd(OAc)_2 \cdot 2H_2O$] (65 mg, 0.24mmol) was dissolved in *n*-octylamine (*n*-OA, 5.6g, 0.043mol) in a septum-capped Schlenktube and heated in a70- ℃ oil bath for 1h. Selenourea (52 mg, 0.42mmol) was dissolved in *n*-OA (1.2 g, 0.0093mol) in the glove box, and then sonicated in a bench-top sonicator for dissolution.

The selenourea solution was injected into the $Cd(OAc)_2$ solution at room temperature (20-25 ^oC) without stirring. During the first hour, the reaction mixture underwent a change from colorless (0 min) to a cloudy greenish-yellow. Some brown precipitate also formed.

After another 5-20 h under ambient conditions, a white precipitate formed under a light-red supernatant.

The reaction mixture was subsequently heated at 70^{o}C in an oil bath for 1h. During this time, the solution turned dark red and a small amount of black or gray precipitate was mixed in with the white precipitate. The black solid and red solution were the byproduct elemental selenium, which was subsequently converted to TOP=Se by addition of TOP. TOP (0.5-1.0 mL) was injected into the reaction mixture, whereupon the red supernatant quickly turned clear and colorless, and the remaining precipitate was white.

The white precipitate was centrifuged in a bench-top centrifuge (700 *g*) for 5 min, and the supernatant was discarded. The white slush so obtained was washed with a TOP solution (10 mL, 5-10 % w/w in toluene). This purification process was repeated 5-6 times using a TOP-toluene solution. (To ensure removal of the last traces of TOP, pure toluene can be used in the last few purification cycles; however, the resulting product is less thermally stable toward nanocluster growth.) The residual solvent was removed in vacuo, leaving [$(CdSe)_{13}$(*n*-octylamine)$_{13}$] as a white slushy solid (75 mg, 0.018 mmol, 95.9%). Anal.Calcd for [$(CdSe)_{13}$(*n*-octylamine)$_{13}$]: C, 29.97; H, 5.97; N, 4.37. Found, C, 30.89; H, 5.84; N, 4.57. All values are given as percentages. UV-vis (toluene) λ_{max}, nm (logε): 312 (3.35), 335 (4.28), 350 (4.27).

The purification procedure in the paragraph above can be applied to the white precipitate before or after the heating step. To optimize the stability of [$(CdSe)_{13}$(*n*-octylamine)$_{13}$], we typically store the [$(CdSe)_{13}$(*n*-octylamine)$_{13}$], TOP, toluene mixture obtained just prior to purification, and purify aliquots of this mixture as needed.

Dissolution of $[(CdSe)_{13}(oleylamine)_{13}]$. This procedure was conducted under an ambient, air atmosphere. An aliquot(ca. 0.02 mL, 5.09×10^{-5}mmol of $[(CdSe)_{13}(n\text{-octylamine})_{13}]$) from the as-made $[(CdSe)_{13}(n\text{-octylamine})_{13}]$, TOP, toluene mixture was diluted into toluene (3 mL) in a small vial, to which oleylamine (0.5 mL, 1.06×10^{-3}mmol)was added. The mixture was sonicated for at least 5 h at room temperature. The resulting clear, colorless dispersion was free $[(CdSe)_{13}(oleylamine)_{13}]$, which was used directly for further analyses. (See Scheme1-1) UV-vis (toluene) λ_{max}, nm: 312, 339, 350.

Isolation of $[(CdSe)_{13}(oleylamine)_{13}]$ from ligand exchange. This procedure was conducted in air. An aliquot (ca. 3.00 mL, 7.63×10^{-3}mmol of $[(CdSe)_{13}(n\text{-octylamine})_{13}]$) from the as-made $[(CdSe)_{13}(n\text{-octylamine})_{13}]$, TOP, toluene mixture was centrifuged and the supernatant discarded. The residual solid was washed 3-5 times with toluene (3 mL each) to remove TOP, and the solid was redispersed in oleylamine (6 mL) and allowed to stand at room temperature without stirring for more than one week. The vial was manually shaken (10-15 s) once each day. In the first two days, some precipitate still remained at the bottom of the vial, which was bundled $[(CdSe)_{13}(n\text{-octylamine})_{13}]$. As ligand exchange proceeded, the precipitate gradually diminished, eventually leaving a solution with a small amount of white slush. After more than one week, the mixture was centrifuged (700 *g*, 30 min) and the supernatant discarded. The white slush so obtained was washed with toluene (3 mL), the mixture centrifuged, and the supernatant discarded. This purification process was repeated 5-7 times. The residual solvent was removed *in vacuo*, leaving $[(CdSe)_{13}(oleylamine)_{13}]$ as a white slushy solid. Anal.Calcd for $[(CdSe)_{13}(oleylamine)_{13}]$: C, 47.04; H, 8.06; N, 3.05. Found, C, 47.25; H, 8.34; N, 4.60. UV-vis (toluene) λ_{max}, nm: 312, 339, 350.

Direct synthesis of $[(CdSe)_{13}(oleylamine)_{13}]$. All synthetic procedures were conducted under dry N_2. (See Scheme 1-2) Cadmium acetate dihydrate [$Cd(OAc)_2$ $2H_2O$] (65 mg, 0.24mmol) was dissolved in oleylamine (2.0 g, 7.48 mmol) in a septum-capped Schlenk tube and heated in a70 ℃ oil bath for 1h. Selenourea (50 mg, 0.41mmol) was dissolved in oleylamine (6.8 g, 0.025mol) in the glove box, and then sonicated in a bench-top sonicator for dissolution. The selenourea solution was injected into the $Cd(OAc)_2$solutionat room temperature (20-25 ^oC) without stirring. The color changed from colorless to light yellow in one minute, and then turned to cloudy orange after 200 minutes. After one week, a white precipitate formed under a red supernatant. The purification procedure was the same as that used in the synthesis [$(CdSe)_{13}$(*n*-octylamine)$_{13}$] (see above). After washing by toluene for more than 5 times, the residual solvent was removed *in vacuo*, leaving [$(CdSe)_{13}$(oleylamine)$_{13}$] as a white slushy solid (97 mg, 0.016mmol, 86.6%). Anal.Calcd for [$(CdSe)_{13}$(oleylamine)$_{13}$]: C, 47.04; H, 8.06; N, 3.05. UV-vis (toluene) λ_{max}, nm: 310, 338,349.

Measurement of $[(CdSe)_{13}(oleylamine)_{13}]$ growth kinetics in the presence of small, polar ligands. These procedures were performed at room temperature in air. An aliquot (ca.0.10 mL, 1.70 $\times 10^{-6}$mmol of [$(CdSe)_{13}$(oleylamine)$_{13}$)] from the dissolution of [$(CdSe)_{13}$(oleylamine)$_{13}$] was diluted into toluene (2 mL) in a quartz cuvette. Various quantities of MeOH, *i*-propanol, or acetone were then measured into a separate vial (0.06 mL, 0. 13 mL, 0.25 mL, and 0.5 mL for methanol; 0.50 mL, 0.75 mL, 1.00 mL for *i*-propanol or acetone), and quantitatively transferred into the cuvette. The UV-visible spectrometer was configured to record the absorbance value at 350 nm at 10-s intervals for 1800 s at room

temperature. During data collection the cuvette was stirred by a small stirring bar.

The data collected at 350 nm were plotted in Figure 1-6 as $-\ln[(A_t-A_b)/(A_0-A_b)]$ vs. time, where A_t is the absorbance at time t, A_0 is the absorbance at t = 0 s, and A_b is the background absorbance measured at t = 1800 s. The slopes were extracted by linear least-squares fitting using Origin software (http://originlab.com/). The errors in the reported k_{obs} and $t_{1/2}$ values were propagated from the standard deviations in the slopes from individual linear least-squares fits.

Absorption spectroscopy (UV-vis). UV-visible spectra were obtained from a Perkin Elmer Lambda 950 UV/Vis spectrometer at room temperature. The $(CdSe)_{13}$ solution sample was prepared by diluting one drop of as-made sample with a certain amount of toluene in a 1-cm path length quartz cuvette, and the same background solution was used prior to each measurement.

Transmission electron sicroscopy (TEM). TEM images of bundled and sheets-like $(CdSe)_{13}$ were collected from a JEOL-2000 FX microscope with an acceleration voltage of 200 kV. Samples were prepared as described below. For bundled sample, ten drops of as-made sample were diluted into toluene (3 mL) in air. The mixture was then centrifuged in a bench-top centrifuge (700 *g*) for 5 min to form a white precipitate at the bottom of test tube along with colorless supernatant. The supernatant was discarded, and the precipitate was then redispersed into toluene (3 mL). This purification process was conducted at least 5 times. In final step, white slushy solid was dispersed into toluene (3 mL) and shaken a few times to yield a white dispersion. For unbundled sheets-like sample, 30 min was required for centrifuging to obtain a white precipitate since unbundled sample had better solubility in

toluene. Carbon-coated copper grids (Ted Pella, PELCO ® 300 Mesh Grids) were dipped into the solution and then taken out to evaporate the solvent at ambient atmosphere. This process was repeated twice to load enough sample. TEM analysis was taken immediately after grids were prepared.

Elemental analysis (EA). Data were collected by Galbraith Laboratories, Inc. Samples were prepared as gray slushy solid after purification. Details about purification process were described in "Synthesis of [$(CdSe)_{13}$(*n*-octylamine)$_{13}$]", "Direct synthesis of [$(CdSe)_{13}$(oleylamine)$_{13}$]", "Isolation of [$(CdSe)_{13}$(oleylamine)$_{13}$] from ligand exchange".

Rutherford backscattering spectrometry (RBS). Data were collected using MAS 1700 pelletron tandem ion accelerator (5SDH) equipped with charge exchange RF plasma source by National Electrostatics Corporation (NEC). Ion detector was fixed at 165^{o} during measurement. The experiment was performed by characterization facility of university of Minnesota. For preparing the sample, 0.5 mL of as-made $(CdSe)_{13}$ mixture was diluted in toluene (3 mL), and centrifuged in a bench-top centrifuge (700 *g*) for at least 5 min. This gave a white precipitate with a colorless supernatant. The supernatant was discarded, and the white slushy solid was redispersed in toluene (3 mL). This purification process was repeated at least 3 times. And the slushy solid was then diluted in 3 mL toluene. The mixture was shaken or sonication for fully dispersion if necessary. Then the pale white mixture was dropwise added onto a 10 x 10 mm^2 silicon wafer to form a thin film after evaporated solvents in a ambient atmosphere. The thickness of this thin film was between 300 -500 Å.

Laser desorption ionization mass spectrometry analysis (LDI-MS). While this analysis was usually carried out in the presence of matrix, the acidity of matrices and the presence of solvents in the matrix preparation could destroy the clusters. Therefore, the sample was analyzed without matrix. The as-made [$(CdSe)_{13}$(*n*-octylamine)$_{13}$] nanoclusters were purified by pure toluene (around 5 mL) under an ambient atmosphere for at least 5 times to remove TOPSe, TOP and excess *n*-octylamine. White gray slurry solid was collected at the bottom of test tube and redissovled in very little amount toluene to form highly concentrated $(CdSe)_{13}$ sample. The highly concentrated $(CdSe)_{13}$ toluene sample was then dropped directly onto a 384-position stainless-steel MALDI plate. The sample was left to dry for several minutes in glove box under N_2 and no matrix was applied. All MS experiments were performed on an UltrafleXtreme^{TM}MALDI TOF TOF (Bruker, Billerica, MA) in both the linear and reflectron modes. External calibration of the plate was done with insulin.

References

(1) Liu, Y. H., Wang, F. D., Wang, Y. Y., Gibbons, P. C., & Buhro, W. E. *J. Am. Chem. Soc.* **2011**, *133*, 17005.

(2) Yu, J. H., Liu, X. Y., Kewon, K. E., Joo, J., Park, J., Ko, K. T., Lee, D. W., Shen, S. P., Tivakornsasithorn, K., Son, J. S., Park, J. H., Kim, Y. W., Hwang, G. S., Dobrowolska, M., Furdynal, J. K. & Hyeon, T. *Nat.Mater.* **2010**, *9*, 47.

(3) Kim, H. S., Jang, S. W., Chung, S. Y., Lee, S; Lee, Y. H., Kim, B. S., Liu, C., Neuhauser, D. *J.Phys.Chem.B* **2010**, *114*, 471.

(4) Bowers, M. J., II McBride, J. R., Rosenthal, S. J. *J. Am. Chem. Soc.* **2005**, *127*, 15378.

(5) Cossairt, B. M., Owen, J. S. *Chem.Mater.* **2011**, *23*, 3114.

(6) Riehle, F. S., Bienert, R., Thomann, R., Urban, G. A., Kruger, M. *Nano Letters* **2009**, *9*, 514.

(7) Scholes, G. D. *Nature Materials* **2011**, *10*, 906.

(8) Kasuya, A., Sivamohan, R., Barnakov, Y. A., Dmitruk, I. M., Nirasawa, T., Romanyuk, V. R., Kumar, V., Mamykin, S. V., Tohji, K., Jeyadevan, B., Shinoda, K., Kudo, T., Terasaki, O., Liu, Z., Belosludov, R. V., Sundararajan, V., Kawazoe, Y. *Nat.Mater.* **2004**, *3*, 99.

(9) Dukes, A. D., McBride, J. R., Rosenthal, S. J. *Chem.Mater.* **2010**, *22*, 6402.

(10) Kudera, S., Zanella, M., Giannini, C., Rizzo, A., Li, Y.Q., Gigli, G., Cingolani, R., Ciccarella, G., Spahl, W., Parak, W. J., Manna, L. *Adv.Mater.* **2007**, *19*, 548.

(11) Noda, Y., Maekawa, H., Kasuya, A. *Eur.Phys.J.D* **2010**, *57*, 43.

(12) Kraetschmer, W., Lamb, L. D., Fostiropoulos, K., Huffman, D. R. *Nature* **1990**, *347*,

354.

(13) Son, J. S., Wen, X. D., Joo, J., Chae, J., Baek, S. I., Park, K., Kim, J. H., An, K., Yu, J. H., Kwon, S. G., Choi, S. H., Wang, Z. W., Kim, Y.W., Kuk, Y., Hoffmann, R., Hyeon, T. *Angew.Chem., Int. Ed.* **2009**, *48*, 6861.

(14) Del Ben, M., Havenith, R. W. A., Broer, R., Stener, Mauro *J.Phys.Chem.C* **2011**, *115*, 16782.

(15) Nguyen, K. A., Day, P. N., Pachter, R. *J.Phys.Chem.C* **2010**, *114*, 16197.

Chapter 2
Preparation of Primary Amine Derivatives of the Magic-Size Nanocluster $(CdSe)_{13}$

Introduction

Cadmium selenide (CdSe) nanoclusters, especially $(CdSe)_{13}$ and $(CdSe)_{34}$ have attracted intense interests since Kasuya's group published the first reports of $(CdSe)_{33}$ and $(CdSe)_{34}$ formation.[42] Before previous research from our group,[43] studies of $(CdSe)_{13}$ relied mainly on theory due to the lack of systematical experiment data.[44] Moreover, since CdSe nanoclusters were not previously available on the gram scale, their intrinsic physical features (size, melting points and etc.) along with chemical properties (reactivity, crystal structure, etc.) were not accessible to researchers.

In this chapter, several discrete $[(CdSe)_{13}(RNH_2)_{13}]$ derivatives (R = *n*-propyl, *n*-pentyl, *n*-octyl, and oleyl) are prepared by reaction of $Cd(OAc)_2{\cdot}2H_2O$ and selenourea in the corresponding primary-amine solvent via a soft-template method. Nanoclusters grow in spontaneously formed amine-bilayer templates, and are characterized by elemental analysis, IR spectroscopy, UV-vis spectroscopy, TEM, and low-angle XRD. Derivative $[(CdSe)_{13}(n\text{-propylamine})_{13}]$ is isolated as a yellowish-white solid (MP 98 ℃) on the gram scale. These compounds are the first derivatives of magic-size CdSe nanoclusters to be isolated in purity.

In this chapter, a novel $(CdSe)_{13}$ derivative synthesized in ethylenediamine (en) is also described. TEM images show $(CdSe)_{13}$ assembled in sheet-like structures. UV-visible spectroscopy indicated that nanoclusters passivated by en were more robust. They were more stable at high temperature (70-80 ℃), and in polar solvents, and had better solubility in solution compared with those passivated by primary amines. These features give $(CdSe)_{13}$ prepared in en a potential advantageous for crystal structure study in the future.

Discretely sized semiconductor nanoclusters have been spectroscopically detected since the early work of Henglein and co-workers,[45] and observed as intermediates in the growth of larger colloidal nanocrystals.[46] Nanoclusters of CdSe have been of intense experimental[30, 47] and theoretical[44a, 48] interest since their mass-spectrometric characterization by Kasuya and co-workers in 2004.[42] Among these so-called magic-size nanoclusters $(CdSe)_{13}$, $(CdSe)_{19}$, $(CdSe)_{33}$, and $(CdSe)_{34}$ have been most studied. Until recently,[43] magic-size CdSe nanoclusters had been prepared only in mixtures of various sizes,[47a,30,49] and no single, discrete-size nanocluster had been isolated in purity.

Our interest in magic-size CdSe nanoclusters began when we observed them as reaction intermediates in the low-temperature synthesis of wurtzitic CdSe nanoribbons or quantum belts.[50] In the course of our initial work, we isolated pure $[(CdSe)_{13}(n\text{-octylamine})_{13}]$ and $[(CdSe)_{13}(\text{oleylamine})_{13}]$.[43] As such compounds now appear to be useful nanocrystal synthons,[50] we sought to prepare a suitable derivative in gram quantities.

We now report full details of the synthesis and characterization of four primary amine derivatives of $(CdSe)_{13}$, each having the stoichiometry $[(CdSe)_{13}(RNH_2)_{13}]$. We show that each results from a templated synthesis in which the nanoclusters grow within amine-bilayer mesophases. The $[(CdSe)_{13}(n\text{-propylamine})_{13}]$ derivative is conveniently prepared on the gram scale. We hope that access to preparative quantities of $(CdSe)_{13}$ will promote further experimental studies of its structure, reactivity, physical properties, and use as a nanocrystal precursor.

Results and Discussion

We previously reported the room-temperature synthesis of [$(CdSe)_{13}$(*n*-octylamine)$_{13}$] by reaction of cadmium acetate (dihydrate) and selenourea in *n*-octylamine solvent.[43] Reaction monitoring established the chemical pathway summarized in Scheme 2-1. Combination of cadmium acetate and *n*-octylamine resulted in spontaneous formation of an amine-bilayer mesostructure[51] in which bilayers of *n*-octylamine separated cadmium acetate layers. This lamellar mesostructure served as a template for growth of $(CdSe)_{13}$ nanoclusters upon addition of selenourea. A mixture of magic-size CdSe nanoclusters was initially formed, including $(CdSe)_{13}$, $(CdSe)_{19}$, $(CdSe)_{33}$, and $(CdSe)_{34}$, which equilibrated exclusively to $(CdSe)_{13}$ over 5-7 h at room temperature.[43] We previously suggested that $(CdSe)_{13}$ is thermodynamically the most stable magic size within the amine-bilayer mesophase.[13]

A white slushy solid isolated from the equilibrated mixture was shown to be [$(CdSe)_{13}$(*n*-octylamine)$_{13}$] by a combination of elemental analysis, UV-vis spectroscopy, mass spectrometry, and Rutherford backscattering spectrometry (showing a Cd:Se ratio of 1:1).[43] Some have argued that mass-spectrometry evidence for magic-size-nanocluster mass distributions is questionable, because various specimens having apparently different distributions of magic-size nanoclusters appear to give very similar mass distributions.[16] However, our reported mass spectrum for $(CdSe)_{13}$ was markedly different than those published previously,[42] especially in that $(CdSe)_{13}$ was the base peak, present in much greater intensity than the peaks for other $(CdSe)_x$ species.[43]

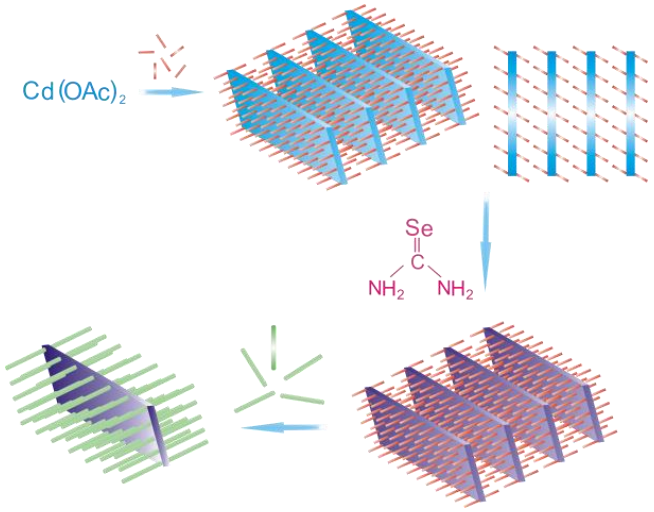

Scheme 2-1. Templated Chemical Pathway for Synthesis of $[(CdSe)_{13}(RNH_2)_{13}]$.[a 43, 50a] Combination of $Cd(OAc)_2$ and the primary amine solvent forms a lamellar, bilayer template structure (blue, orange). Addition of selenourea results in the growth of $[(CdSe)_{13}(RNH_2)_{13}]$ nanoclusters within the planar galleries of the template (purple, orange). Ligand exchange with oleylamine liberates sheet-like aggregates of $[(CdSe)_{13}(RNH_2)_{13}]$ (purple, green) from the bundled template.

The template mesostructure remained intact in the as-synthesized $[(CdSe)_{13}(n\text{-octylamine})_{13}]$, with the $(CdSe)_{13}$ nanoclusters entrained within. We found that individual sheets of aggregated $[(CdSe)_{13}(n\text{-octylamine})_x(\text{oleylamine})_{13-x}]$ were exfoliated (Scheme 2-1) when the initially bundled template mesostructure was allowed to stand in oleylamine solution, during which partial ligand exchange occurred. Sonication of the sheet structures in oleylamine solution completed the ligand exchange, degraded the sheet aggregates, and released molecular $[(CdSe)_{13}(\text{oleylamine})_{13}]$ nanoclusters into solution.[43]

In this study, additional primary-amine derivatives of $(CdSe)_{13}$ were similarly prepared in the corresponding primary-amine solvent. $[(CdSe)_{13}(RNH_2)_{13}]$ nanoclusters were isolated as slushy solids except for $[(CdSe)_{13}(n\text{-propylamine})_{13}]$, which was a yellowish-white solid having a melting point of 98 ℃. Satisfactory elemental analyses were obtained for $[(CdSe)_{13}(RNH_2)_{13}]$, R = *n*-propyl and *n*-pentyl. Elemental analysis for

$[(CdSe)_{13}(n\text{-octylamine})_{13}]$ was slightly high in C, and that for $[(CdSe)_{13}(\text{oleylamine})_{13}]$ was significantly high in C, H, and N, reflecting our difficulty in successfully washing away the excess long-chain alkylamine (used as solvent) from these slushy solids. As expected, IR spectra of the $[(CdSe)_{13}(RNH_2)_{13}]$ compounds exhibited absorbances corresponding only to the primary amine ligands, with the characteristic NH stretches and NH_2 deformations[52] clearly observed (Figure 2-1). The IR spectra of $Cd(OAc)_2{\cdot}2H_2O$, *n*-octylamine, and $[(CdSe)_{13}(n\text{-octylamine})_{13}]$ are compared in Figure 2-2, to establish that the observed absorbances of $[(CdSe)_{13}(n\text{-octylamine})_{13}]$ are displaced from those of the acetate ligand.

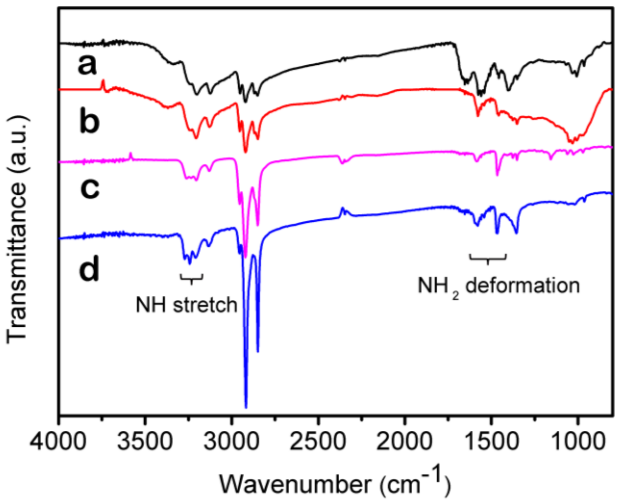

Figure 2-1. Infrared spectra (in KBr) of $[(CdSe)_{13}(RNH_2)_{13}]$ complexes; R = *n*-propyl (a), *n*-pentyl (b), *n*-octyl (c), and oleyl (d). All absorbances were assigned to the amine ligands. Regions characteristic for NH stretching and NH_2 deformation are identified.

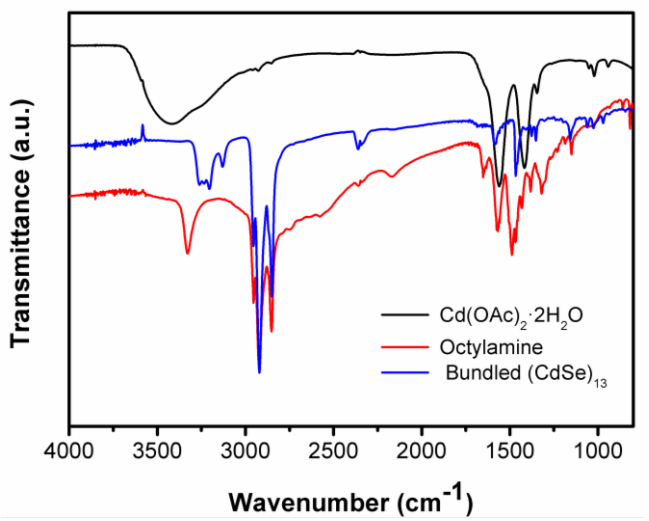

Figure 2-2. IR spectra from KBr pellets of the starting material $Cd(OAc)_2{\cdot}2H_2O$ (black curve), the solvent *n*-octylamine (red curve), and the bundled [$(CdSe)_{13}$(*n*-octylamine)$_{13}$] (blue curve).

Evidence for the $(CdSe)_{13}$ stoichiometry of the as-synthesized nanoclusters was obtained by UV-vis spectroscopy (Figure 2-3). As we previously reported,[43] [$(CdSe)_{13}$(*n*-octylamine)$_{13}$] exhibited three absorbances (311, 337, and 349 nm), which closely approached the electronic spectrum of $(CdSe)_{13}$ calculated theoretically (315, 330, and 345 nm).[9] Spectra of all four primary-amine derivatives were closely similar (Figure 2-3a), with small differences in peak positions and widths (Figure 2-3b) likely induced by the amine ligands. (The 315 nm absorbances were not resolved in the spectra of [$(CdSe)_{13}$(*n*-propylamine)$_{13}$] and [$(CdSe)_{13}$(*n*-pentylamine)$_{13}$].) Small variations in peak positions and line shapes in the absorption spectra of CdSe nanoclusters upon changes in surface ligation have been attributed to small perturbations of surface or electronic structure,[53] which seems to have occurred here as well.

Three of the Figure 2-3 spectra featured long scattering tails to longer wavelength, as a result of the bundled nature of the as-synthesized materials. This scattering tail was absent in the spectrum of [$(CdSe)_{13}$(oleylamine)$_{13}$], because exfoliation occurred readily upon

solvent dispersion of this derivative for spectral analysis. Notably, absorbances at 363, 389, and 413 nm, previously assigned to $(CdSe)_{19}$, $(CdSe)_{33}$, and $(CdSe)_{34}$,[44a, 50a] were absent from all four spectra, establishing the spectroscopic purity of the $[(CdSe)_{13}(RNH_2)_{13}]$ nanoclusters.

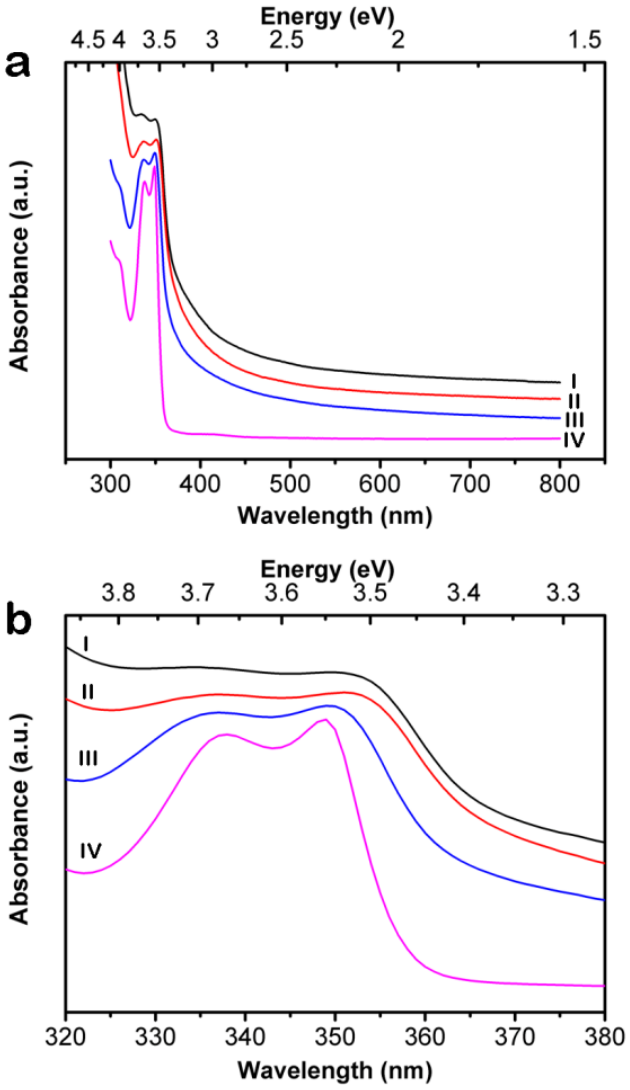

Figure 2-3. Absorption (extinction) spectra (in toluene dispersion) of $[(CdSe)_{13}(RNH_2)_{13}]$ complexes; R = *n*-propyl (I), *n*-pentyl (II), *n*-octyl (III), and oleyl (IV). (a) full spectrum showing the characteristic absorbances of the $(CdSe)_{13}$ nanocluster. Note the scattering tails in spectra I-III. (b) Spectral expansions in the region of the characteristic absorptions near 337 and 349 nm (see text).

The bundled and exfoliated template features were determined by TEM imaging (Figure 2-4). Figure 2-4a shows bundled aggregates of $[(CdSe)_{13}$(*n*-octylamine)$_{13}]$.[43, 50a] Arrows indicate regions in which parallel stripes may be observed, constituting side views of the

lamellar template depicted in Scheme 2-1. Exfoliation of individual layers from the lamellar mesophases as described above produced images like that in Figure 2-4b, in which triangular sheet-like aggregates of [$(CdSe)_{13}$(*n*-octylamine)$_x$(oleylamine)$_{13-x}$] were separated from the bundled templates. The zebra-stripe pattern evident in Figure 2-4b revealed additional structural order within the individual sheets or layers.[43, 50a]

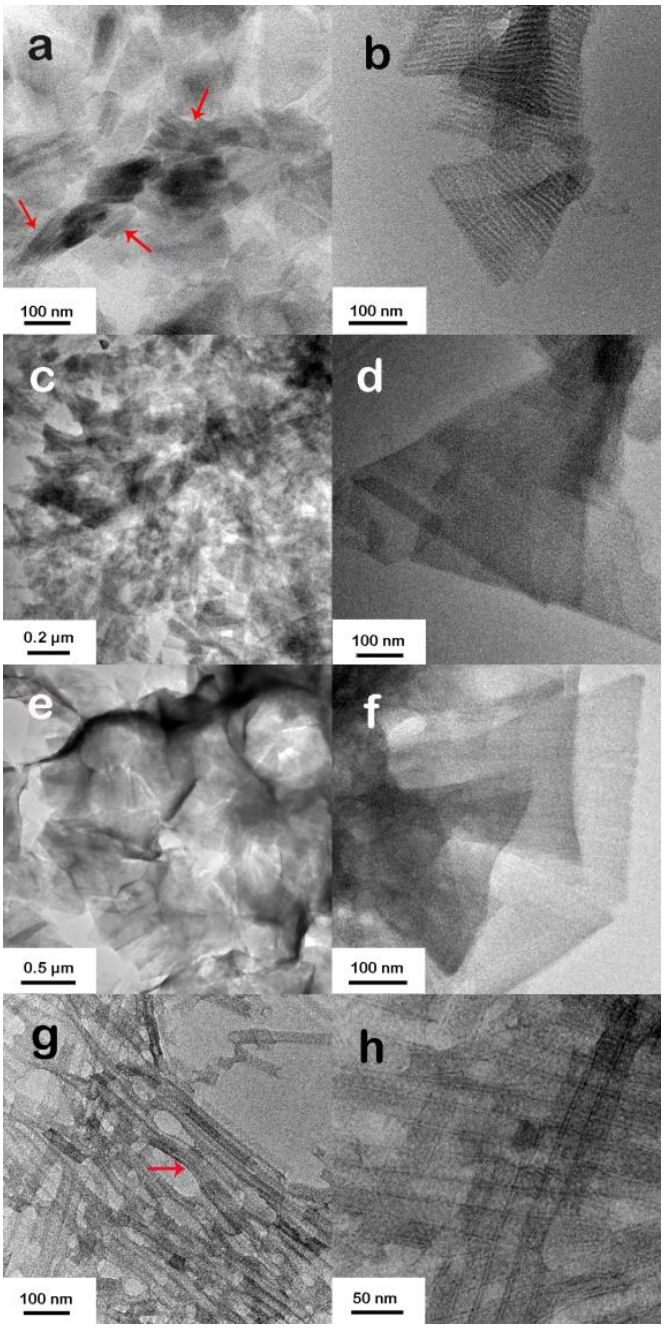

Figure 2-4. TEM images of the as-synthesized bundled (left column) and unbundled (right column) $[(CdSe)_{13}(RNH_2)_{13}]$; R = *n*-octyl (a, b), *n*-propyl (c, d), *n*-pentyl (e, f), and oleyl (g, h). Arrows in parts a and g identify bundled regions.

Images of the bundled and unbundled aggregates of $[(CdSe)_{13}(n\text{-propylamine})_{13}]$ and $[(CdSe)_{13}(n\text{-pentylamine})_{13}]$ are shown in Figure 2-4c-f. The lamellar-stripe pattern was not observed in the bundled aggregates of these compounds (Figure 2-4c and 4e), suggesting them to be less well ordered than the bundled aggregates of $[(CdSe)_{13}(n\text{-octylamine})_{13}]$

(Figure 2-4a). This observation was supported by low-angle XRD (see below). Exfoliation of these compounds produced individual triangular sheets, like those for [$(CdSe)_{13}$(*n*-octylamine)$_{13}$] (Figure 2-4b), confirming the initial lamellar architectures.

Images of "bundled" and unbundled aggregates of [$(CdSe)_{13}$(oleylamine)$_{13}$] (Figure 2-4g and 4h) contrasted with those of the other primary-amine derivatives. The most prominent feature in images of the as-synthesized [$(CdSe)_{13}$(oleylamine)$_{13}$] were rolled sheets resembling half-cylinders. Parallel-stripe patterns were observed in some regions of the images (see the arrow in Figure 2-4g), indicative of a bundled, lamellar architecture. We note that the bundled aggregates of [$(CdSe)_{13}$(oleylamine)$_{13}$] are the most easily exfoliated, as addition of oleylamine to the other bundled [$(CdSe)_{13}(RNH_2)_{13}$] mesophases induces spontaneous exfoliation upon ligand exchange. We therefore surmise that solvent dispersion of the bundled [$(CdSe)_{13}$(oleylamine)$_{13}$] material for TEM sample preparation resulted in extensive exfoliation, as confirmed by the Figure 2-3h image. Low-angle XRD evidence is provided below for the bundled, lamellar structure of the as-synthesized material.

The low-angle XRD patterns (Figure 2-5) of the bundled [$(CdSe)_{13}(RNH_2)_{13}$] mesophases provided strong confirmatory evidence for their lamellar structures. Each contained a series of basal, 00ℓ reflections (Table 2-1) corresponding to the layered architectures. Peaks were sharpest for [$(CdSe)_{13}$(*n*-octylamine)$_{13}$], showing it to be the most highly ordered mesophase.

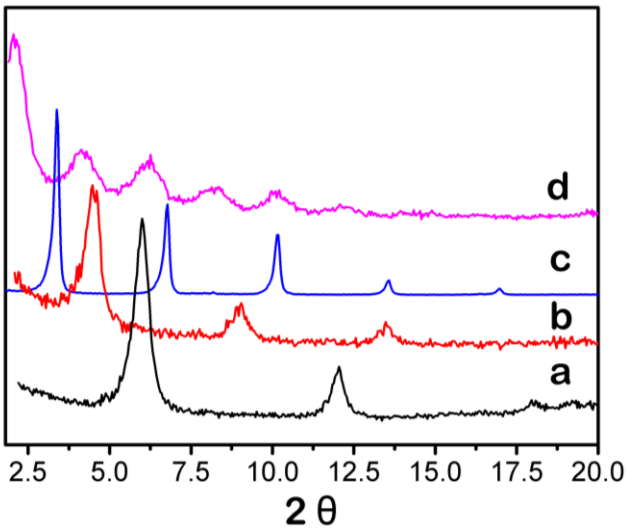

Figure 2-5. Low-angle XRD patterns of as-synthesized (bundled) $[(CdSe)_{13}(RNH_2)_{13}]$ showing the basal reflections produced by the lamellar mesostructures; R = *n*-propyl (a), *n*-pentyl (b), *n*-octyl (c), and oleyl (d).

Table 2-1. Experimental (Exp) and Calculated (Calcd) XRD Basal-Reflection Positions in $[(CdSe)_{13}(RNH_2)_{13}]$ Compounds.

00ℓ	**$[(CdSe)_{13}$ (oleylamine)$_{13}]$** Exp, ℃θ (Calcd, ℃θ)	**$[(CdSe)_{13}$ (*n*-octylamine)$_{13}]$** Exp, ℃θ (Calcd, ℃θ)	**$[(CdSe)_{13}$ (*n*-pentylamine)$_{13}]$** Exp, ℃θ (Calcd, ℃θ)	**$[(CdSe)_{13}$ (*n*-propylamine)$_{13}]$** Exp, ℃θ (Calcd, ℃θ)
001	2.06	3.38	4.48	6.00
002	4.14 (4.12)	6.78 (6.76)	9.04 (8.96)	12.0 (12.0)
003	6.26 (6.18)	10.2 (10.1)	13.5 (13.4)	18.1 (18.0)
004	8.34 (8.24)	13.6 (13.5)		
005	10.2 (10.3)	17.0 (16.9)		
006	12.3 (12.4)			

The *d* spacings calculated from the XRD patterns gave the interlayer spacings in the four lamellar mesostructures, which are plotted versus the number of carbon atoms in the primary-amine ligands in Figure 2-6. Data gave the expected linear relationship,[54] except for the oleylamine point, which departed from the line because of the double bond in the ligand's chain. The line should extrapolate approximately to the interamine-head-group spacing at the *y* intercept, which was 0.80 nm. This value is close to the theoretical diameter of the $(CdSe)_{13}$ nanocluster.[48a] The result indicated that one monolayer of $(CdSe)_{13}$

nanoclusters was interspersed between the amine bilayers, represented as the planar features in Scheme 2-1, in the lamellar-template mesostructures.

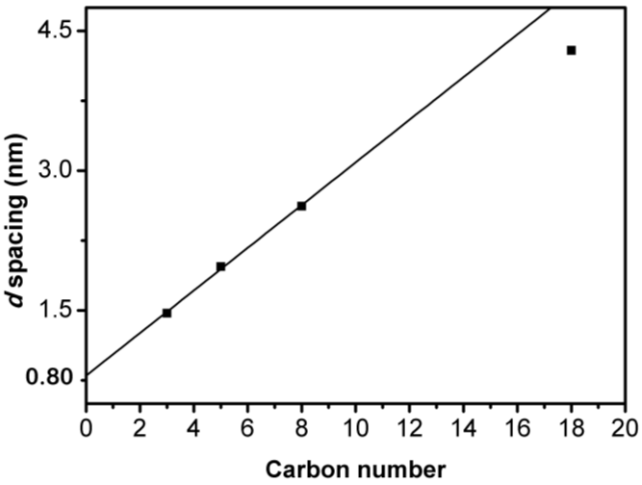

Figure 2-6. Plot of the measured basal-plane *d* spacing in the lamellar $[(CdSe)_{13}(RNH_2)_{13}]$ mesostructures obtained from the XRD data versus the number of carbon atoms in the primary-amine ligands.

The results reported here establish that the four $[(CdSe)_{13}(RNH_2)_{13}]$ derivatives (R = *n*-propyl, *n*-pentyl, *n*-octyl, and oleyl) are accessible by a common synthetic method, are formed by a common templated-mesophase pathway, and possess a common stoichiometry. The solid derivative $[(CdSe)_{13}(n\text{-propylamine})_{13}]$ is readily prepared on the gram scale. Because $[(CdSe)_{13}(RNH_2)_{13}]$ compounds are useful low-temperature precursors to crystalline CdSe quantum belts[50a] and presumably other CdSe nanocrystals and because ligand exchange in $[(CdSe)_{13}(RNH_2)_{13}]$ occurs readily, we expect that $[(CdSe)_{13}(n\text{-propylamine})_{13}]$ will prove to be a useful, isolable form of $(CdSe)_{13}$.

Experimental structure determinations have not been completed for any magic-size CdSe nanocluster, including $(CdSe)_{13}$. Indeed, no single-*x*, magic-size $(CdSe)_x$ nanocluster had been isolated in purity until 2012 (Chapter 1).[43] However, the structure of $(CdSe)_{13}$ has been determined theoretically,[42, 44a, 48] and the lowest energy C_3 isomer found by Nguyen, Day,

and Pachter is plotted in Figure 2-7.[48a] These researchers also found ligated nanoclusters of the type [$(CdSe)_x$(*n*-methylamine)$_x$] to be stable with one amine ligand datively bound to each Cd atom.[48a] The structure of [$(CdSe)_{13}$(*n*-methylamine)$_{13}$] was not reported, the $(CdSe)_{13}$ component of which may differ from that in Figure 2-6. Calculations of the structural and spectral properties of [$(CdSe)_{13}$(*n*-methylamine)$_{13}$] are currently in progress.[55]

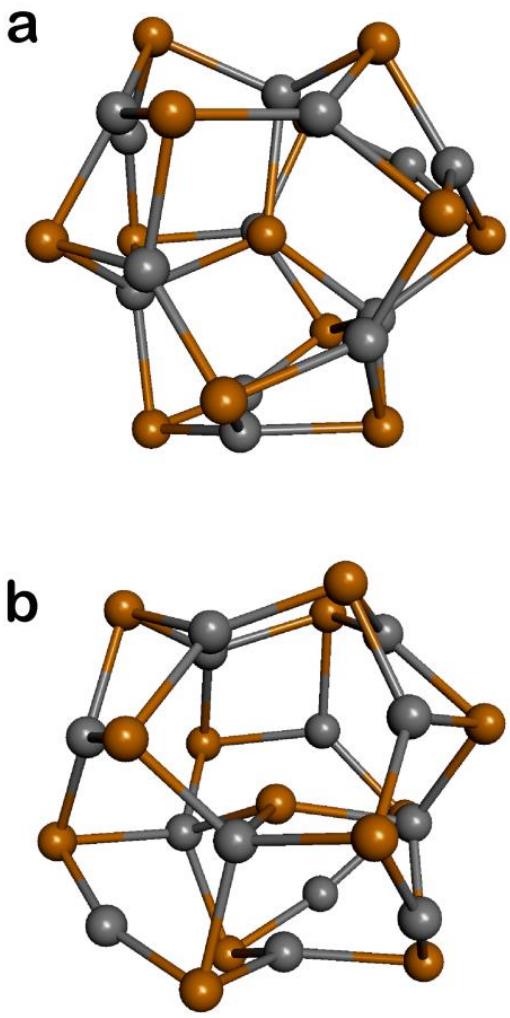

Figure 2-7. Two views of the lowest-energy isomer of unligated $(CdSe)_{13}$ determined theoretically.[6] The Cd atoms are gray, and the Se atoms are orange. (a) view with the C_3 axis perpendicular to the plane of the page; (b) view with the C_3 axis oriented vertically in the plane of the page. Plots were made using Accelrys Discovery Studio Visualizer.

We measured the diameter of the $(CdSe)_{13}$ nanocluster in Figure 2-6 to be 0.78 nm using

molecular-modeling software. This value is close to the interamine-head-group spacing (0.80 nm) determined by analysis of the low-angle XRD data for the as-synthesized, bundled $[(CdSe)_{13}(RNH_2)_{13}]$ mesophases. The similarity of these values supports our claim that a single monolayer of $(CdSe)_{13}$ nanoclusters lies in each interamine-head-group lamellar gallery.

Ethylenediamine (en) passivated magic-size nanoclusters $(CdSe)_{13}$ was another $(CdSe)_{13}$ derivative worthy of investigation. As expected, the IR spectrum of the $(CdSe)_{13}$ en derivative exhibited absorbances corresponding only to the en ligand, with the characteristic NH stretches and NH_2 deformations[52] clearly observed (Figure 2-8), and no residual acetate or water absorptions. Ethylenediamine is potentially a bidentate, chelating ligand (Figure 2-9b). Since each N atom in en binds one surface Cd atom in $(CdSe)_{13}$, then the additional observed stability of the en derivative might be explained as a consequence of the chelate effect.

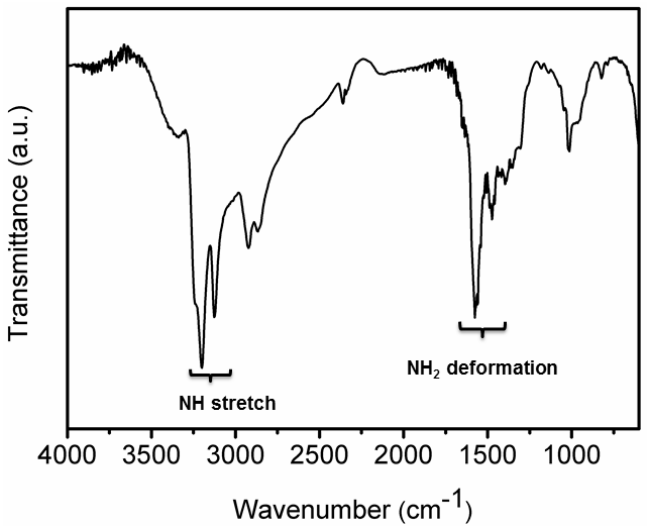

Figure 2-8. Infrared spectrum (in KBr) of $(CdSe)_{13}$ in en complexes. All absorbances were assigned to the amine ligands. Regions characteristic for NH stretching and NH_2 deformation are identified.

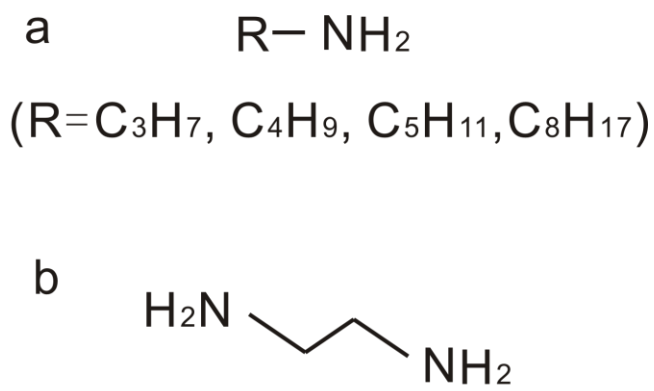

Figure 2-9. Molecular formula of (a) primary amine (R = *n*-propyl-, *n*-butyl-, *n*-pentyl-, and *n*-octyl-) and (b) ethylenediamine.

The UV-vis absorption spectrum reported here contained three absorption features at 311, 338 and 352 were highly consistent with those of $(CdSe)_{13}$, (Figure 2-10, black curve), and absorbances at 363, 389, and 413 nm, which belong to $(CdSe)_{19}$, $(CdSe)_{33}$, and $(CdSe)_{34}$,[44a, 50a] were absent, indicating the nanoclusters synthesized in ethylenediamine were spectroscopically pure $(CdSe)_{13}$ nanoclusters. The large scattering tail at longer wavelength demonstrated that the $(CdSe)_{13}$ nanoclusters were formed within a lamellar-bilayer template and had the same "bundled" nature as those generated in primary amine solvents. However, after sonication in a oleylamine-toluene mixture for 1 h, the scattering tail at longer wavelength still existed compared with $[(CdSe)_{13}(n\text{-octylamine})_x(oleylamine)_{13-x}]$ (Chapter 1, Figure 1-3a), indicating that only a small amount $(CdSe)_{13}$ nanoclusters were unbundled. The result demonstrated that the en template was much more stable and robust than those corresponding to primary amine.

As we had already shown that at high reaction temperature (T > 70 ^{o}C) $(CdSe)_{13}$ formed in primary amine lamellar bilayer templates were not stable, and grew and converted to CdSe quantum belts. However, in the en template, $(CdSe)_{13}$ was stable even at 80 ^{o}C (Figure 2-11) The morphology of the $(CdSe)_{13}$ aggregates passivated by ethylenediamine was different

from those in primary amine, which was proved by TEM images in Figure 2-12. Instead of forming triangular structures, $(CdSe)_{13}$ aggregates in en were generated in sheet-like structures, which may be caused by the monodentate Vs. bidentate amine employed (Figure 2-9 a, b).

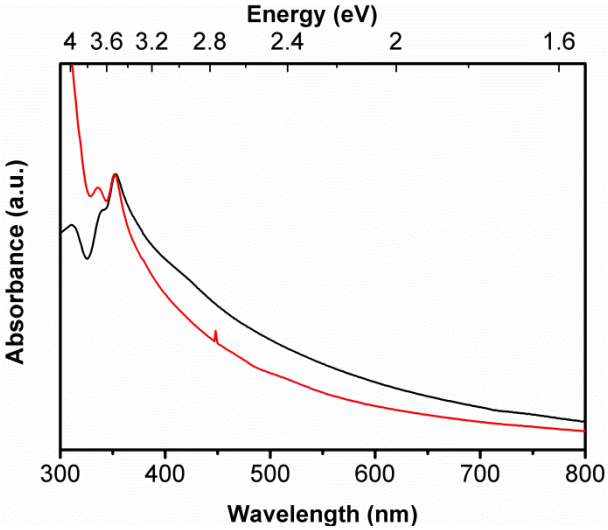

Figure 2-10. Absorption (extinction) spectra (in toluene dispersion) of $(CdSe)_{13}$ in the en templates. Spectrum from bundled sample (black curve), and spectrum from partially unbundled sample (red curve).

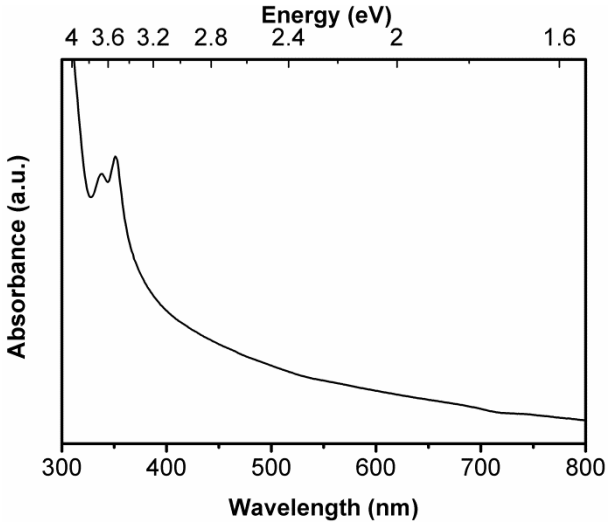

Figure 2-11. Absorption (extinction) spectrum (in toluene dispersion) of $(CdSe)_{13}$ synthesized in en at 80 ^{o}C.

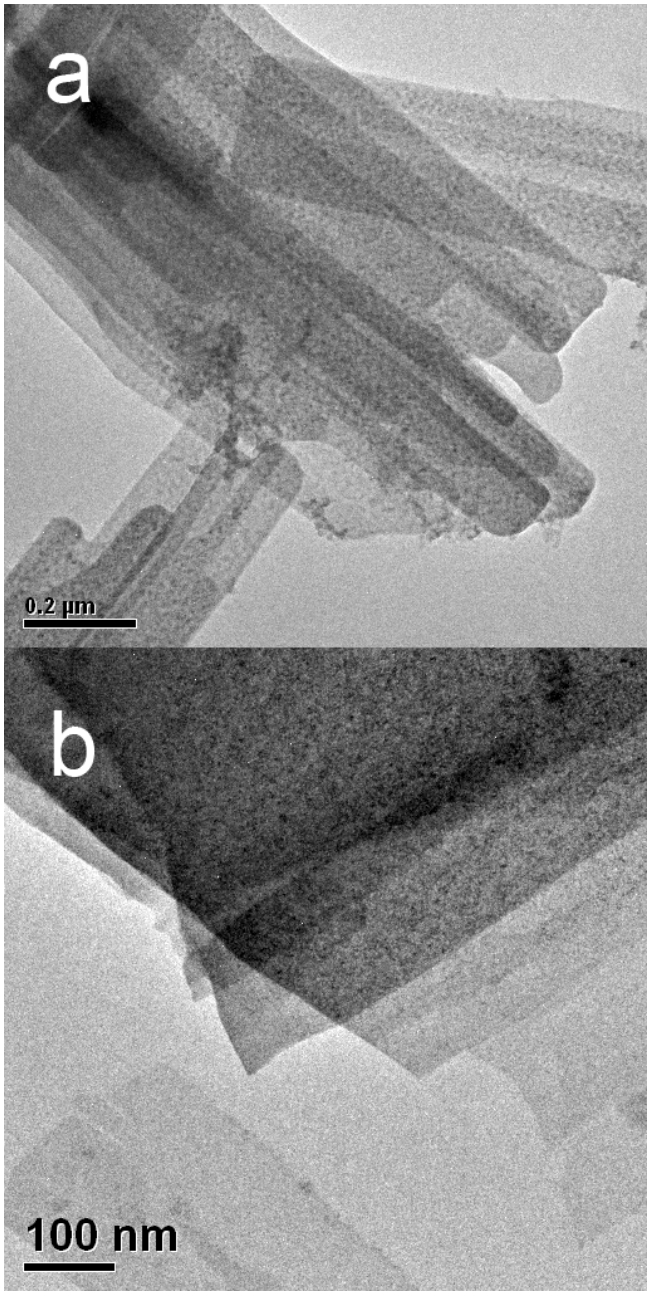

Figure 2-12. TEM images of the as-synthesized $(CdSe)_{13}$ in ethylenediamine (a) at low magnification and (b) at higher magnification.

The state of the magic-size CdSe nanocluster field may be compared to that of the carbon-fullerene field just prior to the reported isolation of C_{60} by Krätschmer and Huffman in 1990.[56] At that time, C_{60} had been characterized by mass spectrometry, its structure had been determined theoretically, and some of its spectroscopic properties were known. After pure C_{60} became available in gram quantities,[56] the carbon-fullerene field grew rapidly.

Similarly, we propose that access to gram quantities of [$(CdSe)_{13}$(*n*-propylamine)$_{13}$] should enable experimental structure determination, reactivity studies, and further determinations of the physical and spectroscopic properties of $(CdSe)_{13}$.

Conclusion

A convenient chemical synthesis affords the four [$(CdSe)_{13}(RNH_2)_{13}$] derivatives (R = *n*-propyl, *n*-pentyl, *n*-octyl, and oleyl). These are the first derivatives of magic-size CdSe nanoclusters to be isolated in purity. The results establish the derivatives to have a common stoichiometry and to have formed by a common amine-bilayer-template pathway. Remarkably, even the shorter chain primary amines are able to generate amine-bilayer templates, which ultimately afford the [$(CdSe)_{13}(RNH_2)_{13}$] products in mesophase architectures. Diffraction data collected from the [$(CdSe)_{13}(RNH_2)_{13}$] mesophases allowed the first experimental estimate of the diameter of the $(CdSe)_{13}$ nanocluster (0.80 nm), which is close to the theoretical diameter. Access to gram quantities of $(CdSe)_{13}$ will enable further experimental studies.

Experimental Section

Materials. *n*-Propylamine (+98%), *n*-pentylamine (+99%), *n*-octylamine (+99%), oleylamine (technical grade, 70%), ethylenediamine (BioXtra), methanol (ACS reagent, ≥ 99.8%) $Cd(OAc)_2 \cdot 2H_2O$ and trioctylphosphine (TOP, 97%) were purchased from Aldrich, and selenourea (99.9%, metal basis) from Alpha Aesar. All were used as received and stored under N_2. Toluene from Sigma-Aldrich (CHROMASOLV, for HPLC, ≥ 99.9%) was purged with dry N_2 for at least 1 h and stored under N_2 prior to use.

Analyses. Elemental analyses (C, H, N) were obtained from Galbraith Laboratories, Inc. (Knoxville, TN). UV-vis spectra were obtained from a Perkin Lambda 950 UV/vis spectrometer. IR spectra were obtained from a Perkin-Elmer Spectrum BX FT-IR System. XRD patterns were obtained from a Rigaku Dmax A vertical powder diffractometer with Cu Kα radiation (λ=1.5418 Å). Low-resolution TEM images were obtained from a JEOL 2000FX microscope operating at 200 KV. Melting point was obtained on a Mel-temp II Laboratory Device. Analysis by Rutherford backscattering spectrometry (RBS) was provided by the Characterization Facility at the University of Minnesota (Minneapolis, MN). LDI mass spectra were recorded on a Bruker ultrafleXtreme MALDI-TOF/TOF mass spectrometer. No matrix was employed in these mass-spectral analyses.

Preparation of $[(CdSe)_{13}(n\text{-propylamine})_{13}]$. All synthetic procedures were conducted under N_2. In a large-scale synthesis, $Cd(OAc)_2 \cdot 2H_2O$ (1.30 g, 4.80 mmol) was dissolved in *n*-propylamine (40.0 g, 0.681 mol) in a septum-capped Schlenk tube, heated in a 50 ℃ oil bath for 1 h, and allowed to cool to room temperature. Selenourea (1.0 g, 8.2 mmol) was added in *n*-propylamine (10.0 g, 0.170 mol) in the glovebox, and then sonicated

in a benchtop sonicator for dissolution.

The selenourea solution was injected into cadmium-precursor solution at room temperature (20-25 ℃) without stirring. The color of the reaction mixture changed immediately after injection from colorless (0 min) to light-yellow (viscous, 5 s), yellow (cloudy with a white precipitate, 1 min), and red (cloudy with a white precipitate, 1 h). After another 2 h under N_2 without stirring, $(CdSe)_{13}$ was deposited as reddish-white precipitate under a light-red supernatant.

The reaction mixture was subsequently heated at 50 ℃ in an oil bath for 40 min, during which the mixture turned a darker shade of red, with a white precipitate. The red solution contained elemental selenium as the colored side-product, which was removed by addition of TOP (1.3 g) to form TOP = Se, resulting in a colorless solution with a white precipitate.

White precipitate was separated using a benchtop centrifuge (700 g, 30 s), and colorless supernatant was discarded. The remaining white slush was combined with a propylamine solution (20 mL, 20% w/w in toluene), and the mixture was recentrifuged and the supernatant discarded. This purification process was repeated 5 times in total. The residual solvent was removed *in vacuo*, leaving $[(CdSe)_{13}(n\text{-propylamine})_{13}]$ as a yellowish-white solid (1.19 g, 0.365 mmol, 97.5%).

Smaller-scale syntheses were conducted similarly, typically using $Cd(OAc)_2 \cdot 2H_2O$ (65 mg, 0.24 mmol) in *n*-propylamine (5.7 g, 0.097 mol) and selenourea (50 mg, 0.41 mmol) in *n*-propylamine (1.2 g, 9.3 mmol). The elemental-selenium side-product was removed with added TOP (65 mg). Product precipitate was purified with a propylamine solution (5 × 5 mL, 20% w/w in toluene) as described above, leaving $[(CdSe)_{13}(n\text{-propylamine})_{13}]$ as a

yellowish-white solid (59.3 mg, 0.018 mmol, 97.1%).

Characterization: MP (98 ± 2 ℃). IR (KBr, cm^{-1}, 25 ℃): 3346 (w, NH stretch), 3245 (sh, NH stretch), 3202 (m), 3122 (m), 2953 (m), 2921 (s), 2869 (m), 2851 (m), 1646 (s, NH_2 deformation), 1559 (s, NH_2 deformation), 1458 (w), 1404 (s), 1351 (w), 1032 (w), 1007 (m), 965 (w) (Figure 2-1). UV-vis (toluene) λ_{max}, nm: 334, 349 (Figure 2-2). Anal. Calcd for [$(CdSe)_{13}$(*n*-propylamine)$_{13}$]: C, 14.37; H, 3.59; N, 5.59. Found: C, 14.80; H, 3.46; N, 5.51. All values are given as percentages.

Preparation of [$(CdSe)_{13}$(*n*-pentylamine)$_{13}$]. All synthetic procedures were conducted under the same general conditions for the [$(CdSe)_{13}$(*n*-propylamine)$_{13}$] preparation, except for the reaction solvent. $Cd(OAc)_2$ $2H_2O$ (65 mg, 0.24 mmol) was dissolved in *n*-pentylamine (5.7 g, 0.066 mol), heated in a 70 ^oC oil bath for 1 h, and allowed to cool to room temperature. Selenourea (50 mg, 0.41 mmol) was dissolved in *n*-pentylamine (1.2 g, 0.013 mol).

After injecting the selenourea solution into the $Cd(OAc)_2$ solution at room temperature without stirring, the reaction mixture turned from colorless (0 min) to green yellow (1 min), light yellow (cloudy, 5 min), and yellow (cloudy with a white precipitate, 15 min), and light red (cloudy with a white precipitate, 2 h). After another 5 h, a white precipitate formed under a red supernatant. The mixture was heated at 70 ^oC for 40 min. TOP (65 mg) was injected to remove the elemental-selenium side-product. The remaining white precipitate was separated from the colorless supernatant using a purification process described above but with *n*-pentylamine solution (5 × 5 mL, 20% w/w in toluene). The residual solvent was removed *in vacuo*, leaving [$(CdSe)_{13}$(*n*-pentylamine)$_{13}$] as a slushy white solid (62.9 mg, 0.017 mmol, 92.6%). To ensure removal of the last traces of *n*-pentylamine for elemental

analysis, pure toluene (5 × 5 mL) was used in the purification steps.

Characterization: IR (KBr, cm^{-1}, 25 ℃): 3368 (w, NH stretch), 3238 (sh, NH stretch), 3205 (m), 3128 (m), 2953 (w), 2920 (s), 2868 (sh), 2849 (s), 1577 (s, NH_2 deformation), 1458 (w), 1352 (w), 1031 (w), 1007 (w), 969 (w) (Figure 2-1). All values are given as percentages. UV-vis (toluene) λ_{max}, nm: 337, 351 (Figure 2-2). Anal. Calcd for $[(CdSe)_{13}(n\text{-pentylamine})_{13}]$: C, 21.54; H, 4.67; N, 5.02. Found: C, 21.44; H, 4.42; N, 4.82.

Preparation of $[(CdSe)_{13}(n\text{-octylamine})_{13}]$. All synthetic procedures were conducted under the same general conditions for the $[(CdSe)_{13}(n\text{-propylamine})_{13}]$ synthesis, except for the reaction solvent. $Cd(OAc)_2 \cdot 2H_2O$ was dissolved in *n*-octylamine (5.7 g, 0.044 mol), heated in a 70 ^oC oil bath for 1 h, and allowed to cool to room temperature. Selenourea was dissolved in *n*-octylamine (1.2 g, 0.0093 mol).

After injecting selenourea solution into the $Cd(OAc)_2$ solution at room temperature, the reaction mixture turned from colorless(0 min) to green yellow (1 min), white yellow (cloudy, 5 min), yellow (cloudy, 15 min), and light red (cloudy, 2 h). After another 5 - 10 h, a white precipitate formed under a red supernatant. The reaction mixture was subsequently heated at 70 ^oC in an oil bath for 40 min. TOP (65 mg) was injected to remove elemental-selenium side-product. The purification procedure was the same as that used in the synthesis $[(CdSe)_{13}(n\text{-propylamine})_{13}]$ but with *n*-octylamine solution (5 × 5 mL, 20% w/w in toluene). The residual solvent was removed *in vacuo*, leaving $[(CdSe)_{13}(n\text{-octylamine})_{13}]$ as a white slushy solid (75 mg, 0.018 mmol, 95.9 %). To ensure removal of the last traces of *n*-octylamine for elemental analysis, pure toluene (5 × 5 mL) was used in the purification steps.

Characterization: IR (KBr, cm^{-1}, 25 ℃): 3260 (w, NH stretch), 3234 (w, NH stretch), 3204 (w), 2952 (m), 2922 (vs), 2850 (vs), 1584 (s, NH_2 deformation), 1466 (s), 1376 (w), 1352 (w), 1165 (w), 1062 (w), 1026 (w), 972 (w) (Figure 2-1). UV-vis (toluene) λ_{max}, nm: 311, 337, 349 (Figure 2-2). MS *m/z* (relative intensity): 6507.5149 ($(CdSe)_{34}$, 7.69%), 6318.0317 ($(CdSe)_{33}$, 5.38%), 3638.1176 ($(CdSe)_{19}$, 10.8%), 2488.5692 ($(CdSe)_{13}$, 100%).[43] RBS: Cd:Se = 1.05:0.95.[43] Anal. Calcd for [$(CdSe)_{13}$(*n*-octylamine)$_{13}$]: C, 29.97; H, 5.97; N, 4.37. Found: C, 30.89; H, 5.84; N, 4.57.[13] All values are given as percentages.

Preparation of [$(CdSe)_{13}$(oleylamine)$_{13}$]. All synthetic procedures were conducted under the same general conditions for the [$(CdSe)_{13}$(*n*-propylamine)$_{13}$] synthesis, except for the reaction solvent. $Cd(OAc)_2$ $2H_2O$ was dissolved oleylamine (1.5 g, 5.6 mmol), heated in a 70 ^oC oil bath for 1 h, and allowed to cool to room temperature. Selenourea was dissolved in oleylamine (6.8 g, 0.025 mol). The color changed much slower after injecting selenourea solution into the $Cd(OAc)_2$ solution at room temperature. It changed from colorless (0 min) to bright green-yellow (transparent, 30 sec), and orange (viscous, overnight), and orange-red (cloudy, over 20 h). After two days, a white-orange precipitate formed under a red supernatant. TOP (65 mg) was injected to remove side-product elemental-selenium. The purification procedure was the same as that used in the synthesis [$(CdSe)_{13}$(*n*-propylamine)$_{13}$] but with oleylamine solution (5 × 5 mL, 20% w/w in toluene). The residual solvent was removed in vacuo, leaving [$(CdSe)_{13}$(oleylamine)$_{13}$] as a white slushy solid (97 mg, 0.016mmol, 86.6%). To ensure removal of the last traces of oleylamine for elemental analysis, pure toluene (5 × 5 mL) was used in the purification steps.

Characterization: IR (KBr, cm^{-1}, 25 ℃): 3271 (w, NH stretch), 3242 (m, NH stretch),

3208(m), 2955 (m), 2918 (vs), 2849 (vs), 1596 (sh, NH_2 deformation), 1578 (m, NH_2 deformation), 1466 (s), 1355 (s), 1018 (w), 963 (w) (Figure 2-1). UV-vis (toluene) λ_{max}, nm: 310, 338, 349 (Figure 2-2). Anal. Calcd for [$(CdSe)_{13}$(*n*-oleylamine)$_{13}$]: C, 47.04; H, 8.06; N, 3.05. Found: C, 49.26; H, 8.84; N, 5.03. All values are given as percentages.

Preparation of $(CdSe)_{13}$ in ethylenediamine (en). All synthetic procedures were conducted under the same general conditions used for the [$(CdSe)_{13}$(*n*-propylamine)$_{13}$] synthesis, except for the reaction solvent. $Cd(OAc)_2$ $2H_2O$ (65 mg, 0.24 mmol) was dissolved ethylenediamine (5.7 g, 0.095 mol), heated in a 70 ^oC oil bath for 1 h, and allowed to cool to room temperature, forming a white milky mixture. Selenourea (50 mg, 0.41 mmol) was dissolved in ethylenediamine (1.2 g, 0.020 mol). The selenourea solution was injected into the $Cd(OAc)_2$ solution at room temperature without stirring. The reaction mixture changed from white milky (0 min) to yellow white (30 sec), orange white (cloudy, 15 min), and orange-red with a white precipitate (cloudy, over 5 h). A white-orange precipitate formed under a red supernatant after the reaction mixture stood overnight at room temperature. TOP (65 mg) in 0.5 mL toluene and 2 mL methanol was injected to remove the selenium side product. The purification procedure was the same as that used in the synthesis [$(CdSe)_{13}$(*n*-propylamine)$_{13}$] but using an ethylenediamine solution (5 × 5 mL, 20% w/w in toluene and methanol). To ensure removal of the last traces of ethylenediamine, pure toluene (5 × 5 mL) was used in the last purification steps. The residual solvent was removed in vacuo, leaving [$(CdSe)_{13}(en)_x$] as a white slushy solid (97 mg, 0.016 mmol, 87%).

Characterization: IR (KBr, cm^{-1}, 25 ℃): 3350 (w, NH stretch), 3200 (sh, NH stretch), 3124 (m), 2922 (s), 2869 (m), 2864 (m), 1646 (s, NH_2 deformation), 1576 (s, NH_2

deformation), 1474 (w), 1394 (s), 1352 (w), 1046 (w), 1014 (m), 964 (w) (Figure 2-10). UV-vis (toluene) λ_{max}, nm: 311, 338 and 352 (Figure 2-10).

Melting-point analysis. Measurement was performed on a Mel-temp II Laboratory Device. As-synthesized $(CdSe)_{13}$(*n*-propylamine)$_{13}$ nanoclusters were dried as a yellowish-white solid prior to analysis. The solid sample was ground to powder in a glovebox, and only milligram samples were transferred into the melting-point capillary.

Absorption spectroscopy (UV-vis). UV-visible spectra were obtained from a Perkin Elmer Lambda 950 UV/Vis spectrometer at room temperature. The $(CdSe)_{13}$ solution was prepared by diluting one drop of as-made sample with a certain amount of toluene in a 1-cm path length quartz cuvette, and the same background solution was used prior to each measurement.

X-ray diffraction analysis (XRD). Data were collected from a Rigaku Dmax A vertical powder diffractometer with Cu Kα radiaton (λ= 1.5418 Å) and Materials Data Incorporated (MDI) automation. Typically, 3-5 mL as-synthesized nanoclusters were used to prepared the sample for XRD measurement. The purification process was as described below. As-synthesized nanoclusters (3 mL of dispersion) were diluted in pure toluene (5 mL) at room temperature. The mixture was allowed to stand on the bench for at least 15 min to settle the precipitate at the bottom of test tube. The colorless supernatant was discarded and the white slushy solid was redispersed in toluene (5 mL). This process was repeated once. The slushy solid was then dispersed in a small amount of toluene (< 1 mL) to form a highly concentrated mixture which was transferred onto a glass XRD sample holder. Measurement was conducted immediately after the residual solvent was evaporated. The diffractometer

step size was 0.04 ºand the retention time was 1 sec for the low-angle range 2.2 - 20° 2θ.

Transmission electron microscopy (TEM). TEM images of bundled and sheet-like $(CdSe)_{13}$ were collected from a JEOL-2000 FX microscope at 200 kV. Samples of $(CdSe)_{13}$ in primary amine were prepared as described below. For bundled samples, ten drops of the as-prepared sample were diluted into toluene (3 mL) in air. The mixture was then centrifuged in a bench-top centrifuge (700 *g*) for 5 min to form a white precipitate at the bottom of the test tube under a colorless supernatant. The supernatant was discarded, and the precipitate was then redispersed into toluene (3 mL). This purification process was conducted at least 5 times. In a final step, the white slushy solid was dispersed into toluene (3 mL) and shaken a few times to yield a white dispersion. For unbundled sheet-like samples, 30 min of centrifugation was required to obtain a white precipitate since unbundled samples had better dispersibility in toluene. Carbon-coated copper grids (Ted Pella, PELCO ® 300 Mesh Grids) were dipped into the solution and then removed to evaporate the solvent at ambient atmosphere. This process was repeated twice to load enough sample. TEM analysis was taken immediately after the grids were prepared. For $(CdSe)_{13}$ nanoclusters in ethylenediamine, the purification process was slightly different from those synthesized in primary amine, since en had lesser solubility in toluene, but higher solubility in polar solvents. Thus, methanol was used as a co-solvent in the purification process. The volume ratio of methanol to toluene was roughly 3:1.

Elemental analysis (EA). Data were collected by Galbraith Laboratories, Inc. Samples were prepared as gray slushy solids after purification.

References

(1) Kasuya, A., Sivamohan, R., Barnakov, Y. A., Dmitruk, I. M., Nirasawa, T., Romanyuk, V. R., Kumar, V., Mamykin, S. V., Tohji, K., Jeyadevan, B., Shinoda, K., Kudo, T., Terasaki, O., Liu, Z., Belosludov, R. V., Sundararajan, V., Kawazoe, Y. *Nat. Mater.* **2004**, *3*, 99.

(2) Wang, Y. Y., Liu, Y.H., Zhang, Y., Wang, F.D., Kowalski, P. J., Rohrs, H. W., Loomis, R. A., Gross, M. L., Buhro, W. E. *Angew. Chem., Int. Ed.* **2012**, *51*, 6154.

(3) Ben, M. D., Havenith, R. W. A., Broer, R., Stener, M. *J. Phys. Chem. C* **2011**, *115*, 16782.

(4) Kim, H. S., Jang, S.W., Chung, S.Y., Lee, S. *J. Phys. Chem. C* **2009**, *114*, 471.

(5) Fojtik, A., Weller, H., Koch, U., Henglein, A. *Ber.Bunsenges. Phys. Chem.* **1984**, *88*, 969.

(6) Peng, Z. A., Peng, X.G. *J. Am. Chem. Soc.* **2002**, *124*, 3343.

(7) Soloviev, V. N., Eichhofer, A., Fenske, D., Banin, U. *J. Am. Chem. Soc.* **2001**, *123*, 2354.

(8) Cumberland, S. L., Hanif, K.M., Javier, A., Khitrov, G.A., Strouse, G.F., Woessner, M., Yun, C.S. *Chem. Mater.* **2002**, *14*, 1576.

(9) Cossairt, M., Owen, J. S. *Chem. Mater.* **2011**, *23*, 3114.

(10) Kudera, S., Zanella, M. Giannini, C., Rizzo, A., Li, Y.Q., Gigli, G. Cingolani, R., Ciccarella, G., Spahl, W., Parak, W.J., Manna, L. *Adv. Mater.* **2006**, *19*, 548.

(11) Kui, Y. *Adv.Mater.* **2012**, *24*, 1123.

(12) Noda, Y., Maekawa, H., Kasuya, A. *Eur. Phys. J. D* **2010**, *57*, 43.

(13) Nguyem, K. A., Day, P. N., Pachter, R. *J. Phys. Chem. C* **2010**, *114*.

(14) Singh, T., Mountziaris, T. J., Maroudas, D. *Appl. Phys. Lett* **2012**, *100*, 053105.

(15) Dukes III, A. D., McBride, J. R., Rosenthal, S. J. *Chem. Mater.* **2010**, *22*, 6402.

(16) Liu, Y. H., Wang, F. D., Wang, Y. Y., Gibbons, P. C., Buhro, W. E. *J. Am. Chem. Soc.* **2011**, *133*, 17005.

(17) Liu, Y. H., Wayman, V. L., Gibbons, P. C., Loomis, R. A., Buhro, W. E. *Nano. Lett.* **2010**, *10*, 352.

(18) Yener, D. O., Sindel, J., Randall, C. A., Adair, J. H. *Langmuir* **2002**, *18*, 8692.

(19) Evans, C. M., Love, A. M., Weiss, E.A. *J. Am. Chem. Soc.* **2012**, *134*, 17298.

(20) Lambert, J. B., Shurvell, H.F., Verbit, L., Cooks, R.G., Stout, G.H. In *Organic Structural Analysis*; Macmillan Publishing Co.,Inc.: New York, 1976.

(21) Cossairt, B. M., Juhas, P., Billinge, S.L., Owen, J. S. *J. Phys. Chem. Lett.* **2011**, *2*, 3075.

(22) Ikawa N., O., Y.,Kimura, T. *J. Mater. Sci* **2008**, *43*, 4198.

(23) Beaulac, R., Ochsenbein, S.T., Gamelin, D.R. In *Nanocrystal Quantum Dots, Second Edition*; CRC Press; 2 edition: United States, 2010.

(24) Pachter, R., Nguyen, K. A., personal communication.

(25) Krätschmer, W., Lamb, L. D., Fostiropoulos, K., Huffman, D. R. *Nature* **1990**, *347*, 354.

Chapter 3
The Magic-Size Nanocluster $(CdSe)_{34}$ as a Low-Temperature Nucleant for Cadmium Selenide Nanocrystals; Room-Temperature Growth of Crystalline Quantum Platelets

Introduction

This chapter provides kinetic evidence indicating that the metastable, magic-size $(CdSe)_{34}$ nanocluster is near the critical-nucleus size for CdSe, and supports the growth of wurtzite CdSe *nanocrystal* platelets at room temperature (20-25 ^{o}C). Typical conditions for the synthesis of CdSe nanocrystals are temperatures above 200 ^{o}C.[57] To our knowledge, the growth of CdSe quantum platelets (QPs) reported here, via the intermediacy of $(CdSe)_{34}$ nanoclusters, constitutes the lowest temperature at which crystalline CdSe has been produced. We ascribe the low-temperature crystal growth to facile nucleation resulting from $(CdSe)_{34}$ being near to the critical size, such that the nucleation barrier has largely been surmounted in the formation of this magic-size nanocluster.

A crystal nucleation and growth process that is driven by a chemical reaction requires a proper ordering of nucleation, growth, and reaction barriers (activation energies, Scheme 3-1). According to the classic crystal-growth model,[58] nucleation barriers are higher than the activation energies for growth steps, such that conditions resulting in nucleation will also support crystal growth. We argue that the barrier for a monomer-generating chemical reaction must be *higher* than the nucleation barrier to support nanocrystal growth (Scheme 3-1, curve a). Here, monomers are defined as small $(CdSe)_n$ molecules or clusters. If the nucleation barrier *exceeds* the reaction barrier (Scheme 3-1, curve b), then monomer is produced by the reaction under conditions that preclude crystal formation, and thus amorphous aggregates and precipitates are formed instead.

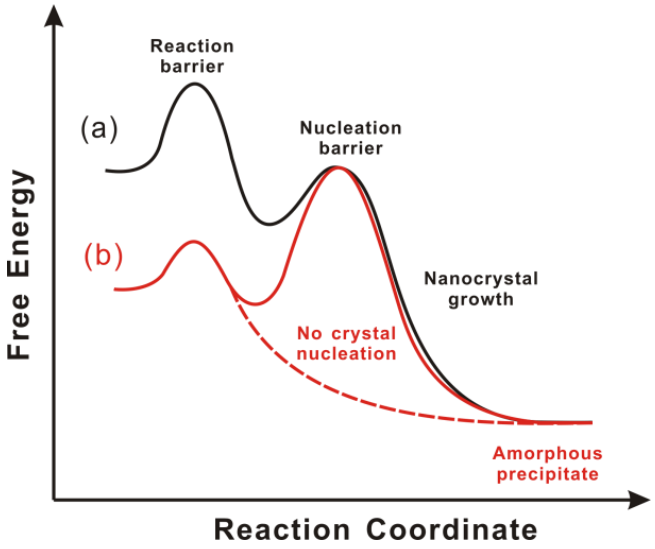

Scheme 3-1. Reaction-coordinate diagrams for alternate ordering of the monomer-generating-reaction and crystal-nucleation barriers. (a) The reaction barrier is higher than the nucleation barrier, and nanocrystal growth occurs on the black free-energy curve. (b) The reaction barrier is lower than the nucleation barrier, precluding nucleation and crystal growth. Instead, amorphous aggregates are formed on the red dashed curve.

We suspect that the high temperatures typically employed in semiconductor-nanocrystal syntheses reflect high nucleation barriers for assembling the critical-size nucleus, such that high-barrier chemical reactions are also required. However, if a critical-size nucleus could be assembled under milder conditions, then in principle semiconductor-nanocrystal nucleation and growth could be achieved at lower temperatures. We propose that $(CdSe)_{34}$ is near the critical size, such that its binary combination exceeds the critical size. If so, then the critical-nucleus size for CdSe under our conditions is in the range of $(CdSe)_{34}$ – $(CdSe)_{68}$.

We previously reported syntheses of CdSe quantum belts (nanoribbons) in lamellar, *n*-octylamine-bilayer templates at the comparatively mild temperatures of 70-80 ^{o}C.[59] Similar syntheses were also reported by Hyeon and coworkers.[60] We determined that the magic-size nanocluster $(CdSe)_{13}$ was an intermediate in the formation of the quantum belts, and later isolated and characterized a series of $[(CdSe)_{13}(\text{primary amine})_{13}]$ adducts.[61]

We now report that crystalline, wurtzite, CdSe quantum platelets (QPs; also known as nanoplatelets,[62] or quantum disks[63]) are formed at room temperature by employing di-*n*-alkylamine cosolvents, or by varying the primary-amine solvent. Reaction monitoring and mechanistic analyses indicate that $(CdSe)_{34}$ is the magic-size nanocluster intermediate under these conditions, which converts to CdSe QPs at room temperature by first-order kinetics with no detectable induction period. Alternatively, at 0 ^{o}C $(CdSe)_{34}$ converts to $(CdSe)_{13}$, which then requires temperatures above 40 ^{o}C to form CdSe QPs. Our interpretation of these results is that $(CdSe)_{34}$ is nearer to the CdSe critical-nucleus size.

A ligated derivative of $(CdSe)_{34}$ is obtained as a slushy solid that is stable indefinitely at 0 ^{o}C. We suggest that this derivative, $[(CdSe)_{34}(n\text{-octylamine})_{16}(\text{di-}n\text{-pentylamine})_2]$, may effectively function as CdSe crystal nuclei that may be stored in a bottle. Its use in templates of varying geometries may afford low-temperature routes to CdSe nanocrystals having other controlled morphologies.

Results and Discussion

Room-Temperature Growth of CdSe QPs. We previously reported that reaction of $Cd(OAc)_2 \cdot 2H_2O$ and selenourea in *n*-octylamine solvent at room temperature selectively produced magic-size $(CdSe)_{13}$ nanoclusters entrained within a spontaneously formed, double-lamellar, *n*-octylamine-bilayer template (eq 1, Scheme 2).[59] These intra-template $(CdSe)_{13}$ nanoclusters were subsequently converted to crystalline, CdSe quantum belts (QBs) at relatively mild temperatures (70-80 ^{o}C, eq 1). The lengths, widths, and thicknesses of the quantum belts were determined by the dimensions within the spontaneously formed,

double-lamellar templates (Scheme 3-2).[59] We sought to purposefully vary these dimensions by varying the nature of the amine solvent, and those efforts led to experiments using di-*n*-alkylamine cosolvents.

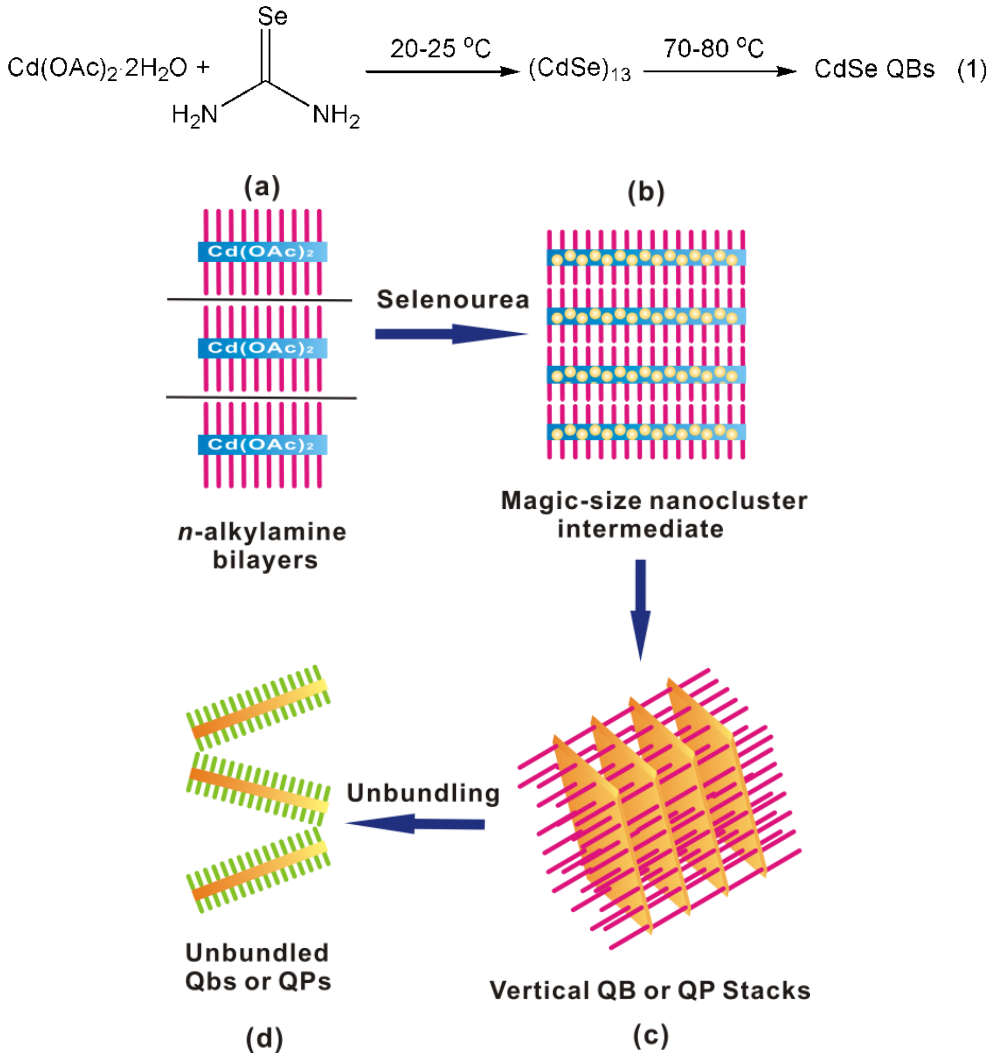

Scheme 3-2. Low-temperature growth of crystalline CdSe QPs within a double-lamellar, primary-amine bilayer template. (a) $Cd(OAc)_2$ and the primary-amine solvent forms a lamellar, amine-bilayer mesophase (blue and purple). (b) Magic-size $(CdSe)_{34}$ clusters are initially formed within the template when primary- and secondary- amine cosolvents are employed (yellow dots, blue and purple). (c) $(CdSe)_{34}$ clusters are converted to bundled QPs at room temperature in the cosolvent mixtures (orange and purple). (d) Addition of a long-chain primary amine results in the spontaneous exfoliation of the QPs by ligand exchange at room temperature (orange and green).

Reaction of $Cd(OAc)_2\ 2H_2O$ and selenourea in an *n*-octylamine, di-*n*-octylamine cosolvent mixture at room temperature gave a yellow precipitate, which contrasted with the white (colorless) [$(CdSe)_{13}$(*n*-octylamine)$_{13}$] isolated from the eq-1 reaction.[61a] The UV-visible spectrum of the yellow precipitate dispersed in toluene (Fig. 3-1) closely matched those previously obtained for CdSe QBs,[59] and could not be assigned to $(CdSe)_{13}$ or other magic-size nanoclusters. TEM images (Fig. 3-2) revealed the formation of pseudo-rectangular CdSe QPs having mean widths and lengths of 7 and 50 nm, respectively. Because the QPs have the electronic properties of quantum wells,[62a, 64] their spectrum depended only on thickness, and was effectively indistinguishable from those previously obtained for 1.8-nm thick QBs.[64] The sharp PL spectrum (Fig. 3-1) also matched those of the corresponding CdSe QBs.[64] Like the QBs, the QPs gave high PL quantum efficiencies (PL QE = 25%). We surmised that, in the cosolvent mixture, the reaction proceeded through magic-size nanocluster intermediates (see below) to CdSe QP nanocrystals at room temperature (eq 2).

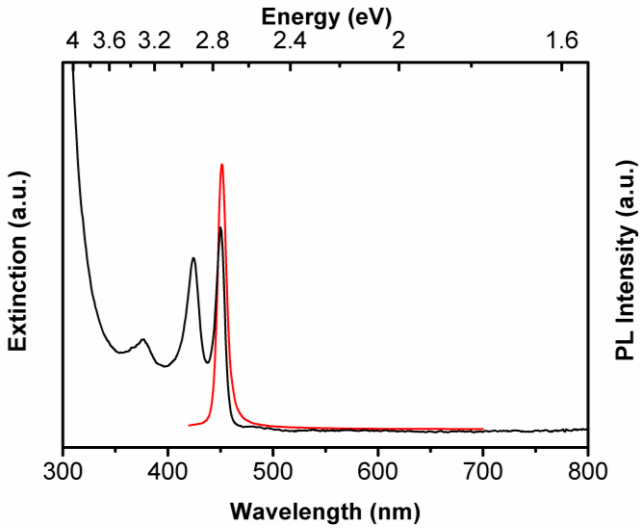

Figure 3-1. A UV-visible extinction spectrum in a toluene dispersion (black curve) and a photoluminescence spectrum in an oleylamine-toluene solution (12% w/w, red curve) of 1.8-nm thickness CdSe QPs.

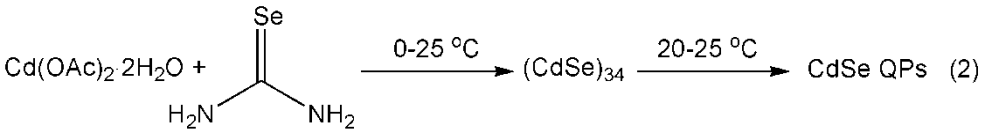

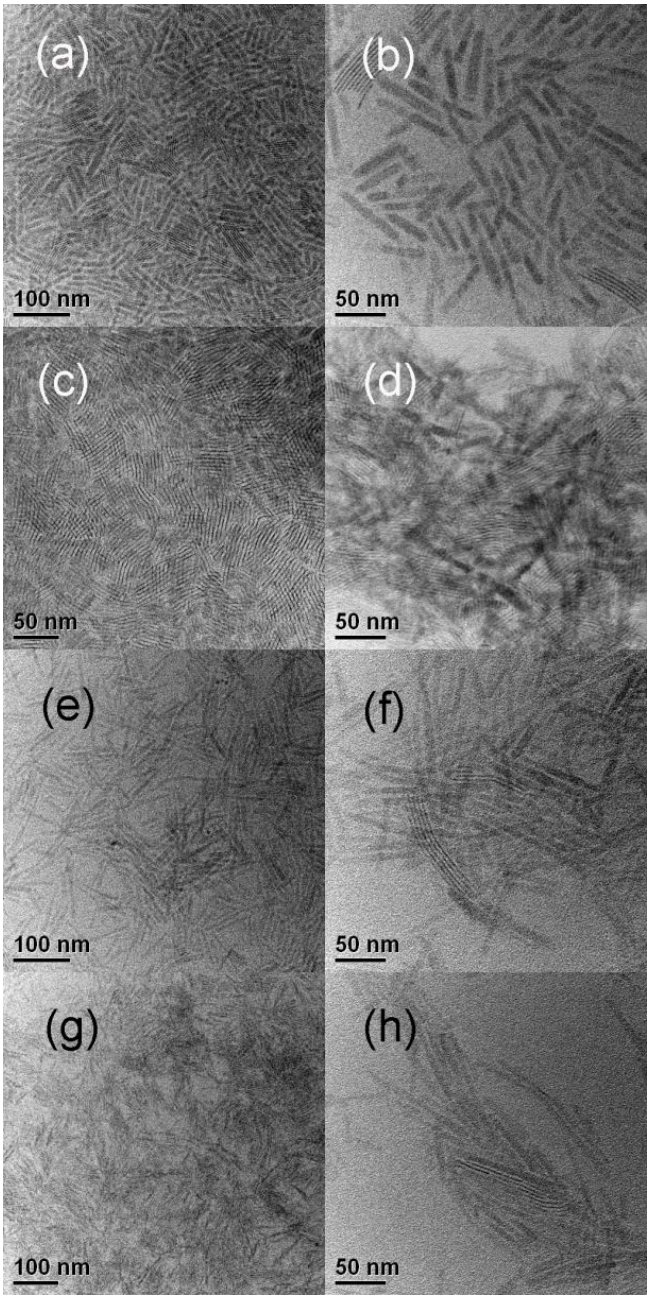

Figure 3-2. TEM images of CdSe QPs synthesized in *n*-octylamine and various di-*n*-alkylamine cosolvents. (a, b) di-*n*-octylamine, (c, d) di-*n*-pentylamine, (e, f) di-*n*-propylamine, (g, h) diethylamine. The right panels are at higher magnification.

We next sought to establish the crystallinity of the QPs grown by the room-temperature synthesis. An XRD pattern of the as-prepared material (Fig. 3-3 and 3-4) matched those previously obtained for wurtzite CdSe QBs.[64] Like those QBs, the QPs exhibited a lattice contraction associated with the surface tension of the thin nanocrystals.[60a] The lattice parameters extracted from the XRD data (a = 4.07 ± 0.02 Å, c = 6.82 ± 0.03 Å) were smaller than the bulk values (a = 4.30 Å, c = 7.02 Å) by nearly the same amounts as those of the QBs.[64]

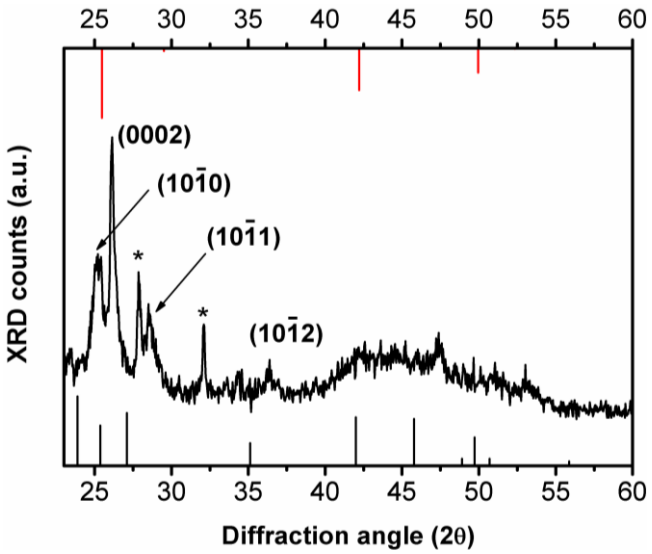

Figure 3-3. An XRD pattern of 1.8-nm thickness CdSe QPs. The black sticks are the peak positions for bulk CdSe in the wurtzite structure, and the red sticks are the peak positions for bulk CdSe in the zinc-blende structure. The indexed reflections for the wurzite QPs are shifted to higher angle than in the bulk pattern because of the lattice contraction (see the text and ref. 22). The asterisks identify unassigned peaks.

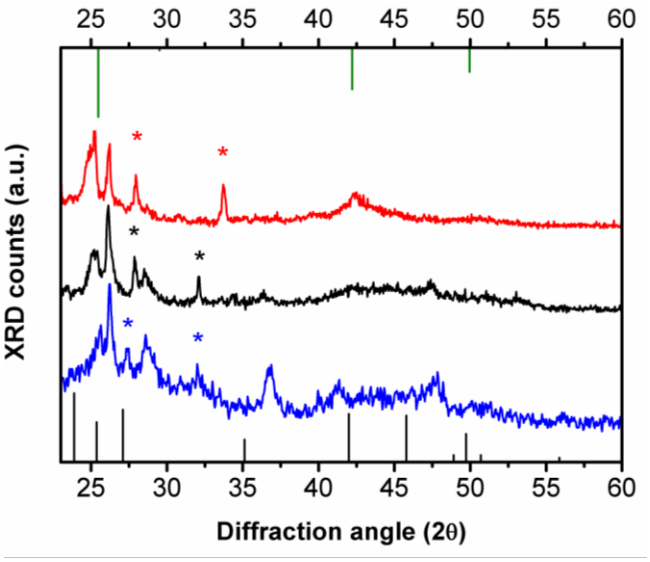

Figure 3-4. An XRD pattern of 1.4-nm thickness CdSe QPs (blue curve), 1.8-nm thickness CdSe QPs (black curve), and 2.2-nm thickness CdSe QPs (red curve). The black sticks are the peak positions for bulk CdSe in the wurtzite structure, and the green sticks are the peak positions for bulk CdSe in the zinc-blende structure. The indexed reflections for the wurzite QPs are shifted to higher angle than in the bulk pattern because of the lattice contraction (see the text and ref. 22). The asterisks identify unassigned peaks.

High-resolution TEM images were also consistent with crystalline CdSe QPs. Figure 3-5a views a stack of bundled QPs parallel to the QP edges (individual QPs are identified by arrows). The 0002 lattice spacings appearing as parallel fringes were clearly evident, and provided another measure of the lattice parameter $c = 6.86 \pm 0.04$ Å. A Fourier transform of the HRTEM image of the face of a QP was consistent with the $(11\bar{2}0)$ plane of wurtzite (Fig. 3-5b inset), as with the previously reported QBs.[64] The lattice parameter $a = 4.04 \pm 0.08$ Å was extracted from the fringe pattern in the image of the face (Fig. 3-5b).

Although amorphous nanoparticles may be crystallized under the electron beam in the TEM, we did not observe such a process; the QPs were crystalline from the outset of TEM observations. Thus, the sharp extinction and PL spectra (Fig. 3-1), the comparatively sharp XRD pattern that clearly indexed to wurtzite (Fig. 3-3), and the high-resolution TEM data (Fig. 3-5) all indicated that the CdSe QPs obtained from the room-temperature synthesis were

crystalline as formed.

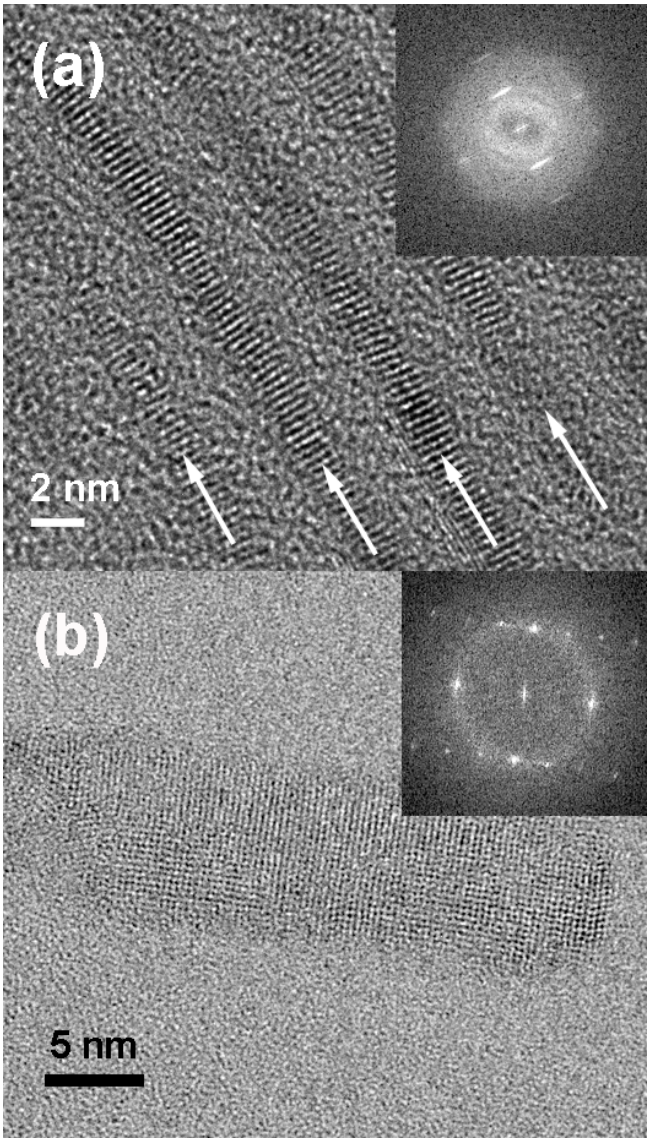

Figure 3-5. HRTEM images of the 1.8-nm thickness CdSe QPs. (a) Edge view of bundled QPs. (b) Face view of a single QP. Fast Fourier transforms of the images are inset. White arrows in (a) indicate the length dimension of the bundled QPs.

The QP synthesis was repeated using other combinations of primary and secondary amines. Experiments were conducted using *n*-octylamine and various di-*n*-alkylamine cosolvents. As summarized in Table 3-1, the secondary amine influenced the mean lengths of the QPs, without strongly affecting widths or thicknesses. Interestingly, the mean QP lengths were inversely proportional to the lengths of the alkyl groups on the di-*n*-alkylamine

cosolvent (Fig. 3-6). We do not understand the origin of this effect.

Table 3-1. Dependence of QP dimensions on the di-*n*-alkylamine cosolvent.

R_2NH; R=	Thickness (nm)	Width Range (nm)	Mean Length (nm)
n-octyl	1.8	5-10	50.3 ± 3.4
n-pentyl	1.8	5-10	63.2 ± 5.6
n-propyl	1.8	5-10	99.1 ± 6.5
ethyl	1.8	5-10	151 ± 6.8

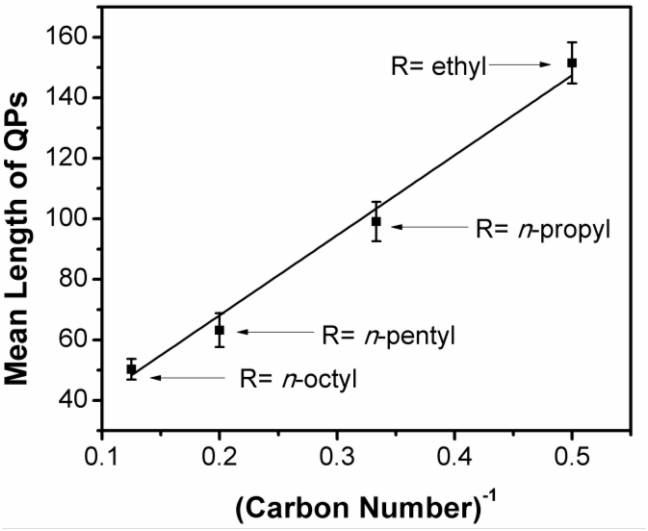

Figure 3-6. A plot of the QP mean length vs. the inverse of the carbon number of the di-*n*-alkylamine cosolvent alkyl chain. The carbon number is the number of carbon atoms in the alkyl chain

Another set of experiments was conducted in which the primary amine was varied and the secondary amine held constant. In contrast to the above, systematic dependences of the QP sizes or morphologies on the primary amine were not observed. However, the results established, as described below, that the top and bottom QP facets were predominantly passivated by the primary amine. The QPs were produced in bundled stacks that were derived from the lamellar, amine-bilayer templates in which they grew (see Scheme 3-2, Fig. 3-2, and Fig. 3-5a).[59] Consequently, the inter-QP spacing (*d* spacing) provided a measure of

the amine-bilayer thickness. Low-angle XRD patterns of QPs obtained from various primary-amine and di-ethylamine cosolvents are given in Fig. 3-7. The *d* spacing was dependent on the primary amine, and consistent with the lengths of the alkyl chains. The experiments described above in *n*-octylamine and di-*n*-alkylamine cosolvents gave *d* spacings consistent with *n*-octylamine, with no influence by the di-*n*-alkylamine (Fig. 3-8). These results required that the primary amine was responsible for lamellar, amine-bilayer template formation, and consequently, the large QP facets inherited primary-amine passivation from the growth template.

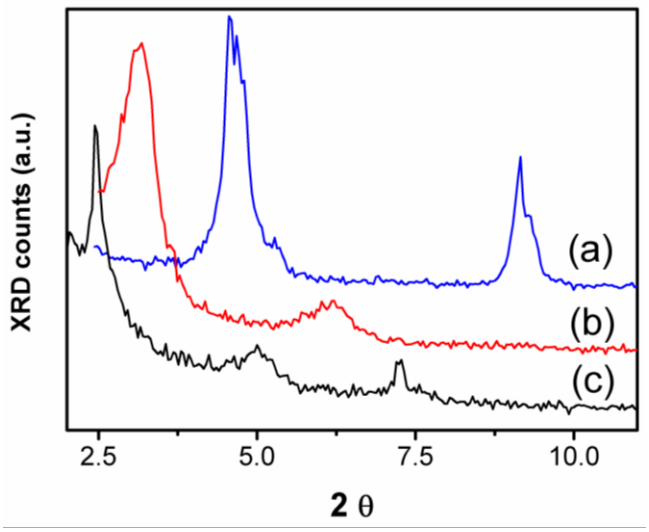

Figure 3-7. Low-angle XRD patterns of CdSe QPs synthesized in in diethylamine and various primary amine cosolvents. (a) *n*-pentylamine, (b) *n*-octylamine, (c) *n*-dodecylamine. These data demonstrate that the interlamellar *d* spacing within the template is determined by the primary amine, and thus that the top and bottom QP facets are passivated by the primary, rather than the secondary, amine.

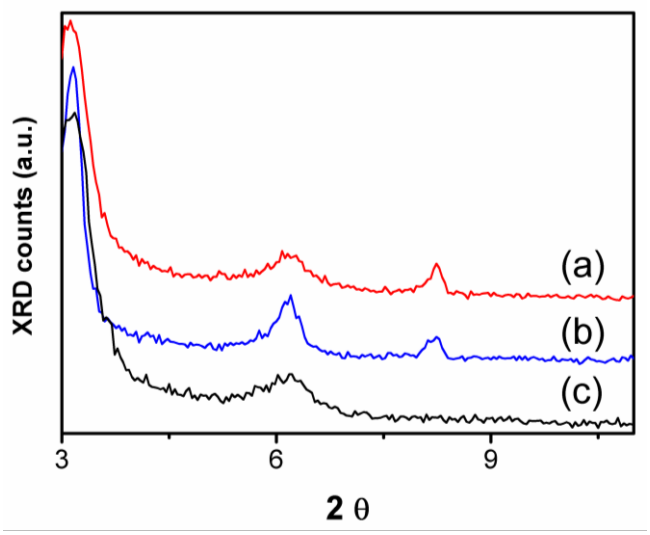

Figure 3-8. Low-angle XRD patterns of CdSe QPs synthesized in *n*-octylamine and various secondary amine cosolvents. (a) di-*n*-octylamine, (b) di-*n*-pentylamine, (c) diethylamine. These data demonstrate that the interlamellar *d* spacing within the template is not influenced by the secondary amine.

Many combinations of primary and secondary amines were investigated as cosolvents (Table 3-2). The best results were achieved when the length of the alkyl chain on the primary amine ($CH_3(CH_2)_nNH_2$) was equal to or longer than the length of the alkyl chains on the secondary amine $[CH_3(CH_2)_m]_2NH$ ($n \geq m$). When this empirical rule was violated, the UV-visible spectra of the resulting QPs were broadened and in some cases contained absorptions for platelets of other discrete thicknesses (Fig. 3-9).

Table 3-2. Various combinations of primary and second amines used as cosolvents

Primary Amine	Secondary Amine	Temperature	Thickness (nm)
Phenethyl	NA	40 °C	1.4
n-propyl *n*-pentyl *n*-octyl *n*-dodecyl	ethyl	RT	1.8
n-propyl *n*-pentyl *n*-octyl	*n*-propyl	RT	1.8
n-propyl *n*-pentyl *n*-octyl	*n*-pentyl	RT	1.8
n-propyl *n*-pentyl *n*-octyl	*n*-octyl	RT	1.8
n-octyl	*n*-octyl	70 °C	2.2

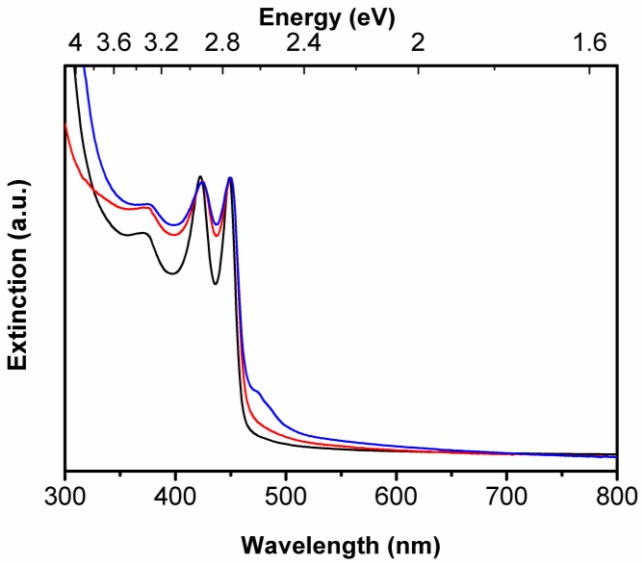

Figure 3-9. UV-visible extinction spectra in toluene dispersions of CdSe QPs synthesized in di-*n*-pentylamine and various primary amine cosolvents. Black curve: *n*-octylamine; blue curve: *n*-butylamine; red curve: *n*-propylamine.

Each of the syntheses conducted at room temperature and as described above gave QPs with a discrete thickness of 1.8 nm. The 2.2-nm thickness QPs were obtained with an *n*-octylamine, di-*n*-octylamine cosolvent mixture when the synthesis was conducted at 70 °C. Low-resolution TEM images of the QPs (Fig. 3-10a, b) showed widths of 10-20 nm, and a

mean length of 50 nm. A discrete QP thickness of 2.2 nm was established by high-resolution TEM (Fig. 3-10c). As expected,[59, 62b, c] the three characteristic QP absorptions were red-shifted from those of the 1.8-nm thickness QPs (Fig. 3-11). The 2.6-nm thickness QPs were obtained by conversion of the 2.2-nm thickness QPs at 90 ^{o}C. These thickness QPs gave the most red-shifted absorptions (Figure 3-11).

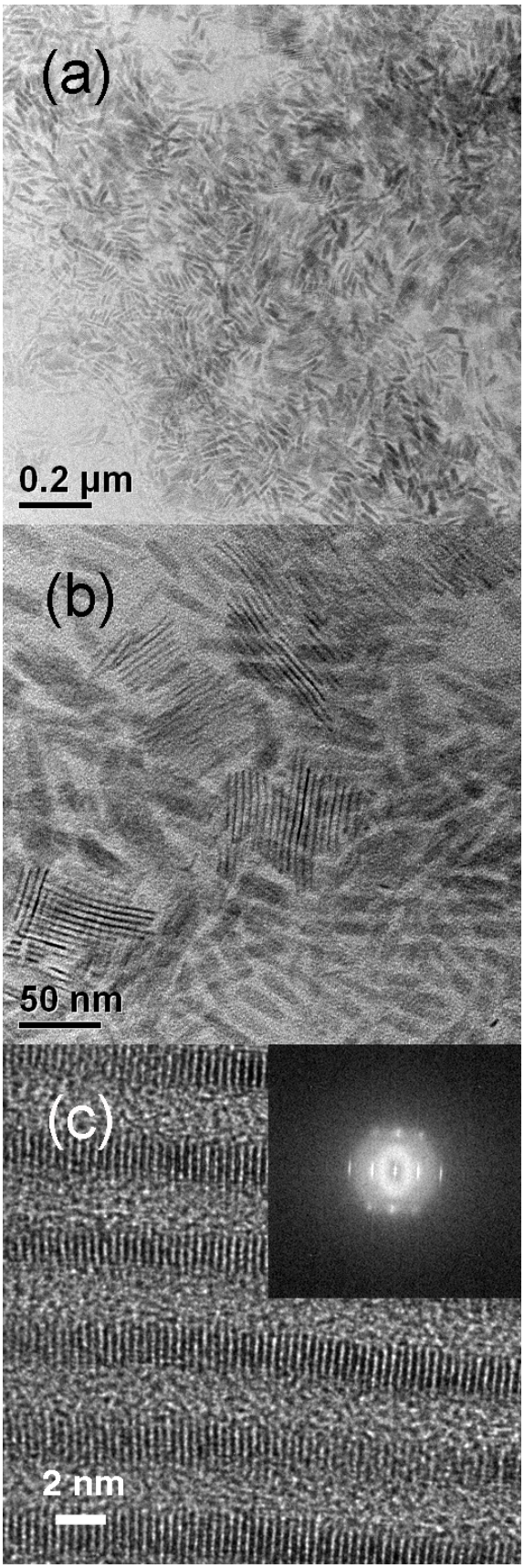

Figure 3-10. TEM and HRTEM images of bundles of the 2.2-nm thickness CdSe QPs. (a, b) TEM image and (c) HRTEM image of the QPs viewed from the edge. Inset is the fast Fourier transform of the image.

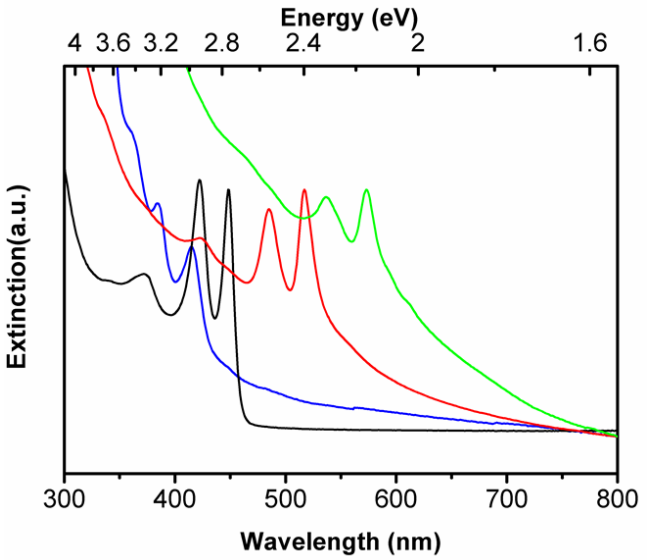

Figure 3-11. UV-visible extinction spectra in toluene dispersions of bundled 1.4-nm thickness CdSe QPs (blue curve), 1.8-nm thickness CdSe QPs (black curve), 2.2-nm thickness CdSe QPs (red curve) and 2.6-nm thickness CdSe QPs (green curve).

1.4-nm thickness QPs were obtained in the solvent 2-phenethylamine at 40 ^{o}C with no secondary-amine cosolvent. Low-resolution TEM images of the QPs (Fig. 3-12a, b) showed widths of 2-4 nm, and a mean length of 700 nm. We note that these lengths are closer to QBs along the QP – QB length spectrum than the cases discussed above. A discrete QP thickness of 1.4 nm was established by high-resolution TEM (Fig. 3-12c). In this case the three characteristic QP absorptions were blue-shifted from those of the 1.8-nm thickness QPs (Fig. 3-11). Thus, we have prepared CdSe QPs of four discrete thicknesses (1.4, 1.8, 2.2 and 2.6 nm). By comparison, Dubertret and coworkers have also prepared CdSe QPs of four discrete thicknesses.[62b]

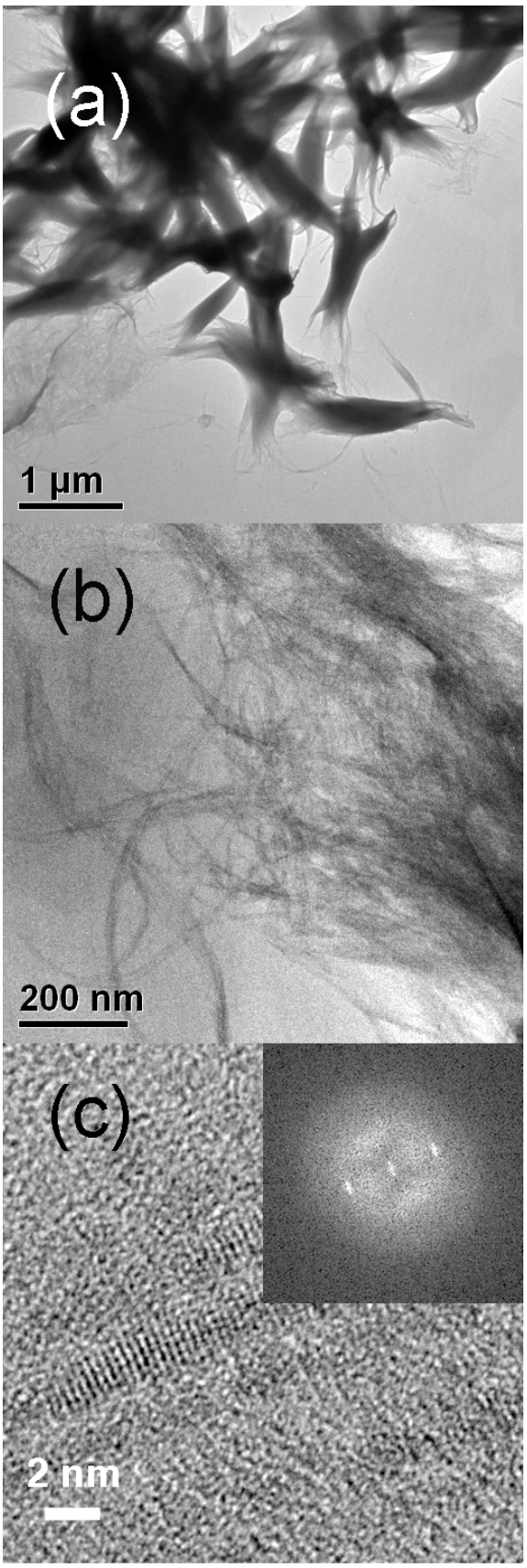

Figure 3-12. TEM and HRTEM images of bundles of 1.4-nm thickness CdSe QPs (1.4-nm thickness). (a, b) TEM image and (c) HRTEM image. Inset is the fast Fourier transform of the image.

Spectroscopic Monitoring of $(CdSe)_{34}$ Formation and Conversion. Our prior study established magic-size CdSe nanoclusters to be intermediates in the formation of CdSe QBs.[59] However, the eq-1 reaction in primary-amine solvents at room temperature gave $(CdSe)_{13}$,[61b] whereas the eq-2 reaction in primary-amine, secondary-amine cosolvents at room temperature gave CdSe QPs. Thus, we monitored the eq-2 reaction by UV-visible spectroscopy to determine if magic-size nanocluster intermediates participated in the reaction.

The eq-2 reaction was conducted in an *n*-octylamine, di-*n*-octylamine cosolvent mixture at room temperature as described above. An aliquot removed from the reaction mixture after 1 h gave the spectrum in Fig. 3-13, which has been previously assigned to the magic-size nanocluster $(CdSe)_{34}$.[12, 60d] In our prior study,[59] we mistakenly assigned one of these spectroscopic features to $(CdSe)_{66}$, but the results reported here (see below) demonstrate that the spectrum does indeed correspond to $(CdSe)_{34}$. A second aliquot was removed from the reaction mixture after 2 days, which gave the spectrum in Fig. 3-13, clearly assignable to CdSe QPs. Thus, spectroscopic monitoring suggested that $(CdSe)_{34}$ was an intermediate in the formation of the QPs; other magic-size nanoclusters were not observed.

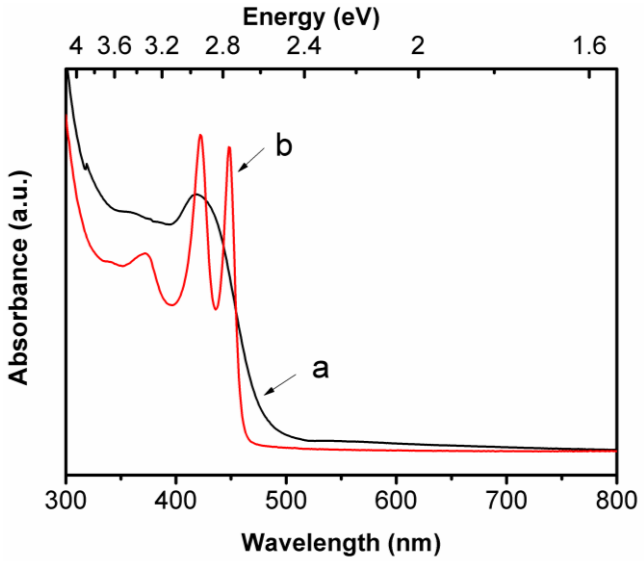

Figure 3-13. Spectral evolution upon transformation of $(CdSe)_{34}$ to 1.8-nm thickness CdSe QPs in an *n*-octylamine, di-*n*-octylamine cosolvent at room temperature. UV-visible extinction spectra of (a) $(CdSe)_{34}$ was observed after 1 h (black curve). (b) 1.8-nm thickness CdSe QPs (1.8-nm thickness) were observed after 2 days (red curve).

We then combined the eq-2 reactants in an *n*-octylamine, di-*n*-pentylamine cosolvent mixture at the lower temperature of 0 ^{o}C to determine if other nanocluster intermediates would be detected. (The reaction was conducted in a different cosolvent mixture because *n*-octylamine, di-*n*-octylamine mixtures are solid at 0 ^{o}C.) The spectrum of an aliquot taken after 12 h at 0 ^{o}C corresponded exclusively to $(CdSe)_{34}$ (Fig. 3-14a). The mixture was then monitored for over 1 month at 0 ^{o}C. The spectrum after 14 days corresponded to a mixture of $(CdSe)_{34}$ and $(CdSe)_{13}$ (Fig. 3-14b). After 1 month the $(CdSe)_{34}$ was completely converted to $(CdSe)_{13}$ (Fig. 3-14c). For a similar reaction conducted at 0 ^{o}C in a *n*-propylamine, di-*n*-ethylamine cosolvent mixture, the conversion of $(CdSe)_{34}$ to $(CdSe)_{13}$ was complete in about 1 week (Fig. 3-15). The results established that, under these conditions, $(CdSe)_{13}$ was more thermodynamically stable than $(CdSe)_{34}$, a conclusion supported by another observation (see below).

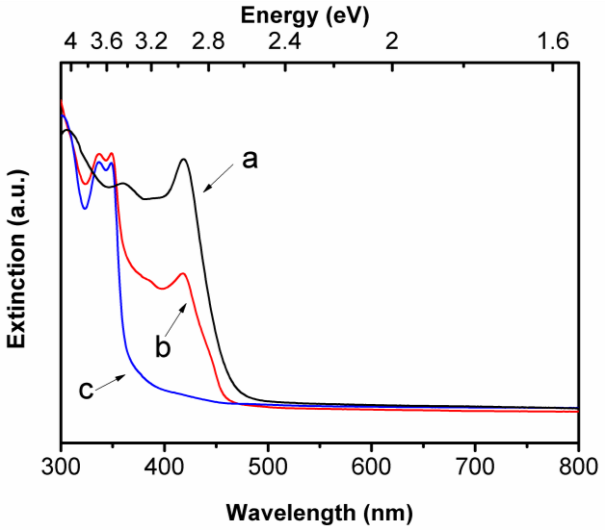

Figure 3-14. Spectral evolution upon transformation of $(CdSe)_{34}$ to $(CdSe)_{13}$ in an *n*-octylamine, di-*n*-pentylamine cosolvent at 0 ℃. UV-visible extinction spectra of (a) $(CdSe)_{34}$ after 12 h (black curve), (b) a mixture of $(CdSe)_{34}$ and $(CdSe)_{13}$ after 14 days, and (c) $(CdSe)_{13}$ after 1 month.

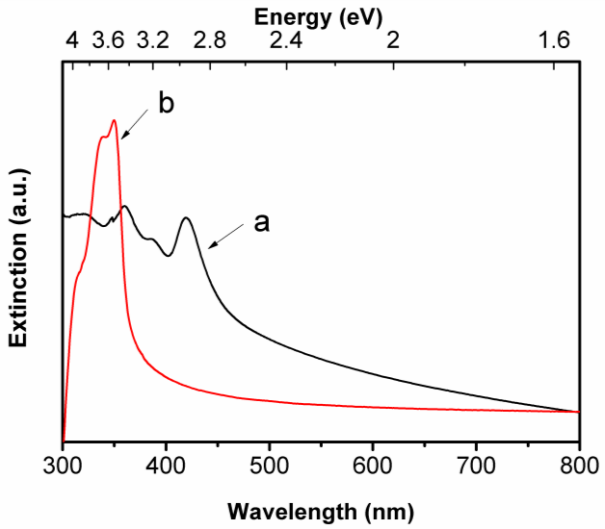

Figure 3-15. Spectral evolution upon transformation of $(CdSe)_{34}$ to $(CdSe)_{13}$ in *n*-propylamine and diethylamine cosolvent at 0 ℃. UV-Visible extinction spectra of (a) $(CdSe)_{34}$ after 6 h (black curve). (b) Mixture of $(CdSe)_{34}$ and $(CdSe)_{13}$ after 1 week.

We next sought to determine if the secondary-amine cosolvent was merely an inert diluent of the primary-amine component (an inert cosolvent), or was an active participant in the initial, selective formation of $(CdSe)_{34}$. Consequently, the room-temperature synthesis described above was conducted using the inert cosolvent 1-octadecene in place of the

secondary-amine cosolvent. Reaction monitoring after 5 min revealed the (unselective) formation of a mixture of $(CdSe)_{13}$ and $(CdSe)_{34}$, from which the $(CdSe)_{34}$ was gradually converted to a mixture of $(CdSe)_{13}$ and CdSe QPs. The results indicated that $(CdSe)_{34}$ is a kinetic product, and its conversion to the thermodynamically more stable $(CdSe)_{13}$ is actively hindered in the presence of a secondary amine.

The conversion kinetics of $(CdSe)_{34}$ to CdSe QPs was determined by UV-visible spectroscopy. Figure 3-16 shows the spectrum of $(CdSe)_{34}$ prepared in an *n*-octylamine, di-*n*-pentylamine cosolvent mixture at 0 ^{o}C, as described above, having a prominent absorption feature at 418 nm (black curve). Over the course of several hours at room temperature a sharp absorption feature emerged at 448 nm corresponding to the lowest-energy transition in the spectrum of CdSe QPs (red and blue curves). A second QP feature grew in at 423 nm, only slightly shifted from the 418-nm absorption of $(CdSe)_{34}$. The blue curve in Figure 3-16 corresponds to the fully transformed sample. The kinetics of the appearance of CdSe QPs and the disappearance of $(CdSe)_{34}$ were monitored by curve fitting of the 418-, 423-, and 448-nm absorptions (Fig. 3-17).

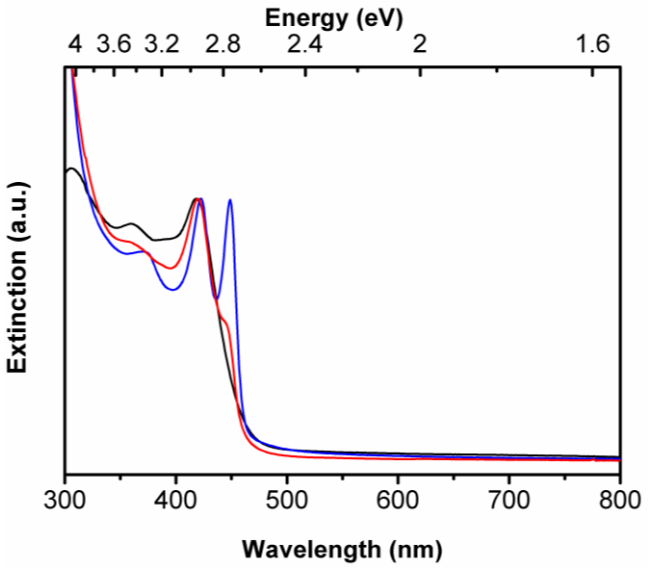

Figure 3-16. Spectral evolution upon transformation of $(CdSe)_{34}$ to CdSe QPs in an *n*-octylamine, di-*n*-pentylamine cosolvent. UV-visible extinction spectra of $(CdSe)_{34}$ at 0 ℃ (black curve) at time zero. A mixture of $(CdSe)_{34}$ and CdSe QPs was observed after 5 h (red curve). Fully transformed CdSe QPs were observed after 12 h (blue curve).

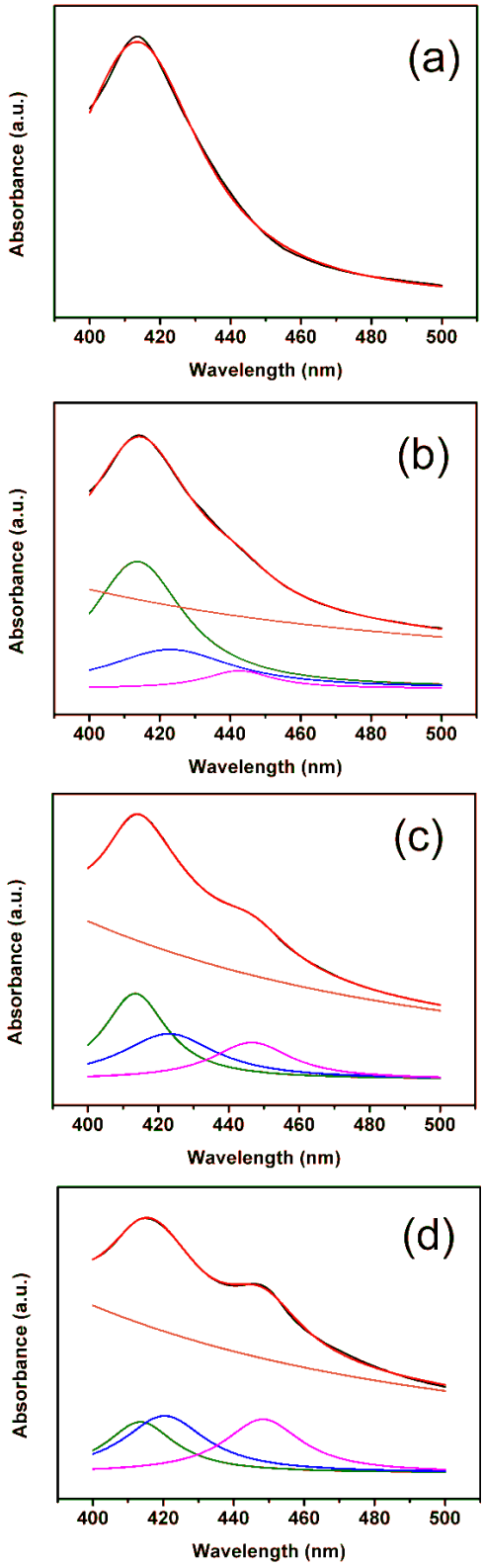

Figure 3-17. Curve fitting of the 418-nm absorption of $(CdSe)_{34}$, and the 423- and 448-nm absorptions of CdSe QPs observed during the conversion of $(CdSe)_{34}$ to CdSe QPs at room temperature at time (a) 0 h, (b) 5 h, (c) 10h, (d) 12h. In a-d the black curve is data, the red curve the fit, the orange curve the fitted background, and the green, blue, and magenta curves the fitted Lorentzians to the 418-, 423-, and 448-nm features, respectively. The areas of the Lorentzian fits were used in the kinetic analyses.

For kinetic analysis, $(CdSe)_{34}$ was diluted into a cosolvent mixture having a lower *n*-octylamine:di-*n*-pentylamine ratio (which increased the conversion rate). The appearance of CdSe QPs at room temperature was followed by the integrated area of the QP absorption at 448 nm derived from the curve fitting. As shown in Figure 20, the log of the integrated absorption vs. time was linear over three half-lives ($k_{obs} = (4.94 \pm 0.47) \times 10^{-5}$ s^{-1}; $t_{1/2} = 233 \pm 22.2$ min), establishing a first-order process. The inverse of the integrated absorption vs. time was non-linear, ruling out second-order kinetics (Fig. 3-18). Significantly, no induction (nucleation) period was observed; first-order QP growth began immediately upon warming the $(CdSe)_{34}$ solution to room temperature.

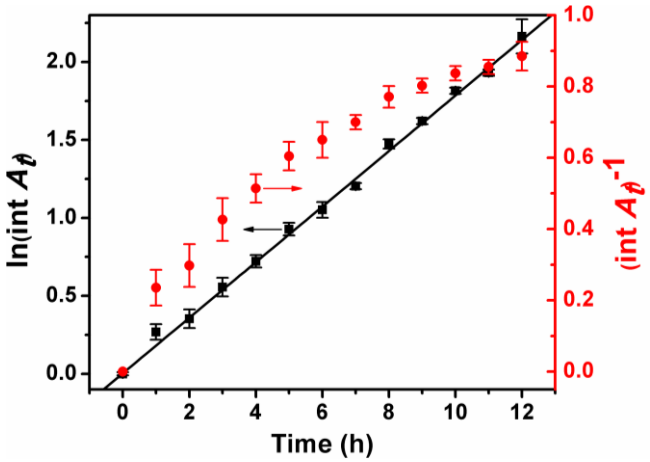

Figure 3-18. Kinetic data for the conversion of $(CdSe)_{34}$ to CdSe QPs at room temperature. The black squares in the first-order plot (left axis) were obtained from the integrated area of the 448-nm QP absorption (see the text). The black line is the linear least-squares fit. The data are also plotted for second-order kinetics (red points), which are nonlinear.

The kinetics were also analyzed by the disappearance of the fitted 418-nm $(CdSe)_{34}$ feature, and the appearance of the fitted 423-nm CdSe QP feature. These data also gave linear first-order plots over three half-lives (Figs. 3-19 and 3-20). The kinetic parameters for the disappearance of $(CdSe)_{34}$ were determined to be $k_{obs} = -(4.69 \pm 0.81) \times 10^{-5}$ s^{-1}; $t_{1/2} = 247 \pm 42.6$ min. This rate constant is, within experimental error, the opposite of that for the

appearance of CdSe QPs (see above), establishing that the conversion of $(CdSe)_{34}$ to CdSe QPs occurs without the accumulation of an intermediate. The appearance of CdSe QPs analyzed using the 423-nm feature gave $k_{obs} = (5.14 \pm 1.03) \times 10^{-5}$ s^{-1}; $t_{1/2} = 225 \pm 50.5$ min, in good agreement with the more-precise 448-nm data. Thus, the conversion was demonstrated to be a first-order process, with no induction period.

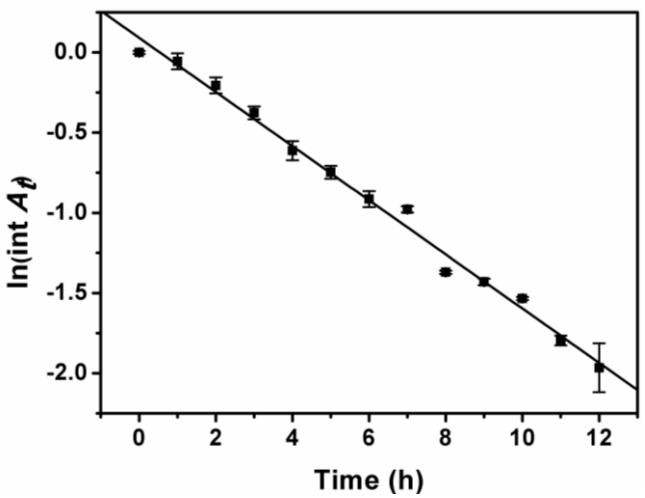

Figure 3-19. Kinetic data from conversion of $(CdSe)_{34}$ to CdSe QPs at room temperature. The first-order plot (black dots and curve) was constructed by monitoring decreasing of the integrated area of $(CdSe)_{34}$ absorbance at 418- nm derived from the curve fitting. A_t is the integrated area of $(CdSe)_{34}$ absorbance at 418-nm at time *t*.

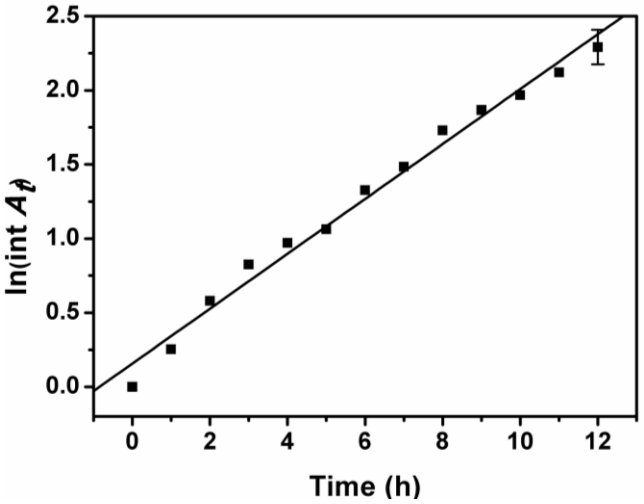

Figure 3-20. Kinetic data from conversion of $(CdSe)_{34}$ to CdSe QPs at room temperature. The first-order plot (black dots and curve) was constructed by monitoring increasing of the integrated area of the QP absorbance at 423- nm derived from the curve fitting. A_t is the integrated area of the QP absorbance at 423-nm at time *t*.

The room-temperature conversion rates of $(CdSe)_{34}$ were influenced by the alkyl-chain lengths on the primary and secondary amine cosolvents, and on the primary:secondary amine ratio. Shorter chain lengths on both the primary and secondary amines increased the rates of room-temperature conversion of $(CdSe)_{34}$ to CdSe QPs, presumably by enhancing diffusion. Lower primary:secondary amine ratios increased the room-temperature conversion rates of $(CdSe)_{34}$ to CdSe QPs, perhaps by the increased lability of secondary-amine ligands on $(CdSe)_{34}$. Higher primary:secondary amine ratios decreased the room-temperature conversion rates of $(CdSe)_{34}$ to CdSe QPs, by facilitating the conversion of $(CdSe)_{34}$ to $(CdSe)_{13}$. The cluster $(CdSe)_{13}$ seems particularly stabilized by primary-amine ligation.

Characterization of [$(CdSe)_{34}$(*n*-octylamine)$_{16}$(di-*n*-pentylamine)$_2$]. A ligated derivative of $(CdSe)_{34}$ as a slushy, greenish-yellow solid was obtained from preparations conducted in *n*-octylamine and di-*n*-pentylamine cosolvents. The UV-visible spectrum (Figure 3-21) matched those of $(CdSe)_{34}$ in Figures 3-14a and 3-16. Although no features assignable to other magic-size nanoclusters were detected, the presence of $(CdSe)_{13}$, $(CdSe)_{19}$, or $(CdSe)_{33}$ in small amounts was not ruled out, because their absorptions appear at shorter wavelengths and may have been obscured by the absorptions of $(CdSe)_{34}$.

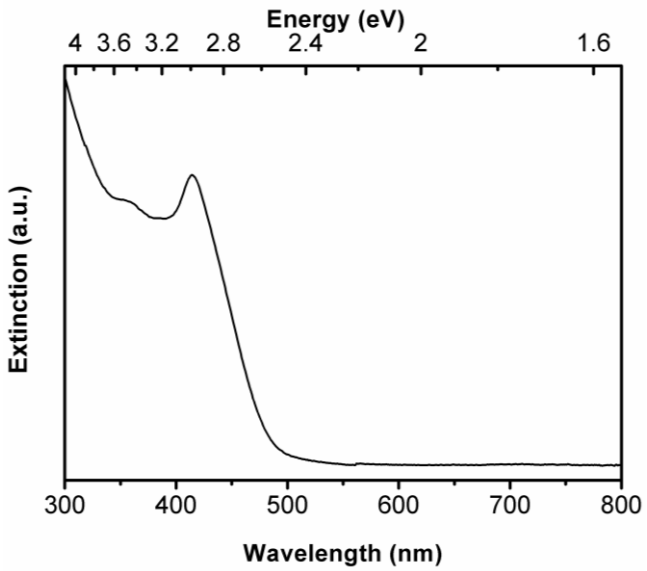

Figure 3-21. UV-visible extinction spectrum in toluene dispersion of isolated slushy, greenish-yellow [$(CdSe)_{34}$(*n*-octylamine)$_{16}$(di-*n*-pentylamine)$_2$] solid, prepared in *n*-octylamine and di-*n*-pentyalmine.

The isolated $(CdSe)_{34}$ specimen was further characterized by laser-desorption-ionization (LDI) mass spectrometry (see Figure 3-22). The spectrum contained a prominent ion centered at of *m/z* 6508 corresponding to the bare $(CdSe)_{34}$ nanocluster, indicating ligand desorption had occurred during the experiment. Peaks were also present for each fragment nanocluster $(CdSe)_x$, over the range x = 33-13. The $(CdSe)_{19}$ (*m/z* 3652) and $(CdSe)_{33}$ (*m/z* 6320) ions were slightly more abundant, and the $(CdSe)_{13}$ (*m/z* 2502) ion significantly more abundandant, than those of the other fragment ions. Significantly, the Figure-3-22 LDI mass spectrum differed markedly from that we previously reported for isolated [$(CdSe)_{13}$(*n*-octylamine)$_{13}$],[61a] and was consistent with a simple fragmentation process from the $(CdSe)_{34}$ parent. However, the data did not confirm that $(CdSe)_{34}$ had been isolated in a pure form, because of the presence of the fragment ions corresponding to the other magic sizes $(CdSe)_{13}$, $(CdSe)_{19}$, and $(CdSe)_{33}$. The results did establish that the sample was at least highly enriched in $(CdSe)_{34}$.

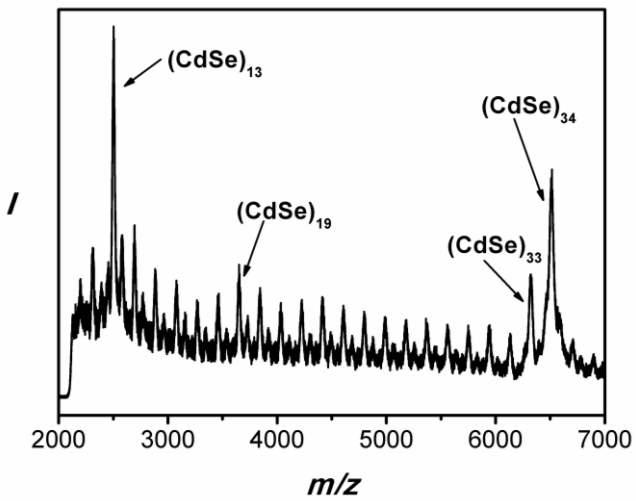

Figure 3-22. An LDI mass spectrum of [$(CdSe)_{34}$(*n*-octylamine)$_{16}$(di-*n*-pentylamine)$_2$]. The peaks for the magic-size CdSe nanoclusters are labeled.

The composition of the ligand shell was determined by calibrated mass spectrometry (see the Supporting Information). Analysis of the isolated $(CdSe)_{34}$ derivative gave an *n*-octylamine:di-*n*-pentylamine ligand ratio of 8.1 ± 0.5. That ratio was used to fit the C, H, and N analyses, providing an excellent fit to the formula [$(CdSe)_{34}$(*n*-octylamine)$_{16}$(di-*n*-pentylamine)$_2$]. On the basis of that formula, the $(CdSe)_{34}$ derivative was isolated in a 96% yield.

Nanoclusters of $(CdSe)_{34}$ dispersed in a di-*n*-alkylamine solvent were stable for over one month at room temperature. Isolated [$(CdSe)_{34}$(*n*-octylamine)$_{16}$(di-*n*-pentylamine)$_2$] was stable at room temperature for over one week, and stable for longer periods when stored at 0 ℃. A color change to reddish orange was observed when the greenish yellow [$(CdSe)_{34}$(*n*-octylamine)$_{16}$(di-*n*-pentylamine)$_2$] was subjected to a vacuum (0.1 torr) for longer than 12 h. However, after re-dispersion of such samples in toluene, analysis by UV-visible spectroscopy showed that the $(CdSe)_{34}$ nanocluster remained intact, with no evidence for other species.

Syntheses of flat CdSe nanocrystals may be categorized in two general types. In the first type, long-chain cadmium carboxylate precursors and high reaction temperatures (≥170 °C) are employed, yielding QPs having zinc-blende structures.[62a-c, 63] The second type, used here, employs simple cadmium salts and amine solvents at comparatively low temperatures (25 – 100 ℃), producing CdSe QPs and QBs having wurtzite structures.[59-60] The spectroscopic properties of the two types of flat CdSe nanocrystals are closely related, and produce comparable quantum-well absorption and emission spectra.[62a, 64]

The preparation of CdSe QPs having four discrete thicknesses, 1.4, 1.8, 2.2 and 2.6 nm, is described here. These discrete thicknesses correspond to integer numbers of CdSe monolayers. The flat II-VI nanocrystals having the WZ structure are oriented to express nonpolar (11-20) facets on the broad top and bottom surfaces, which having equal numbers of Cd and E atoms and are corrugated.[59-60, 65] (Figure 3-23). The broad surfaces are populated by Cd-E dimer units. The monolayers (MLs) here were described as the thinnest, contiguously bonded network, and so two atomic layers constitute a ML, as shown by the red lines in Figure 3-23. As a result, the WZ nanocrystal depicted in Figure 3-23 consists of 4 MLs, but has a thickness of 3.5 ML because of the corrugated nature of the ML. Thus CdSe QPs we reported here had 3.5, 4.5, 5.5 and 6.5 ML thicknesses by this definition, corresponding to 4, 5, 6, and 7 MLs, respectively. In comparison, Dubertret and coworkers[62b] have also prepared CdSe QPs having 4, 5, 6 and 7 monolayers, corresponding to discrete thicknesses of 1.2, 1.5, 1.8, and 2.1 nm. Because of the zinc blende structure and [100] orientation of Dubertret's QPs, the monolayer thickness is $a/2$ = 0.30 nm, explaining the apparent discrepancy between the monolayer and actual thicknesses of the two sets of

nanocrystals.

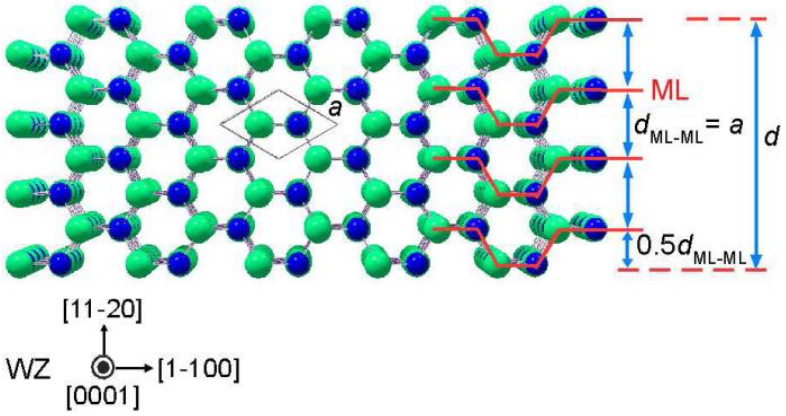

Figure 3-23. Schematic illustration of the atomic arrangements of the thin edges for pseudo-2D CdE (E = S, Se, Te) nanocrystals with WZ[59-60] crystal structures. Red solid lines identify the bi-atomic (Cd-E) monolayers (MLs). d_{ML-ML} and d are defined as the inter-ML distance and the thickness of the nanocrystals, respectively. *a* is the lattice parameter for the hexagonal unit cell. Approximately 4 MLs are identified.

We also report here the isolation of a ligated form of $(CdSe)_{34}$ having the empirical formula $[(CdSe)_{34}(n\text{-octylamine})_{16}(\text{di-}n\text{-pentylamine})_2]$. Our results may be compared to the room-temperature synthesis and isolation of *n*-octylamine-ligated $(CdSe)_{34}$ recently described by Sardar and coworkers.[66] Their nanocluster specimen is a bright yellow solid having a strong, narrow lowest-energy absorption feature at 418 nm, where we observed it in $[(CdSe)_{34}(n\text{-octylamine})_{16}(\text{di-}n\text{-pentylamine})_2]$ (Fig. 3-14a). The Sardar absorption spectrum also contains the two higher-energy features we also observed for our amine-ligated $(CdSe)_{34}$ (Fig. 3-14a). Moreover, Sardar and coworkers reported LDI mass spectra in which the $(CdSe)_{34}$ parent ion was the (most-intense) base peak. By recording LDI mass spectra at varying laser powers, they demonstrated that the lower-mass peaks present in the spectra were fragment ions of $(CdSe)_{34}$. The evidence strongly supported the isolation of a purified, ligated form of $(CdSe)_{34}$, which compares very closely to the $[(CdSe)_{34}(n\text{-octylamine})_{16}(\text{di-}n\text{-pentylamine})_2]$ isolated in this study.

Prominent, reasonably narrow absorption features having λ_{max} values in the range of 410-420 nm have been frequently observed in studies of small CdSe nanocrystals or nanoclusters. In some cases these absorptions have been assigned to magic-size nanocrystals or nanoclusters of unspecified stoichiometry.[57d, 67] More recently, such features have been assigned to $(CdSe)_{33}$, $(CdSe)_{34}$ mixtures,[12, 68] or exclusively to $(CdSe)_{34}$,[66] as in the present study. Cossairt and Owen isolated a nanocluster having a $Cd_{35}Se_{28}$ stoichiometry (with additional charge-balancing ligation), which also gave a prominent absorption at 418 nm.[47a] Whether a variety of small CdSe nanoclusters have absorption features in this range, or whether they equilibrate to the same absorbing species is presently unknown.

The ligand-to-cluster stoichiometry of $[(CdSe)_{34}(n\text{-octylamine})_{16}(\text{di-}n\text{-pentylamine})_2]$ is not readily reconciled with the theoretically proposed structures of the bare $(CdSe)_{34}$ nanocluster. Both cage[69] and core-cage[12] structures have been proposed for $(CdSe)_{34}$, the latter of which has a structure $(CdSe)_{6@28}$, in which 6 formula units of CdSe are in the core of an outer cage structure.[12] If one presumes amine binding to each surface Cd atom, the expected ligand:cluster ratio would be 34 or 28, respectively. That we have measured a ligand:cluster ratio of 18 suggests either that not all surface Cd atoms are ligated, or that the cluster structure has only 18 surface Cd atoms.

In our previously reported synthesis of $(CdSe)_{13}$ at room temperature in primary-amine solvents, an initial mixture of $(CdSe)_{13}$, $(CdSe)_{19}$, $(CdSe)_{33}$, and $(CdSe)_{34}$, was observed to equilibrate exclusively to $(CdSe)_{13}$.[61] The results here show that the same synthesis conducted in a primary-amine, secondary-amine cosolvent mixture initially produces $(CdSe)_{34}$ as the only detectable nanocluster product, at both room temperature and at 0 ℃

(Scheme 3). At the lower temperature, $(CdSe)_{34}$ eventually converts to $(CdSe)_{13}$, establishing that $(CdSe)_{13}$ is more thermodynamically stable under these conditions, and that $(CdSe)_{34}$ is a kinetic product (Scheme 3). The secondary-amine cosolvent slows the conversion of $(CdSe)_{34}$ to $(CdSe)_{13}$. The $(CdSe)_{13}$ generated from $(CdSe)_{34}$ in this manner requires temperatures above 40 ℃ for conversion to CdSe QPs; whereas this conversion occurs readily at room temperature from $(CdSe)_{34}$ (Scheme 3). Thus, $(CdSe)_{34}$ is a more potent nanocrystal precursor than is $(CdSe)_{13}$, because, we propose, $(CdSe)_{34}$ is much closer to the critical crystal-nucleus size.

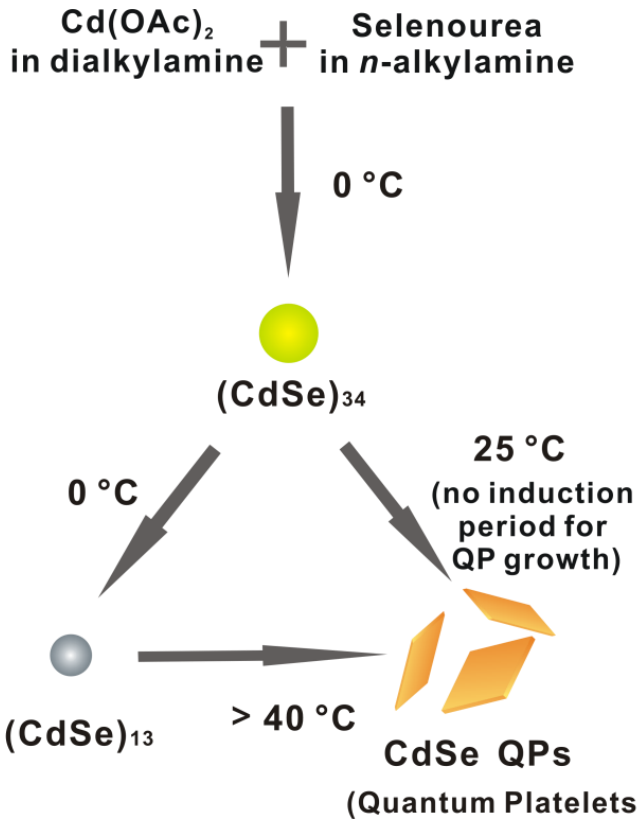

Scheme 3-3. Reaction scheme summarizing the formation and interconversion of CdSe nanoclusters and QPs in primary-amine, secondary-amine cosolvent mixtures. The nanocluster $(CdSe)_{34}$ (yellow-green dot) is the kinetic product at 0 ℃, which slowly converts to the thermodynamic product $(CdSe)_{13}$ (gray dot) at 0 ℃, or to crystalline, wurtzite CdSe QPs (orange platelets) at 25 ℃. Temperatures of > 40 ℃ are required to convert the $(CdSe)_{13}$ generated by the scheme to CdSe QPs.

The room-temperature conversion of $(CdSe)_{34}$ to CdSe QPs occurs by first-order kinetics, with no induction period. The result requires that crystal nucleation is instantaneous under these conditions. The first-order nature of the conversion suggests that an activated, partially ligated form of $(CdSe)_{34}$ is generated by a ligand dissociation in the rate-determining step, which either itself functions as a critical-size nucleus, or coalesces with a fully ligated $(CdSe)_{34}$ nanocluster in a subsequent fast bimolecular collision to exceed the critical-nucleus size. If correct, then the critical-nucleus size $(CdSe)_x$ is in the range of x = 34-68. Other experimental determinations of the CdSe critical-nucleus are in the diameter range of 1.2-1.6 nm.[57a, 70] For comparison, $(CdSe)_{34}$ has a theoretical diameter of 1.45 nm,[12] and thus the critical-size range we elucidate here is consistent with the prior measurements.

The very low temperature (25 ^{o}C) at which crystalline CdSe is produced here is surprising. The early syntheses of CdSe colloids conducted at room temperature within the water pools of inverse micelles gave materials of low crystallinity.[71] The crystalline coherence lengths in such colloids were shown to be much smaller than the particle sizes.[72] Consequently, most syntheses of CdSe nanocrystals are conducted at temperatures well above 200 ^{o}C.[57a-c, 57e, 72] For example, the now-classical CdSe quantum-dot synthesis in TOPO solvent reported by Murray, Norris, and Bawendi employed nanocrystal-growth temperatures of 230-260 ^{o}C.[72] Crystalline CdSe nanosheets[60b, 60d] and quantum belts[59] have been grown at the low temperatures of 100 ^{o}C and 45-80 ^{o}C, respectively, using *n*-octylamine as the solvent and via magic-size nanocluster intermediates. Crystalline CdSe quantum dots have been obtained under aqueous conditions at 55 ^{o}C.[73] To our knowledge, the synthesis of CdSe quantum platelets reported here, via the intermediacy of $(CdSe)_{34}$ nanoclusters, constitutes

the lowest temperature at which crystalline CdSe has been obtained.

In the Introduction, we argue that the monomer-generating reaction and crystal nucleation must be the two highest-barrier processes participating in semiconductor-nanocrystal growth. Therefore, we surmise that the high temperatures typically employed in nanocrystal synthesis reflect either high reaction barriers or high nucleation barriers with the use of conventional precursors and conditions. The very mild conditions for CdSe QP growth found here suggest that the nucleation barrier has nearly been surmounted in $(CdSe)_{34}$. Magic-size nanoclusters should be ideal precursors to support semiconductor-nanocrystal growth, and have been observed as reaction intermediates in nanocrystal synthesis[57b, 57e, 74] since the early observations of Henglein and coworkers.[75]

The critical sizes and stoichiometries of crystal nuclei are likely precursor and condition dependent. To our knowledge, a stoichiometry for the critical-size crystal nucleus has not been previously determined for CdSe, but has been reported to be $(ZnO)_{25\pm4}$ for ZnO and $(ZnSe)_{181\pm109}$ for ZnSe by Gamelin and coworkers.[76] Our phenomenological determination of $(CdSe)_{34\text{-}68}$ for CdSe is nicely consistent with these stoichiometries.

Conclusion

The magic-size nanocluster $(CdSe)_{34}$ has been shown to be a potent, room-temperature precursor for crystalline CdSe QPs. The first-order conversion kinetics suggest that the critical nucleus is achieved in a de-ligated form of $(CdSe)_{34}$, or in its combination with a second $(CdSe)_{34}$, which supports room-temperature crystal growth. The nanocluster is obtained in isolable form as $[(CdSe)_{34}(n\text{-octylamine})_{16}(\text{di-}n\text{-pentylamine})_2]$, which functions

as critical crystal nuclei that may be stored in a bottle.

The results suggest a strategy for making low-temperature nanocrystal synthesis more generally achievable. Magic-size nanoclusters like $(CdSe)_{34}$ of other compositions should be near to the critical size, and function as potent nucleating agents. Incorporating these into other mesophase-template geometries may provide low-temperature routes to well-passivated nanocrystals having a range of compositions and morphologies.

Experimental Section

Materials and General Procedures. Di-*n*-octylamine (+98%), di-*n*-pentylamine (99%), di-*n*-propylamine (99%), diethylamine (>99.5%), phenethylamine (≥ 99%), *n*-dodecylamine (≥ 99%), *n*-octylamine (+99%), *n*-pentylamine (+99%), *n*-propylamine (+98%), $Cd(OAc)_2 \cdot 2H_2O$ (>98%), tri-*n*-octylphosphine (TOP) (97%), and oleylamine (or cis-9-octadecenylamine, technical grade, 70%) were obtained from Sigma-Aldrich. Selenourea (99.9%, metal basis) was obtained from Alpha Aesar. All were used as received and stored under N_2. Toluene was obtained from Sigma-Aldrich (CHROMASOLV® for HPLC, ≥ 99.9%). TEM sample grids (Cu with holey carbon film) were obtained from Ted Pella, Inc.

All synthetic procedures were conducted under dry N_2, except the final washing steps, which were conducted in the ambient atmosphere. The reaction mixtures were not stirred. The synthetic products were generally stored as reaction mixtures, after addition of TOP (see below).

Analyses. Elemental analyses (C, H, N) were obtained from Galbraith Laboratories, Inc. (Knoxville, TN). UV-visible spectra were obtained from a Perkin Lambda 950 UV/Vis spectrometer. Photoluminescence (PL) spectra were obtained from a home-built fluorimeter. The XRD patterns were obtained from a Rigaku Dmax A vertical powder diffractometer with Cu Kα radiation (λ=1.5418 Å). Low-resolution TEM images were obtained from a JEOL 2000FX microscope operating at 200 KV. High-res TEM images were obtained from a JEOL JEM-2100F field emission (FE)- scanning transmission electron microscope. The LDI mass spectra were recorded on an ABI DE-STR MALDI TOF mass spectrometer.

The ligand-ratio study used an Agilent 7200 GC/q-TOF mass spectrometer (Agilent Technologies, Santa Clara, CA) in positive CI (chemical ionization) mode with methane as the CI reagent gas. Spectra were collected from 50-750 m/z. The samples for the calibration curve were introduced into the q-TOF MS through the GC column (Agilent HP-5MS) programmed at 80 ^{o}C for 2 min, 80-300 ^{o}C at 10 ^{o}C /min, and held at 300 ^{o}C for 6 min with 1.0 μl introduction and a split ratio of 3:1. Mass spectra of the $[(CdSe)_{34}(n\text{-octylamine})_{16}(\text{di-}n\text{-pentylamine})_2]$ samples were obtained by introduction via a thermal-desorption probe (TDP) with a short-fused silica transfer line and no column. The thermal profile of the probe was programmed with an initial hold at 40 ^{o}C for 2 min, followed by 40-300 ^{o}C at 10 ^{o}C /min, and then a hold at 300 ^{o}C for 8 min.

Analytical-Sample Preparation. For TEM analyses of CdSe QPs, an aliquot from a reaction mixture (0.1 mL) was diluted into toluene (3-5 mL) in air. The resulting dispersion was centrifuged in a bench-top centrifuge (700 *g*) for 5 min. The colorless supernatant was discarded, and the yellowish slush was re-dispersed into 3-5 mL toluene. This process was repeated an additional 4 times to ensure complete removal of TOP and the amine cosolvents. The slushy QP precipitate was dispersed in toluene (5 mL) for subsequent TEM analysis. TEM grids were dipped into the dispersion to prepare the TEM specimen. The TEM specimens were stable in air for at least one week.

For XRD analyses of CdSe QPs, a large aliquot from a reaction mixture (5 mL) was diluted into toluene (3-5 mL) in air. The purification process was the same as above, but the cycle was conducted a total of 3 times. The resulting yellow slushy QP precipitate was dispersed in toluene (0.5 mL). This concentrated dispersion was transferred onto a glass

XRD slide and dried in a fume hood (10 min). XRD patterns were recorded immediately after sample preparation.

For UV-visible spectroscopy, a small aliquot from a reaction mixture (40 μL) was diluted into toluene (12.5mL) in air. The diluted solution (2.5 mL) was used for absorption analyses. In each spectroscopic analysis, toluene was used in the reference cuvette. Absorption spectra were measured on the day of sample preparation.

For PL analyses of CdSe QPs, the reaction mixture was heated to 70 ^{o}C for 40 min prior to analysis. Toluene was purged with dry N_2 for at least 1 h, stored under N_2, and dried over molecular sieves prior to use. All sample-preparation processes were performed under N_2 at room temperature. In a typical process, a small aliquot (40 μL) from an annealed reaction mixture was diluted into an oleylamine-toluene solution (12% w/w, 12.5 mL). The dilute solution (2.5 mL) was transferred into a quartz cuvette, and the cuvette was then sealed by parafilm. An absorption spectrum was obtained immediately from the freshly prepared sample, followed by the collection of a PL spectrum within 10 min after collection of the absorption spectrum. The excitation wavelength for PL spectroscopy was set at 2.95 eV (420 nm). An oleylamine-toluene solution (12% w/w) was used in the reference cuvette.

Mass-spectral Determination of the Ligand Ratio in [$(CdSe)_{34}$(*n*-octylamine)$_{16}$(di-*n*-pentylamine)$_2$]. A calibration curve for the instrument response was obtained as follows. Stock solutions (1 mM) of *n*-octylamine and di-*n*-pentylamine were prepared in acetonitrile. These stock solutions were diluted to a total concentration of 200 μM for integer ligand ratios of 1:9 to 9:1 of *n*-octylamine to

di-*n*-pentylamine. Mass spectra in the CI mode (CH_5^+) were obtained in triplicate for each solution after on-line GC separation. Four ion signals were retrieved as extracted-ion chromatograms (EICs) in the range of *m*/*z* = 100-200, corresponding to *n*-octylamine, di-*n*-pentylamine, and two isomers of di-*n*-pentylamine. Signal for the ions of *m*/*z* 130.1590, 100.1121, 156.1747, and 186.2216, which were the $[M + H]^+$ of octylamine, and the $[M + H - C_4H_{10}]^+$, $[M + H - H_2]^+$ and $[M + C_2H_5]^+$ of dipentylamine, respectively, were used to quantify the four analyses. The selected ions are derived from the target amines and have little contamination (< 2%), from other sources. *n*-Octylamine:dipentylamine signal ratios were determined from the *n*-octylamine and sum of the three dipentylamine signals at each concentration. The signal ratio plotted linearly against the concentration ratio, yielding the calibration plot.

Samples of $[(CdSe)_{34}(n\text{-octylamine})_{16}(\text{di-}n\text{-pentylamine})_2]$ were subjected to mass-spectral analysis in the CI mode (CH_5^+) by the temperature-programmed desorption described earlier in the experimental section. The integrated signal ratio was determined to be 3.7 ± 0.24, corresponding to an actual ratio of 8.1 ± 0.5. Consequently the *n*-octylamine:di-*n*-pentylamine ligand ratio of 8:1 was used to fit the elemental-analysis data (see above), yielding the molecular formula $[(CdSe)_{34}(n\text{-octylamine})_{16}(\text{di-}n\text{-pentylamine})_2]$.

Direct Synthesis of 1.8-nm Thickness CdSe QPs. In a typical procedure, $Cd(OAc)_2\ 2H_2O$ (65 mg, 0.24 mmol) was dissolved in di-*n*-octylamine (5.7 g, 24 mmol) in a septum-capped Schlenk tube and placed in a bench-top sonicating bath (10 min) to achieve dissolution. In a glove box, selenourea (50 mg, 0.41 mmol) was dissolved in *n*-octylamine (1.2 g, 9.3 mmol) in a septum-capped amber vial. The vial was removed from the glove box

and placed in a bench-top sonicating bath (10 min) to achieve dissolution.

The selenourea solution was injected into the [$Cd(OAc)_2$ $2H_2O$] solution at room temperature (20-25 ^oC). The colorless reaction mixture became cloudy within 10 s, viscous and light green within 5 min, cloudy and yellow green within 60 min, and cloudy and light yellow at longer reaction times. After 2 h, the mixture was nearly clear and colorless with a light-yellow precipitate. After 2 days, the yellow precipitate remained in the presence of a light-red supernatant, the color of which was due to a Se side product from $(CdSe)_{34}$ formation. TOP (0.25-0.50 mL) was injected to scavenge the Se side product through the formation of colorless (n-octyl)$_3$P=Se. The light-yellow precipitate of bundled CdSe QPs was then stored at room temperature in the reaction mixture under N_2 for further analyses.

Direct Synthesis of 2.2-nm Thickness CdSe QPs. The procedure was conducted in the same manner as that for the 1.8-nm thickness CdSe QPs (see above), except the amount of *n*-octylamine used (2.4 g, 18 mmol), and the reaction temperature, which was raised to 70 ^oC. The color changes occurred more rapidly, from colorless (0 min) to viscous and yellow (10 s), cloudy and orange (1 min), and cloudy and orange-red (>120 min). After the reaction mixture stood for 2 days at 70 ^oC, the CdSe QPs were deposited as an orange-red precipitate in the presence of a red supernatant. TOP (0.25-0.50 mL) was injected to scavenge the Se side product from $(CdSe)_{34}$ formation responsible for the red coloration of the supernatant, which became colorless. The dispersion of bundled CdSe QPs was then stored at room temperature in the reaction mixture under N_2 for further analyses.

Synthesis of 2.6-nm Thickness CdSe QPs. CdSe QPs having a thickness of 2.2 nm were prepared at 70 ^oC as described above. The reaction mixture was then warmed to 90

^{o}C , and held at that temperature for 2 days. After 1 day, the color of the mixture changed from orange-red to dark red. The 2.6-nm CdSe QPs were deposited as a dark-red precipitate under a red supernatant. TOP (0.25-0.50 mL) was injected to scavenge the selenium side product, forming a colorless solution. The dispersion of bundled CdSe QPs was then stored at room temperature in the reaction mixture under N_2 for further analyses.

Direct Synthesis of 1.4-nm thickness CdSe QPs. In a typical procedure, $Cd(OAc)_2$ $2H_2O$ (65 mg, 0.24 mmol) was dissolved in phenethylamine (5.74 g, 47 mmol) in a septum-capped Schlenk tube and heated in a 70 ℃ oil bath (1 h) to dissolve the cadmium precursor. In a glove box, selenourea (50 mg, 0.41 mmol) was dissolved in phenethylamine (1.2g, 9.9 mmol) in a septum-capped amber vial. The vial was removed from the glove box and placed in a bench-top sonicating bath (10 min) to achieve dissolution of the selenourea.

The selenourea solution was injected into the [$Cd(OAc)_2$ $2H_2O$] solution at 40 ^{o}C. The clear, colorless reaction mixture became clear and light yellow within 1 h, viscous and white (60-90 min), and then cloudy and white-yellow (> 90 min). After 2 h, the solution became nearly clear and colorless upon formation of a white-yellow precipitate. After 2 days, CdSe QPs were deposited as a white-yellow precipitate in the presence of a light-red supernatant. TOP (0.25-0.50 mL) was injected to scavenge the Se side product from $(CdSe)_{34}$ formation responsible for the red coloration of the supernatant, which became colorless. The white-yellow precipitate of bundled CdSe QPs was then stored at room temperature in the reaction mixture under N_2 for further analyses.

Preparation of [$(CdSe)_{34}$(*n*-octylamine)$_{16}$(di-*n*-pentylamine)$_2$]. In a typical procedure, $Cd(OAc)_2$ $2H_2O$ (65 mg, 0.24 mmol) was dissolved in di-*n*-pentylamine (5.74 g,

36 mmol) in a septum-capped Schlenk tube, and then was stored in an ice bath (0 ℃) placed inside a refrigerator. In a glove box, selenourea (50 mg, 0.41 mmol) was added to *n*-octylamine (1.2 g, 9.3 mmol) in a septum-capped amber vial. The vial was removed from the glove box and placed in a bench-top sonicating bath (10 min) to achieve dissolution of the selenourea.

The selenourea solution was injected into the $Cd(OAc)_2$ $2H_2O$ solution at 0 ℃. The clear, colorless reaction mixture became viscous and light yellow within 6 h, cloudy and yellow within 8 h, and cloudy and green-yellow at longer times (0 ℃). After 18 h at 0 ℃, $(CdSe)_{34}$ was formed as a green-yellow precipitate mixed with colorless supernatant. TOP (0.25-0.50 mL) was injected to scavenge excess selenourea.

The greenish-yellow precipitate was separated using a bench-top centrifuge (700 *g*, 30 s) at room temperature, and the colorless supernatant was discarded. The remaining greenish-yellow slush was re-dispersed into 3-5 mL toluene. This purification process was repeated, for a total of two such cycles, yielding $[(CdSe)_{34}$(*n*-octylamine)$_{16}$(di-*n*-pentylamine)$_2]$ as a slushy, greenish-yellow solid after drying in vacuo for 12 h (0.061 g, 95.7%). UV-Visible (toluene) λ_{max}, nm: 360, 390, 418 (Figure 11). MS *m/z* (relative area, assignment): 6508.2572 (100%, $(CdSe)_{34}$), 6319.5733 (42.6%, $(CdSe)_{33}$), 3651.5768 (17.0%, $(CdSe)_{19}$), 2502.4747 (52.4%, $(CdSe)_{13}$). Anal Calcd for $[(CdSe)_{34}$(*n*-octylamine)$_{16}$(di-*n*-pentylamine)$_2]$: C, 20.00; H, 3.94; N, 2.84. Found, C, 19.94; H, 3.95; N, 2.93. All values are given as percentages.

$[(CdSe)_{34}$(*n*-octylamine)$_{16}$(di-*n*-pentylamine)$_2]$ was generally used immediately for analyses or further reactions. The compound was stable at room temperature for at least 24

h under N_2, and for longer than one month at 0 ℃ under N_2.

Other di-*n*-alkylamine derivatives of $(CdSe)_{34}$ were prepared under the same general conditions, expect for the reaction cosolvents employed. Di-*n*-propylamine or diethylamine were used to replace di-*n*-pentylamine for the $Cd(OAc)_2$ $2H_2O$ solution, while *n*-octylamine was used for the selenourea solution. The purification procedure was the same as that used above.

Conversion of $(CdSe)_{34}$ Nanoclusters to CdSe QPs. The preparation of $(CdSe)_{34}$ was conducted as described above. The reaction mixture was then removed from the ice bath and stored at room temperature (20-25 ^{o}C) an additional 12 h. The reaction mixture was periodically monitored by UV-visible spectroscopy to determine the extent of the conversion, which was found to be complete after 12 h. CdSe QPs were deposited as a light-yellow precipitate in the presence of a light-red supernatant. TOP (0.5-1.0 mL) was injected into the reaction mixture to scavenge the red selenium side product from $(CdSe)_{34}$ formation, resulting in a colorless supernatant. The conversion of $(CdSe)_{34}$ to CdSe QPs was accelerated by adding additional di-*n*-pentylamine to the reaction mixture at room temperature after the formation of $(CdSe)_{34}$.

Measurement of the $(CdSe)_{34}$-to-CdSe-QPs Conversion Kinetics. A $(CdSe)_{34}$ sample was prepared as described above. An aliquot (26mg) taken from the reaction mixture was diluted into a di-*n*-pentylamine (2.5 g) and *n*-octylamine (0.07 g) mixture in a quartz cuvette at room temperature (20-25 ^{o}C). UV-visible spectra were collected in the wavelength range 400-500 nm at 1 h intervals. During data collection the cuvette was stirred by a small stirring bar.

The 418-nm absorption of $(CdSe)_{34}$ and the 423- and 448-nm absorptions of CdSe QPs were extracted from the spectra by non-linear least-squares fitting using Origin software (http://originlab.com/). The initial (t = 0 h) spectrum was fit by a single Lorentzian function, yielding the center position of the 418-nm absorption. The final (t = 12 h) was fit with three Lorentzian functions, the first centered at 418 nm, and a background-scattering function (A/λ^4, where A was an adjustable parameter), yielding the center positions of the 423- and 448-nm QP absorptions. All of the intermediate spectra were fit with three Lorentzian and the one background-scattering functions, with the Lorentzians initially centered at 418, 423, and 448 nm. These peak centers were refined only in the final stages of fitting.

The peak areas determined from the non-linear least-squares fits were used for the kinetic analyses. All three absorptions gave first-order plots of absorption peak area vs. time over three half-lives. The error in the slope of the plots was determined by conducting three kinetic trials, and observing the range in the integrated peak areas in the final (t = 12 h) spectra. The range of slopes that accommodated these final values was assigned as the error in the slopes. The kinetic parameters k_{obs} and $t_{1/2}$ were extracted from the slopes, and their errors determined by propagation in the normal manner. These values are reported in the Results section.

Conversion of $(CdSe)_{34}$ to $(CdSe)_{13}$ Nanoclusters. The preparation of $(CdSe)_{34}$ was conducted as described above. The reaction temperature equilibrated near 0 ℃ in the refrigerator, even after the ice in the bath melted. The reaction mixture was periodically monitored by UV-visible spectroscopy to determine the extent of the conversion. When di-*n*-pentylamine was used as the cosolvent, the complete conversion required longer than 1

month, during which the greenish-yellow precipitate gradually changed to white with formation of a small amount of black precipitate, which was a selenium side product. TOP (0.5-1.0 mL) was injected into the reaction mixture, whereupon the black solid disappeared, leaving $(CdSe)_{13}$ as a white precipitate. When diethylamine or di-*n*-propylamine were used as the cosolvent, the conversion of $(CdSe)_{34}$ to $(CdSe)_{13}$ was more rapid, and completed in 2-3 weeks. The conversion was also accelerated by adding additional *n*-octylamine to the reaction mixture after the formation of$(CdSe)_{34}$.

References

(1) Bullen, C. R., Mulvaney, P. *Nano Lett.* **2004**, *4*, 2303.

(2) Cumberland, S. L., Hanif, K.M., Javier, A., Khitrov, G.A., Strouse, G.F., Woessner, S.M., Yun, C.S. *Chem. Mater.* **2002**, *14*, 1576.

(3) Lovingood, D. D., Oyler, R.E., Strouse, G.F *J. Am. Chem. Soc* **2008**, *130*, 17004.

(4) Murray, C. B., Norris, D.J., Bawendi, M.G. *J. Am. Chem. Soc* **1993**, *115*, 8706.

(5) Peng, Z. A., Peng, X.G. *J. Am. Chem. Soc.* **2002**, *124*, 3343.

(6) LaMer, V. K., Dinegar, R. H. *J. Am. Chem. Soc.* **1950**, *72*, 4847.

(7) LaMer, V. K. *Ind. Eng. Chem.* **1952**, *44*, 1270.

(8) Reiss, H. J. *J. Chem. Phys.* **1951**, *19*, 482.

(9) Sugimoto, T. *Adv. Colloid Interfac. Sci.* **1987**, *28*, 65.

(10) Liu, Y. H., Wang, F. D., Wang, Y. Y., Gibbons, P. C., Buhro, W. E. *J. Am. Chem. Soc.* **2011**, *133*, 17005.

(11) Joo, J., Son, J.S., Kwon, S.G., Yu, J.H., Hyeon, T. *J. Am. Chem. Soc* **2006**, *128*, 5632.

(12) Son, J. S., Wen, X.D., Joo, J., Chae, J., Baek, S., Park, K., Kim, J.H., An, K., Yu, J.H., Kwon, S.G., Choi, S.H., Wang, Z., Kim, Y.W., Kuk, Y., Hoffmann, R., Hyeon, T. *Angew. Chme., Int. Ed.* **2009**, *48*, 6861.

(13) Son, J. S., Park, K., Kwon, S.G., Yang, J., Choi, M.K., Kim, J., Yu, J.H., Joo, J., Hyeon, T. *Small* **2012**, *8*, 2394.

(14) Yu, J. H., Liu, X., Kweon, K.E., Joo, J., Park, J., Ko, K.T., Lee, D.W., Shen, S.P., Tivakornsasithorn, K., Son, J.S., Park, J.H., Kim, Y.W., Hwang, G.S., Dobrowolska, M.,

Furdyna, J.K., Hyeon, T. *Nat. Mater.* **2009**, *9*, 47.

(15) Wang, Y. Y., Liu, Y.H., Zhang, Y., Wang, F.D., Kowalski, P. J., Rohrs, H. W., Loomis, R. A., Gross, M. L., Buhro, W. E. *Angew. Chem., Int. Ed.* **2012**, *51*, 6154.

(16) Wang, Y. Y., Liu, Y.H., Zhang, Y., Kowalski, P. J., Rohrs, H. W.,Buhro, W. E. *Inorg. Chem* **2013**, *52*, 2933.

(17) Ithurria, S., Dubertret, B. *J. Am. Chem. Soc* **2008**, *130*, 16504.

(18) Ithurria, S., Tessier, M.D., Mahler, B., Lobo, R.P.S.M., Dubertret, B., Efros,. A.L. *Nat. Mater.* **2011**, *10*, 936.

(19) Ithurria, S., Bousquet, G., Dubertret, B. *J. Am. Chem. Soc* **2011**, *133*, 3070.

(20) Mahler, B., Nadal, B., Bouet, C., Patriarche, G., Dubertret, B. *J. Am. Chem. Soc* **2012**, *134*, 18591.

(21) Li, Z., Peng, X. *J. Am. Chem. Soc* **2011**, *133*, 6578.

(22) Liu, Y. H., Wayman, V.L., Gibbons, P.C., Loomis, R.A., Buhro, W.E. *Nano Lett.* **2010**, *10*, 352.

(23) Kasuya, A., Sivamohan, R., Barnakov, Y. A., Dmitruk, I. M., Nirasawa, T., Romanyuk, V. R., Kumar, V., Mamykin, S. V., Tohji, K., Jeyadevan, B., Shinoda, K., Kudo, T., Terasaki, O., Liu, Z., Belosludov, R. V., Sundararajan, V., Kawazoe, Y. *Nat. Mater.* **2004**, *3*, 99.

(24) Morrison, P. J., Loomis, R.A., Buhro, W.E. *Chem. Mater.* **2014**, *10.1021/cm5020702*.

(25) Wang, Y. Y., Zhang, Y., Wang, F.D., Giblin, D.E., Hoy, J., Rohrs, H. W., Loomis, R.A., Buhro, W. E. *Chem. Mater.* **2014**, *26*, 2233.

(26) Dolai, S., Nimmala, P. R., Mandal, M., Muhoberac, B. B., Dria, K., Dass, A., Sardar,

R. *Chem. Mater.* **2014**, *26*, 1278.

(27) Bowers, M. J. I., McBride, J.R., Rosenthal, S.J. *J. Am. Chem. Soc* **2005**, *127*, 15378.

(28) Bowers, M. J. I., McBride, J.R., Garrett, M.D., Sammons, J.A., Duckes III, A.D., Schreuder, M.A., Watt, T.L., Lupini, A.R., Pennycook, S.J., Rosenthal, S.J. *J. Am. Chem. Soc* **2009**, *131*, 5730.

(29) Lands, C., El-Sayed, M.A. *J. Phys. Chem. A* **2002**, *106*, 7621.

(30) Yu, K., Hu, M.Z., Wang, R., Piolet, M.L., Frotey, M., Zaman, M.B., Wu. X., Leek., D.M., Tao, T., Wilkinson, D., Li, C. *J. Phys. Chem. C* **2010**, *114*, 3329.

(31) Duckes III, A. D., McBride, J.R., Rosenthal, S.J. *Chem. Mater.* **2010**, *22*, 6402.

(32) Harrell, S. M., McBride, J.R., Rosenthal, S.J. *Chem. Mater.* **2013**, *25*, 1199.

(33) Kasuya, A., Noda, Y., Dmitruk, I., Romanyuk, V., Barnakov, Y., Tohji, K., Kumar, V., Belosludov, R., Kawazoe, Y., Ohuchi, N. *Eur. Phys. J. D* **2005**, *34*, 39.

(34) Cossairt, M., Owen, J. S. *Chem. Mater.* **2011**, *23*, 3114.

(35) Nguyen, K. A., Day, P. N., Pachter, R. *J. Phys. Chem. C* **2010**, *114*, 16197.

(36) Xie, C., Hao, H.X., Chen, W., Wang, J.K. *J. Cryst. Growth* **2008**, *310*, 3504.

(37) Ptatschek, V., Schmidt, T., Lerch, M., Muller, G., Spanhel, L., Emmerling, A., Fricke, J., Foitzik, A.H., Langer, E. *Ber.Bunsenges. Phys. Chem.* **1998**, 85.

(38) Steigerwald, M. L., Alivisatos, A.P., Gibson, J.M., Harris, T.D., Kortan, R., Muller, A.J., Thayer, A.M., Duncan, T.M., Douglass, D.C., Brus, L.E. *J. Am. Chem. Soc* **1988**, 3046.

(39) Bawendi, M. G., Kortan, A.R., Steigerwald, M.L., Brus, L.E. *J. Chem. Phys.* **1989**, *91*, 7282.

(40) Al-Amri, A. M., Yaghmour, S.J., Mahoud, W.E. *J. Cryst. Growth* **2011**, *334*, 76.

(41) Soloviev, V. N., Eichhofer, A., Fenske, D., Banin, U. *J. Am. Chem. Soc.* **2001**, *123*, 2354.

(42) Fojtik, A., Weller, H., Koch, U., Henglein, A. *Ber.Bunsenges. Phys. Chem.* **1984**, *88*, 969.

(43) Bryan, D. J., Schwartz, D.A., Gamelin, D.R. *J. Nanosci. Nanotech.* **2005**, *5*, 1472.

(44) Norberg, N. S., Parks, G.L., Salley, G.M. Gamelin, D.R. *J. Am. Chem. Soc* **2006**, *128*, 13195.

Chapter 4

Conclusion

In this dissertation, a novel soft-template method was introduced for the synthesis of colloidal CdSe magic-size nanoclusters and crystalline CdSe quantum platelets. A lamellar-amine-bilayer mesophase was formed spontaneously when cadmium acetate dissolved in a primary-amine solvent at around 70 ℃. The template structure was stabilized by van de Waals attractions between hydrophobic sidechains of the alkyl amine. This mesophase was constructed of alternating inorganic and organic layers with spacings determined by the size of cadmium precursor and the length of the alkyl chain from primary amine (Scheme 4-1a).

In a primary-amine environment, the $(CdSe)_{13}$(*n*-octylamine)$_{13}$ nanocluster and its primary-amine derivatives were assembled within the bilayer templates at room temperature upon addition of a selenium precursor. (Chapter 1 and 2). The results demonstrated that $(CdSe)_{13}$ under such conditions was the most thermodynamic stable CdSe-nanocluster size, and required heating to about 70 ℃ for conversion to crystalline wurtzite-structures CdSe quantum platelets (Scheme 4-1b). Mechanistic studies established that the ligated $(CdSe)_{13}$ nanocluster was stable in toluene or acetonitrile, but coalesced and grew to larger sizes in methanol, *i*-propanol, or acetone with first-order kinetics, due to the substitution of the primary-amine ligand by the small polar molecules (Chapter 1).

The $(CdSe)_{34}$ nanocluster was formed within the template at room temperature upon addition of the selenium precursor in a mixed primary-amine, secondary-amine environment (Chapter 3). Further studies indicated the $(CdSe)_{34}$ nanocluster with an empirical formula [$(CdSe)_{34}$(*n*-octylamine)$_{16}$(di-*n*-pentylamine)$_2$] was a key intermediate in the formation of crystalline, wurtzite CdSe nanocrysals at room temperature. Because the $(CdSe)_{34}$

nanoclusters were a kinetic product in the primary-amine, secondary-amine cosolvent system, and were near the critical crystal-nucleus size, they spontaneously converted to CdSe nanocrystals at room temperature by first-order kinetics (Scheme 4-1b), with no induction period.

The conversion process from either $(CdSe)_{13}$ nanoclusters or $(CdSe)_{34}$ nanoclusters to colloidal CdSe nanocrystals was achieved within the lamellar-bilayer templates, thus the nanocrystals grew in lateral dimension, and formed sheet-like two-dimensional nanoplatelets having the wurtzite structure (Scheme 4-1b) (Chapter 3).

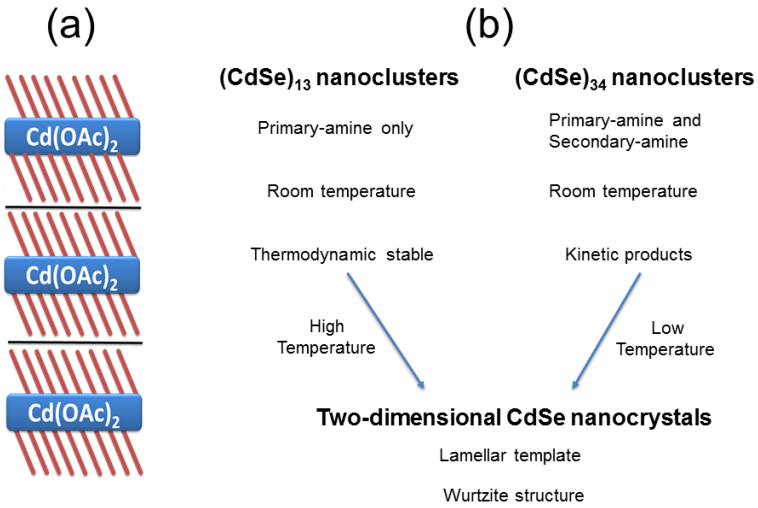

Scheme 4-1. Growth of $(CdSe)_{13}$ nanoclusters, $(CdSe)_{34}$ nanoclusters and crystalline CdSe QPs within a double-lamellar, primary-amine bilayer template. (a) $Cd(OAc)_2$ and the primary-amine solvent forms a lamellar, amine-bilayer mesophase. (b) Room temperature synthesis of $(CdSe)_{13}$ nanoclusters and $(CdSe)_{34}$ nanoclusters and their conversion to crystalline two-dimensional CdSe nanocrystals.

In future work, two research directions relevant to this dissertation will be undertaken. Crystalline, amine-ligated $(CdSe)_{13}$ nanoclusters will be sought, so that their structures may be pursued through NMR and X-ray diffraction techniques. Because gram-scale, solid-phase $(CdSe)_{13}$ derivatives, $(CdSe)_{13}$(*n*-propylamine)$_{13}$ and $(CdSe)_{13}(en)_x$, are now available (Chapters 1 and 2), suitable solvents are required for dissolving and recrystallizing

these $(CdSe)_{13}$ derivatives. The crystal structure of the $(CdSe)_{13}$ nanocluster will illuminate their physical and chemical properties, and further understanding of their functions in nanocrystals syntheses.

Other II-VI magic-size nanoclusters and QPs are also worthy of study. Recent research has focused most on cadmium chalcogenides; few studies are reported on zinc chalcogenides. Our preliminary work indicates that zinc precursors also form lamellar, amine-bilayer templates in primary-amine solvents, which indicates our soft template method may also work in zinc-chalcogenide magic-size nanocluster syntheses. Other II-VI crystalline QPs should be preparable in primary-amine, secondary-amine cosolvent systems; their morphologies and crystal structures will be investigated as well.